MINISTRY OF EDUCATION AND SCIENCE OF UKRAINE

National Aerospace University Named by M. E. Zhukovsky
«Kharkov Aviation Institute»

Airplanedesign Faculty

Airplane and Helicopter Design Department

Explanatory Note to Diploma Project of

Master
(degree)

Subject: Long-Range Passenger Airplane. Winglet airflow analysis

Student of 2 Year 161fd Group
Speciality: 134 Aviation and Aerospace Technologies
Educational program: Planes and Helicopters
Zhang Haoyu
(name)
Supervisor:
(name)
Reviewer
(name)

Kharkiv — 2023

NATIONAL AEROSPACE UNIVERSITY
«Kharkov Aviation Institute»

NATIONAL AEROSPACE UNIVERSITY
«Kharkov Aviation Institute»

Faculty Airplane-design
Chair Airplane and Helicopter Design
Degree Master

Specialty 134 Aerospace Engineering
(Code and Name)
Education Program Aircraft Designing
(Code and Name)

APPROVED by
Head of Chair

PhD, Ass. Prof.
S. V. Trubaev
"___" _____201___

T A S K
FOR STUDENT'S DIPLOMA WORK

Haoyu Zhang
(Name)
Subject of Work Long-Range Passenger Airplane. Winglet airflow analysis

Supervisor of Work ass. prof, PhD, Chumak
(duty, degree, scientific degree, name)
approved by University order from "___"_____20__ No___
Work presentation deadline\ 10.05.23
Initial data for work N_{pas} = 450
L = 10 000 km
V_{cr} = 850 km/h

Content of explanatory note (list of problems to solve)

Summary

1. Designing section

1.1. Automated formation of the aircraft shape

Introduction, aim and tasks of design

1.1.1. Development of the aircraft concept, scientific and technical program to achieve its performance.

1.1.2. Aircraft purpose, tactical and technical requirements, the conditions of its production and operation, restrictions imposed by aviation regulations.

1.1.3. Collection, processing and analysis of statistical data. Selection of basic relative initial parameters of the aircraft.

1.1.4. Aircraft scheme selection and justification, powerplant type selection.

1.1.5. Calculation of the aircraft takeoff mass.

1.1.6. Engines selection.

1.1.7. Definition of geometry of main airplane units.

1.1.8. Determining the position of the center of mass.

1.1.9. Determination of landing gear parameters there are following parameters to three strut landing gear.

1.2. Analysis of optimized aircraft design parameters influence on its aerodynamic and mass characteristics.

1.2.1. Study of wing geometrical parameters to take off characteristics.

1.2.2. Analysis of aircraft geometrical parameters influence to thrust to weight ratio.

1.2.3. Analysis of aircraft geometrical parameters influence to relative mass of power plant.

1.2.4. Analysis of aircraft geometrical parameters influence to relative mass of fuel.

1.2.5. Analysis of aircraft geometrical parameters influence to relative mass of structures.

1.2.6. Calculation of mass of equipment, control system and operational items.

1.2.7. Analysis of the total aircraft mass with respect to wing loading and wing respect ratio.

2. Economics

3. Special task

Winglet airflow analysis

List of drawings

- Master geometry of aircraft surface, general view drawing;
- Three view diagram of the aircraft.

Advisors of work sections

Section	Name and duty of advisor	Sign, Date	
		Task is given	Task is passed
1.	**Chumak A.S.**		
2.	**Pavlenko T.Y.**		
3.	**Chumak A.S.**		
4.			
5.			

Date when task is given_____

CALENDAR PLAN

Nos	Diploma work milestones	Work milestones deadline	Notes

Student _____

(Sign) (Name)

Supervisor of work _____ _____

(Sign) (Name)

SUMMARY

The master project includes 98 pages, 6 Tables, 47 Figures, 17 References.

Object of research: long range passenger aircraft, Variable tip winglets

The purpose of the work: the aim of the diploma project is to create a long-range passenger aircraft for 450 passengers, including the general views of the projected airplane, the determination of the takeoff mass and geometric parameters, calculation of the cost of manufacturing the projected aircraft, analysis of optimized aircraft design parameters influence on its aerodynamic and mass characteristics

Research methods: statistical, analytical methods, methods of building mechanics. Structural modeling in UG. According to the total research, we used some software to help finish our work. They are AutoCAD, EXCEL, ANSYS Fluent.

The results of the project:

(1). Design of a rotating body to achieve wingtip rotation

(2). Wingtip winglets installed on the upper and lower wing surface can impede air flow, thus reducing the lift force caused by vortices induced drag, and reduce the flow of the lift damage.

(3). Rotational position of wingtip a reasonable choice to increase the lift-drag ratio, improving the aircraft climb capabilities, and enhance flight performance.

(4). Research projects for the future of small wing on the aircraft wing can provide a design approach and technical foundation.

TURBOFAN ENGINE, LOW-WING MONOPLANE, AERODYNAMIC PERFORMANCE, ENGINE MOUNT, POWER PLANT SYSTEM, AIRPLANE PRICING, AIRFOIL ANALYSIS.

Contents

1. DESIGNING SECTION

1.1. Automated formation of the aircraft shape

To start developing an aircraft we take the main aspects of aircraft design:

Aerodynamics – Understanding the motion of air around an object (often called a flow field) enables the calculation of forces and moments acting on the object. In many aerodynamics problems, the forces of interest are the fundamental forces of flight: lift, drag, thrust, and weight. Of these, lift and drag are aerodynamic forces, i.e. forces due to air flow over a solid body. Calculation of these quantities is often founded upon the assumption that the flow field behaves as a continuum. Continuum flow fields are characterized by properties such as flow velocity, pressure, density, and temperature, which may be functions of position and time. These properties may be directly or indirectly measured in aerodynamics experiments or calculated starting with the equations for conservation of mass, momentum, and energy in air flows. Density, flow velocity, and an additional property, viscosity, are used to classify flow fields[1].

Propulsion – A powered aircraft is an aircraft that uses onboard propulsion with mechanical power generated by an aircraft engine of some kind.

Aircraft propulsion nearly always uses either a type of propeller, or a form of jet propulsion. Other potential propulsion techniques such as ornithopters are very rarely used.

Controls – A conventional fixed-wing aircraft flight control system consists of flight control surfaces, the respective cockpit controls, connecting linkages, and the

necessary operating mechanisms to control an aircraft's direction in flight. Aircraft engine controls are also considered as flight controls as they change speed.

The fundamentals of aircraft controls are explained in flight dynamics. This article centers on the operating mechanisms of the flight controls.

Mass – is both a property of a physical body and a measure of its resistance to acceleration (a change in its state of motion) when a net force is applied. An object's mass also determines the strength of its gravitational attraction to other bodies.

Structure – The structural parts of a fixed-wing aircraft are called the airframe. The parts present can vary according to the aircraft's type and purpose. Early types were usually made of wood with fabric wing surfaces, when engines became available for a powered flight around a hundred years ago, their mounts were made of metal. Then as speeds increased more and more parts became metal until by the end of WWII all-metal aircraft were common. In modern times, increasing use of composite materials has been made.

1.1.1. Development of the aircraft concept, scientific and technical program to achieve its performance.

The modern aircraft is a complex technical system, elements of which are, individually and collectively, need to have the maximum optimized parameters and high reliability. Aircraft generally must meet specified requirements, and have high efficiency in an appropriate technical level.

When drafting new aircraft is particularly important to achieve a high technical and economic efficiency. These aircraft must not only have good performance at time of entering the airline, but also have the potential for systematic modification to

increase the efficiency throughout the period of normal production and operation.

Creating a computer-aided design has revolutionized the design of aircraft, and their use has become almost scientific discipline. Dramatically expanded opportunities for improving the design of aircraft, improved the quality of technical documentation development, made possible the creation of a parallel based on one of a number of aircraft modifications.

The present trend of simultaneous creation of a family of planes including the various modifications and varying flight distance passenger has become more urgent. This is due to the desire to achieve maximum economic effect due to the basic design and systems (the motors may vary and the individual units, equipment, control). Such an approach based on maximum harmonization, reduce the cost of developing new models and price series of products as well as maintenance of their operation costs. Therefore, the creation of modern competitive aircraft is impossible without the use of integrated computer systems, CAD / CAM / CAE / PLM.

1.1.2. Aircraft purpose, tactical and technical requirements, the conditions of its production and operation, restrictions imposed by aviation regulations

The purpose of the design:

- **Type of aircraft:** long range passenger aircraft;
- **Number of passengers:** 450 passengers;
- **Range:** 10,000km;
- **Cruising speed:** 880 km/h;

- **Take-off distance:** 2500m.

Design tasks: concept development, selection of the aircraft scheme, the calculation of takeoff weight, the calculation of aerodynamic performance, calculation of economic indicators.

Regarding the development prospects of civil airliners in the future, the basic consensus in the industry is that they are safer, more environmentally friendly, more economical, and more comfortable, or the indicators of safety, environmental protection, economy, and comfort continue to improve.

The concept of creating a projected aircraft is necessary for the optimal assignment of his TTT, the conditions of production and use.

Briefly state the concept of its creation:

- The appointment of the volume and frequency of activities on monitoring and maintaining the quality of the aircraft and its systems based on reliability analysis;
- Perfection aircraft structure and its parts in systems operation and maintenance workability (testability, availability, easily removable, easy maintenance, and the like);
- Extensive use of built-in control and on-board automatic second control system for the evaluation of technical condition, solutions of diagnosis and forecasting tasks;
- A purposeful choice composition of maintenance funds;
- High reliability and safety;

- Damage resistance;
- Maintainability;
- Lifetime 80 000 flight hours;
- Ability to continue the take-off in case of failure of one engine.

1.1.3. Collection, processing and analysis of statistical data. Selection of basic relative initial parameters of the aircraft.

The collection and processing of statistical data in the design of the aircraft, you can:

1. Get a clear picture of the current level of development of the aircraft, taking into account:

a) The types of aircraft;

b) The tasks they perform;

c) Flight technical qualities;

g) Means to achieve these qualities: applied aircraft circuits geometric and weight parameters power plant structural materials, production methods, and others.

2. Identify trends and development prospects of the developed type of aircraft, the quantitative and qualitative changes in the TTT to the plane, the evolution of his appointment, the conditions of production and operation.

3. Define number of aircraft parameters. Statistical analysis of the material makes it possible to develop TTT projected plane, select it scheme. The following listed aircraft were chosen to collect statistics are listed in Table 1.1:

Airbus A330-300 (Figure 1.1);

Airbus A350-1000 (Figure 1.2);

Boeing787-9 (Figure 1.3);

Boeing777-300 (Figure 1.4).

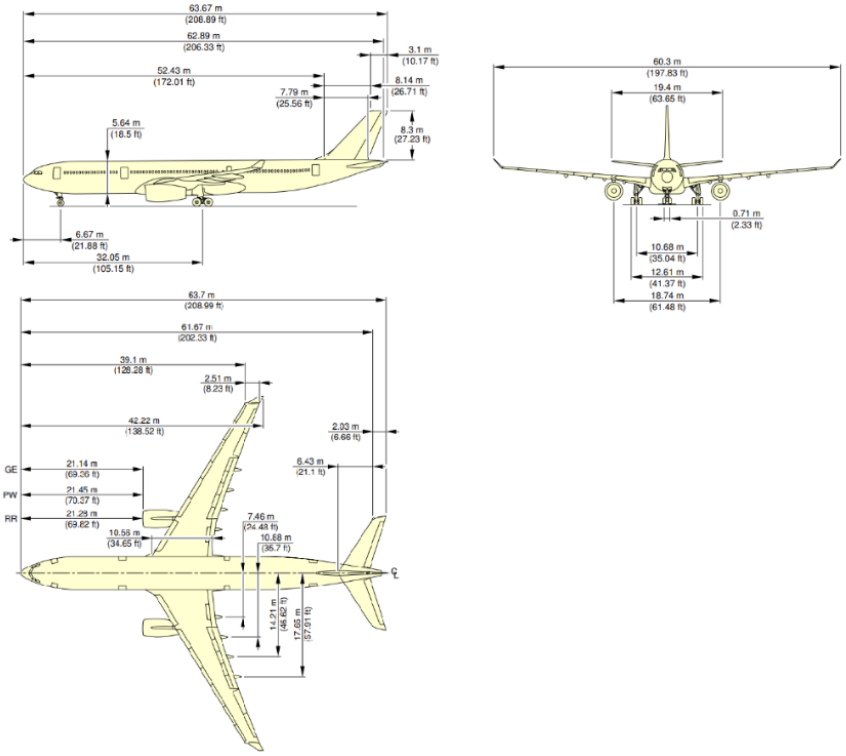

Figure 1.1 – Airbus A330-300

A330-300 - powered by two General Electric CF6-80E1, Pratt & Whitney PW4000, or Rolls-Royce Trent 700 engines, the 63.69 m (208 ft 11 in) long −300 has a range of 11,750 km / 6,350 nmi, typically carries 277 passengers with a 440 exit limit and 32 LD3 containers. It received European and American certification on 21 October 1993 after 420 test flights over 1,100 hours.[118] The −300 entered service on 16 January 1994. The A330-300 is based on a stretched A300 fuselage but with new wings, stabilisers and fly-by-wire systems.

In 2010, Airbus offered a new version of the −300 with the maximum gross weight increased by two tonnes to 235 t. This enabled 120 nmi (220 km; 140 mi) extension of

the range as well as 1.2 t increase in payload. In mid-2012, Airbus proposed another increase of the maximum gross weight to 240 t. It is planned to be implemented by mid-2015. This −300 version will have the range extended by 400 nmi (740 km; 460 mi) and will carry 5t more payload. It will include engine and aerodynamic improvements reducing its fuel burn by about 2%. In November 2012, it was further announced that the gross weight will increase from 235 t to 242 t, and the range will increase by 500 nmi (926 km; 575 mi) to 6,100 nmi (11,300 km; 7,020 mi). Airbus is also planning to activate the central fuel tank for the first time for the −300 model[2].

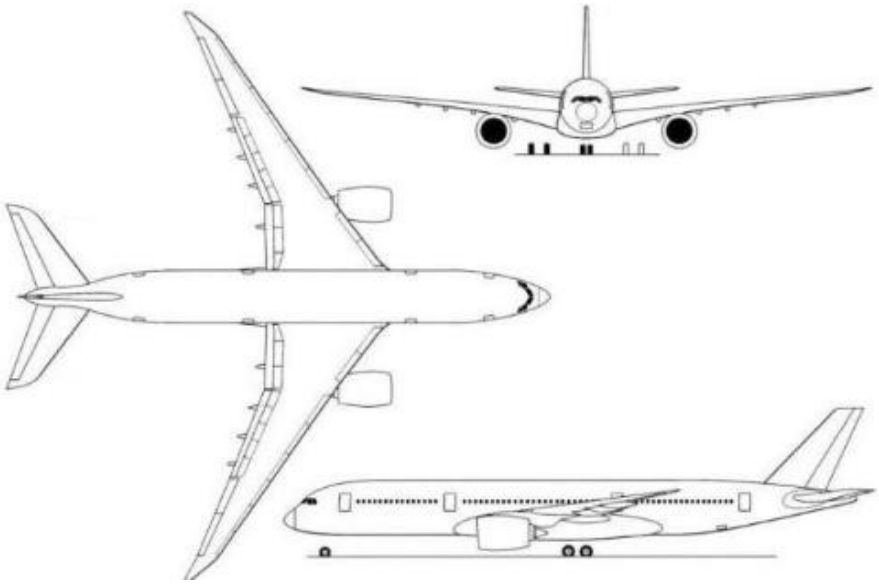

Figure 1.2 – Airbus A350-1000

A350-1000 - the A350-1000 flight test programme planned for 1,600 flight hours; 600 hours on the first aircraft, MSN59, for the flight envelope, systems and powerplant checks; 500 hours on MSN71 for cold and warm campaigns, landing gear checks and high-altitude tests; and 500 hours on MSN65 for route proving and ETOPS assessment, with an interior layout for cabin development and certification. In cruise at Mach 0.854 (911.9 km/h; 492.4 kn) and 35,000 ft, its fuel flow at 259 t (571,000 lb) is 6.8 t (15,000

lb) per hour within 10,000 km, 11 and 1/2 hours early long test flight. Flight tests allowed raising the MTOW from 308 to 316 t (679,000 to 697,000 lb), the 8 t (18,000 lb) increase giving 450 nmi (830 km) more range. Airbus then completed functional and reliability testing.

Type Certification was awarded by EASA on 21 November 2017, along FAA certification. The first serial unit was on the final assembly line in early December. After its maiden flight on 7 December 2017, delivery to launch customer Qatar Airways slipped to early 2018. The delay was due to issues with the business class seat installation[3].

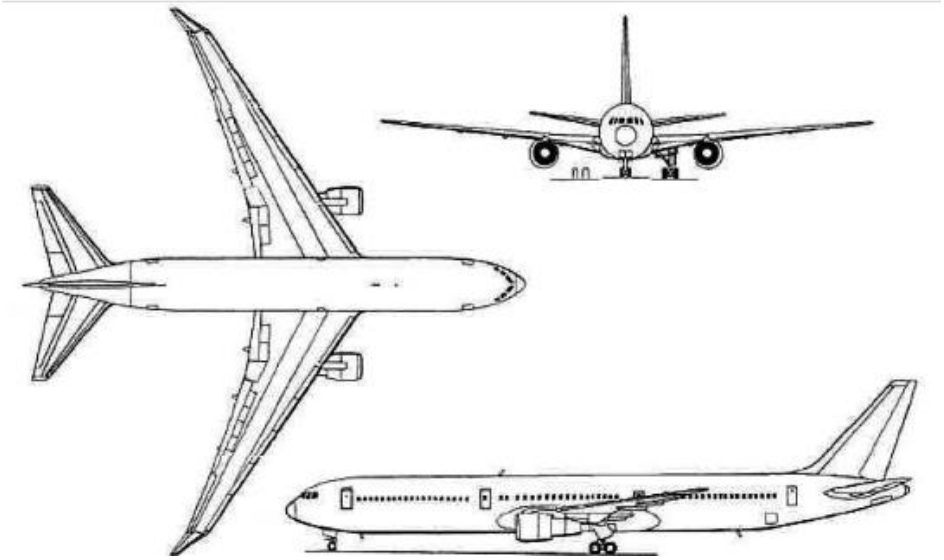

Figure 1.3 – Boeing787-9

B787-9 - the Boeing 787 Dreamliner is a long-haul, widebody, twin-engine jetliner, designed with lightweight structures that are 80% composite by volume; Boeing lists its materials by weight as 50% composite, 20% aluminum, 15% titanium, 10% steel, and 5% other. Aluminum has been used throughout the leading edges of wings and tailplanes, titanium is predominantly present within the elements of the engines and fasteners, while various individual components are composed of steel.

External features include a smooth nose contour, raked wingtips, and engine nacelles with noise-reducing serrated edges (chevrons). The longest-range 787 variant can fly up to 7,635 nmi (14,140 km), or the even longer Qantas QF 9 flight between Perth Airport and London–Heathrow, over 7,828 nmi (14,497 km). Its cruising airspeed is Mach 0.85 (488 kn; 903 km/h). The aircraft has a design life of 44,000 flight cycles[4].

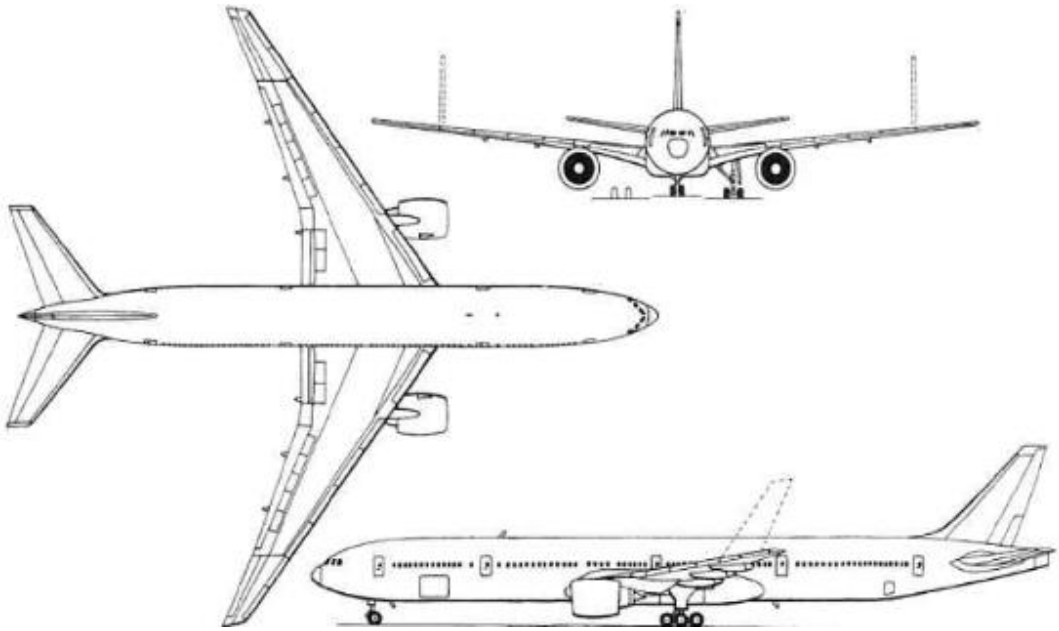

Figure 1.4 – Boeing777-300

B777-300 - Launched at the Paris Air Show on June 26, 1995, its major assembly started in March 1997 and its body was joined on July 21, it was rolled-out on September 8 and made its first flight on October 16. The 777 was designed to be stretched by 20%: 60 extra seats to almost 370 in tri-class, 75 more to 451 in two classes, or up to 550 in all-economy like the 747SR. The 33 ft (10.1 m) stretch is done with 17 ft (5.3 m) in ten frames forward and 16 ft (4.8 m) in nine frames aft for a 242 ft (73.8 m) length, 11 ft (3.4 m) longer than the 747-400. It uses the -200ER 45,200 US gal (171,200 L) fuel capacity and 84,000– 98,000 lbf (374–436 kN) engines with a 580,000

to 661,000 lb (263.3 to 299.6 t) MTOW[5].

Table 1.1 – Statistics prototype aircraft

	Airplane	A330-300	A350-1000	B787-9	B777-300
Flight data	V_{max}, km/h	1053	945	945	945
	H_{max}, km	12.5	13	13	13
	V_{cr}, km/h	1004	903	903	901
	H_{cr}, km	11	12	12	10
	$V_{take-off}$, km/h	278	260	280	290
	V_{land}, km/h	241.4	241.4	222.09	241.4
	L, km	11750	15560	14140	13650
	L_{land}, m	1750	1950	1755	1829
	$L_{take-off}$, m	2600	3000	3100	3200
Weight data	m_{empty}, kg	54600	64410	115200	144250
	$m_{0\ max}$, kg	233000	316000	252651	237680
	N_{pas}, people	330	440	420	451
	m_c, kg	50400	61300	60000	69250
Power plant	$n_{en}\times$ Type	Turbofan,2	Turbofan,2	Turbofan,2	Turbofan,2
	P_0, daN	31600	43200	32000	44000
Geometric data	S, m^2	361.6	440	325	427.8
	l, m	60.3	64.7	60	60.9
	X_{cr}, °	30	35.4	32.2	31.6
	λ	10.06	9.53	11.08	8.77

End of Table 1.1

	η_{cr}	5.9	6.4	5.5	5.7
	L_f, m	62.8	73.8	63	73.9
	D_f, m	5.6	5.9	6	6.2
	S_{ail}, m^2	6.21	7.35	6.89	7.26
	S_{hs}, m^2	89.64	102.4	98.75	101.4
	S_{vt}, m^2	48.51	53.56	50.34	53.05
Derived data	$P_0 = \frac{m_0 g}{10S}$, daN/m^2	631.47	703.8	580.13	685.79
	$t_0 = \frac{10P_0}{m_0 g}$	0.138	0.139	0.129	0.15

After collecting statistical data, we proceed to the development of tactical and technical requirements (TTT). This stage will be carried out on the basis of the analysis of statistical material, supplementing the TTT of the designed aircraft.

Selected TTT are entered in table 1.2.

Table 1.2 – Tactical-technical requirements

R, h	V_{cr} km/h	V_{max} km/h	L, km	$L_{take-off}$ m	N_{pas} people	H_{cr} km	N_{crew} people
80000	880	945	10000	3000	450	10	18

Where R – Lifetime, hours;

V_{cr} – Cruise Speed, km/h;

V_{max} – Maximum Speed, km/h;

H_{cr} – Cruise Altitude, km;

L – Flight Range, km;

$L_{take-off}$ – Take-off Run Distance, m;

N_{crew} – Number of Crew Members, people;

According to statistical data, the main parameters of the wing, plumage, fuselage and governing bodies are determined and recorded in table 1.3.

Table 1.3 – Main aircraft parameters

	Horizontal Stabiliser	Vertical Stabiliser	Main Wing
λ	4.575	1.775	8.67
η	4.286	3.27	5.846
$\mathbf{S_{relative\ area}}$	0.2367	0.1244	1
χ	40	45	31.64
S	101.034	53.111	426.884
L	21.5	9.71	60.84
$\mathbf{b_0}$	7.621	8.378	11.983
$\mathbf{b_{tip}}$	1.778	2.562	2.05
$\mathbf{b_A}$	5.305	5.985	8.188
$\mathbf{Z_A}$	4.261	3.995	11.621
$\mathbf{\tan x}$	0.84	1	0.462
$\mathbf{X_A}$	3.576	9.71	7.161

1.1.4. Aircraft scheme selection and justification, powerplant type selection

Along aircraft design process we should meet the following requirements:

1) Aircraft should provide an opportunity to continue the takeoff, climb, and

long horizontal flight with one engine inoperative. The following conditions must be met:

- in case of failure of one engine at takeoff 1,2Vmin at equal speed with landing gear during take-off position and high lift flap, it should be possible to continue takeoff;
- climb in this case must be at least 2 m/s;
- when an engine failure in flight control loads compensating bodies should not be excessive, and by a mechanism trimmer effect should be reduced to zero;
- Landing with an inoperative engine shall be possible missed.

2) Planes and conditions of its application require some special requirements for its structure, which can be summarized in several main groups:

- the aircraft must be stable and operate on all modes of flight and ground movements at the same control force should be within acceptable limits;
- airframe should have the minimum possible weight, thus must meet the requirements of strength and stiffness;
- airframe and aircraft control system must meet the requirements of survivability in the presence of significant damage;
- the aircraft must be simple to operate, repair and maintenance;
- all parts of the aircraft should be reinforced anti-corrosion treatment;
- the aircraft must be simple and economical to manufacture;

3) All flight control and navigation systems must be highly integrated to

reduce crew workload and provide solutions of tasks automatically. All aircraft equipment must confidently carry out their functions in the presence of strong interference. Apart from the above said aircraft, equipment must be modular design and be easily accessible.

4) For civilian aircraft engine in addition to the normal requirements of the special requirements are imposed due to application features:
    - strong corrosion protection elements;
    - built-in monitoring system state of the engine;
    - engine stability when operating in critical conditions;
    - advanced alarm system deviations in the work;
    - high resistance to damage.

Based on statistical data processing, normal aerodynamic configuration was selected for the projected plane. This scheme is a low-wing aircraft with swept wings. Crew has better observation of the front semi-sphere. Wing is in the pure, undisturbed airflow and is no stabilizers. Height of the landing gear struts and their mass is less, their retraction becomes simpler.

Along with the advantages of this scheme has the following disadvantages:

- the horizontal stabilizer (HS) is in the skewed airflow disturbed by wing; vertical stabilizer (VS) the mass of VS and this reduces its efficiency, causes the necessity of increase of its area and mass, and if HS position is shifted beyond turbulence zone upwards, downwards or on fuselage increases;
- greatest interference drag, but it can be essentially diminished by installation of fillets in a place of a wing-to-fuselage attachment;

- Service of the engines located on wing becomes simpler, but it is necessary to protect an air intake from being hit by foreign objects while moving on ground;
- during landing with bank, there is significant danger that engines may touch the ground;
- anhedral angle of swept wings partially allows to remove disadvantages by distancing engines from ground, but this results in increase of lateral stability and decrease of controllability. It is widely applied on passenger and transport aircraft.

The selected scheme placed on pylons below the wing engines is widespread at subsonic aircraft. Such engine installation scheme has the following advantages:

- Engines unload wing structure in flight, reducing the bending and twisting moments from the external loads, leading to decrease in the weight of the wing by 10 -15%;
- Simplified wing design: Mounting engines on the wing pylons can simplify the design of the wing, allowing for more efficient airflow and potentially reducing the overall weight of the aircraft. Easy access to the engine for maintenance;
- Improved safety: In the event of an engine failure, wing-mounted engines can reduce the risk of debris entering the fuselage or causing damage to other aircraft systems;
- More flexible engine placement: Mounting engines on wing pylons can offer more flexibility in terms of engine placement and allow for larger or

more efficient engines to be used on the aircraft.

The disadvantages of placing the engines on the wing pylons are:

- Increased drag: Placing the engines on the wing pylons creates additional drag, which can decrease the aircraft's overall efficiency;
- Reduced maneuverability: The weight and placement of the engines on the wing pylons can affect the aircraft's maneuverability, making it less agile in flight;
- Increased noise: The position of the engines on the wing pylons can also lead to increased noise levels in the cabin and on the ground;
- Higher maintenance costs: Maintaining engines mounted on pylons can be more difficult and expensive than maintaining engines mounted within the wings or fuselage;
- Increased risk of damage: Engines mounted on pylons are more exposed to damage from debris or bird strikes, which can cause significant damage to the aircraft.

Tricycle landing gear with nose wheel provides a more effective braking when run, substantially reducing the possibility of bouncing, improve visibility during takeoff -landing pilots. In addition, the circuit with the chassis nose wheel has better stability when driving on the airfield. Nose wheel retracts forward into the fuselage, the main - in special fairings on the fuselage. Plane show in Figure 1.5.

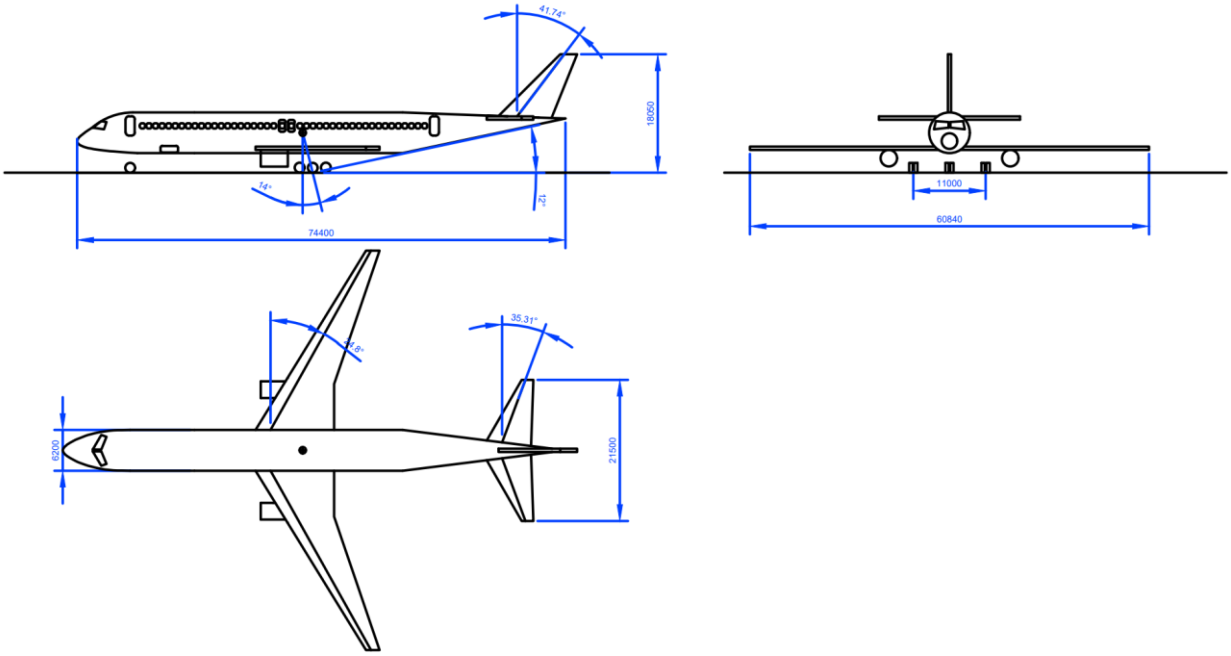

Figure 1.5 – Airplane scheme

1.1.5. Calculation of the aircraft takeoff mass

Determination m0 is available in several approximations updating via relative masses mi obtained by examining statistics of prototypes and comparative analysis of aircraft.

Take-off weight in the zero approximation, given by:

$$m_0 = \frac{m_{p.l} + m_{crew}}{1 - \left(\bar{m}_{airfrm} + \bar{m}_{pow.pl} + \bar{m}_{fuel} + \bar{m}_{ctl.sys}\right)} \qquad (1.1)$$

Here $m_{p.l}$ – mass of payload = 54000kg,

m_{crew} – mass of operational items and crew members, it is assumed that averaged mass of crew member eruals to 80 kilos = 1200kg;

$\bar{m}_{airfrm}$ - relative mass of airframe, which includes relative masses of the wing, fuselage, tail unit and landing gears=0.25;

$\bar{m}_{pow.pl}$ - relative mass of power plant, which includes relative masses of the engines together with facilities for mounting and servicing systems=0.08;

$\bar{m}_{ctl.sys}$ - relative mass of the equipment and control system, including hydraulic, pneumatic, electrical system, navigation equipment, control systems of the rudder, elevator, ailerons, flaps and spoilers=0.09;

$\bar{m}_{fuel}$ – relative mass of fuel, which is calculated according to the following formula:

$$\bar{m}_{fuel} = a + b\frac{L_{fl}}{V_{cruis}} = a + b \cdot t_{fl} \quad (1.2)$$

here $a = \begin{cases} 0.04 \dots 0.05 - for\ light\ non - manuverable\ planes; \\ 0.06 \dots 0.07\ for\ any\ other\ airplanes; \end{cases}$

$b = \begin{cases} 0.05 \dots 0.06 - for\ sub - sonic\ planes; \\ 0.14 \dots 0.15 - for\ supersonic\ planes; \end{cases}$

L_{fl} - flight range in kilometers;

V_{cruis} - cruising flight speed in km/h;

t_{fl} - planned flight duration in hours.

So m_0 = 240000kg.

Thus calculating for each of the separate parameters with the above obtained take off mass we get the following results.

$\bar{m}_{airfrm}$ - mass of fuel= 60000 kg;

$\bar{m}_{pow.pl}$ - mass of the Power Plant= 19200 kg;

$\bar{m}_{ctl.sys}$ -mass of the equipment = 21600 kg;

$\bar{m}_{fuel}$ – mass of the airplane structure= 84000 kg:

1.1.6. Engines selection

P_0 - Starting Thrust of the Engine

$$P_0 = t_0 \cdot M_0 \cdot g \tag{1.3}$$

P_0 =0.395*240000*9.8=929040N

This is the total engine thrust required. We have total number of engines as 2. So thrust required for one engine =464520 N. We select the GE Aviation GE9X engines. As shown on Fig 1.6 below.

Type：Dual rotor, axial flow, high bypass turbofan

Length：224.0 in (5690 mm) [Fan Spinner to TRF aft most flange]

Weight：21,230 lb (9,630 kg)

Compressor：1 fan, 3-stage LP, 11-stage HP

Combustor：Single annular Twin Annulus Premixing Swirler

Turbine：2-stage HP, 6-stage LP

Thrust/weight：5.2

Fan：134 in (340 cm) diameter, 16 wide chord composite blades

Bypass ratio：9.9:1

Overall pressure ratio：60:1, HPC pressure ratio: 27:1

Fan pressure ratio：1.70-1.80

Figure 1.6 – GE9X engine

1.1.7. Definition of Geometry of Main Airplane Units

Wing area is determined by the formula (1.4):

$$S_{wing} = m_0 g/10 p_0, m^2 \quad (1.4)$$

here g = 9.8 – gravity acceleration, m/s^2;

p_0 =481.409 – wing specific load during takeoff determined by statistics, daN/m^2;

m_0 =209700 – take-off mass, kg

So S_{wing} = 426.884 m^2

Wing span is determined by the formula (1.5):

$$L_{wing} = \sqrt{\lambda S_{wing}} = 60.84 \text{ m} \quad (1.5)$$

Wing root chord (along axis of symmetry) b_0, m, and wing tip chord b_{tip}, are determined by formulas (1.6):

$$b_0 = 2\eta S_{wind}/L_{wing}(\eta + 1);\ b_{tip} = b_0/\eta \quad (1.6)$$

Here η = 5.846, so b_0 = 11.983m, b_{tip} = 2.05m.

Mean aerodynamic chord (MAC) in meters is calculated by the formula (1.7):

$$b_A = \frac{2b_0}{3} \cdot \frac{\eta^2 + \eta + 1}{\eta(\eta + 1)} \tag{1.7}$$

So b_A = 8.188 m.

MAC coordinate spanwise in meters is determined by the formula (1.8):

$$Z_A = \frac{L}{6} \cdot \frac{\eta + 2}{\eta + 1} = 11.621 \tag{1.8}$$

Coordinate of MAC nose along OX axis is determined by the formula (1.9):

$$X_A = Z_A \mathrm{tg}\chi_{l.ed.} = 7.161 \text{ m} \text{ or } X_A = \frac{b}{6} \cdot \frac{\eta + 2}{\eta + 1} \mathrm{tg}\chi_{l.ed.}, \text{ m} \tag{1.9}$$

here $\chi_{l.ed.}$ –sweepback angle at leading edge is determined by the formula (1.10):

$$\mathrm{tg}\chi_{l.ed.} = \mathrm{tg}\chi + (\eta - 1)/4(\eta + 2) = 0.616 \tag{1.10}$$

Formulas (1.9), (1.10) are true for wings having straight generatrices of the leading and trailing edges and tip chord parallel to OX axis, for curvilinear contours of wings and chord they are replaced approximately with straight lines.

Calculation of horizontal tail parameters is preformed similar to the calculations of wing parameters.

Horizontal Stabilizer Area is determined by the formula (1.11):

$$S_{HS} = \bar{S}_{HS} S = 101.034\ m^2 \tag{1.11}$$

Horizontal Stabilizer Span is determined by the formula (1.12):

$$L_{HS} = \sqrt{\lambda_{HS} S_{HS}} = 21.5\ m \tag{1.12}$$

Horizontal Stabilizer Root Chord is determined by the formula (1.13):

$$b_{0HS} = \frac{2S_{HS}}{L_{HS}} \frac{\eta_{HS}}{\eta_{HS} + 1} = 7.621\ m \tag{1.13}$$

Horizontal Stabilizer Tip Chord is determined by the formula (1.14):

$$b_{KHS} = \frac{b_{0HS}}{\eta_{HS}} = 1.778\ m \tag{1.14}$$

Horizontal Stabilizer Mean Aerodynamic Chord is determined by the formula (1.15):

$$b_{AHS} = \frac{2b_{0HS}}{3} \cdot\cdot \frac{\eta_{HS}^2 + \eta_{HS} + 1}{\eta_{HS}(\eta_{HS} + 1)} = 5.305\ m \tag{1.15}$$

Coordinate b_{AHS} is determined by the formula (1.16):

$$Z_{AHS} = \frac{L_{HS}}{6}\frac{\eta_{HS} + 2}{\eta_{HS} + 1} = 4.261\ m \tag{1.16}$$

Coordinate of nose b_{AHS} is determined by the formula (1.17):

$$X_{\text{HAHS}} = Z_{\text{AHS}} tg\chi_{nHS} = 3.576\ m \tag{1.17}$$

Vertical Stabilizer Area is determined by the formula (1.18):

$$S_{vS} = \bar{S}_{vS} S = 53.111 m^2 \tag{1.18}$$

Vertical Stabilizer Span is determined by the formula (1.19):

$$L_{vS} = \sqrt{\lambda_{vS} S_{vS}} = 9.71\ m \tag{1.19}$$

Vertical Stabilizer Root Chord is determined by the formula (1.20):

$$b_{oVS} = \frac{2S_{VS}}{L_{VS}}\frac{\eta_{vS}}{\eta_{vS} + 1} = 8.378\ m \tag{1.20}$$

Vertical Stabilizer Tip Chord is determined by the formula (1.21):

$$b_{\text{RVS}} = \frac{b_{0\text{VS}}}{\eta_{\text{VS}}} = 2.562\ m \tag{1.21}$$

Vertical Stabilizer Mean Aerodynamic Chord is determined by the formula (1.22):

$$b_{AVS} = \frac{2b_{0VS}}{3} \cdot \frac{\eta_{VS}^2 + \eta_{VS} + 1}{\eta_{VS}(\eta_{VS} + 1)} = 5.985\ m \tag{1.22}$$

Coordinate b_{AVS} along height is determined by the formula (1.23):

$$Y_{Avs} = \frac{L_{vS}}{3}\frac{\eta_{vS} + 2}{\eta_{vS} + 1} = 3.995\ m \quad (1.23)$$

Coordinate of nose b_{AVS} is determined by the formula (1.24):

$$X_{HAVS} = L_{vS} tg\chi_{nVS} = 9.71\ m \quad (1.24)$$

Fuselage length is determined by the formula (1.25):

$$L_f = \lambda_f d_f, \text{ m} \quad (1.25)$$

Take $\lambda_f = 12,\ d_f = 6.2$, so $L_f = 74.4\ m.$

Fuselage nose section length is determined by the formula (1.26):

$$L_{nf} = \lambda_{nf} d_{nf}, \text{ m} \quad (1.26)$$

Take $\lambda_{nf} = 2.1,\ d_{nf} = 8.5$, so $L_{nf} = 17.86\ m.$

Fuselage aft section length is determined by the formula (1.27):

$$L_{af} = \lambda_{af} d_{af}, m \quad (1.27)$$

Take $\lambda_{af} = 3.5,\ d_{af} = 7.08$, so $L_{af} = 24.8\ m.$

Fuselage cylindrical section length is determined by the formula (1.28):

$$L_{c.f.} = L_f - L_{nf} - L_{af} = 31.74\ m \quad (1.28)$$

1.1.8. Determining the position of the center of mass

Position of the airplane center of mass is determined relative to nose part of wing mean aerodynamic chord. The recommendation distance for the center of mass (point 0) from nose part of mean aerodynamic chord X_m has such values for the airplanes with swept wing.

$$X_m = (0.26 \ldots 0.30) * b_A = 0.28 * b_A = 0.28 * 8.188 = 2.29\ m \quad (1.29)$$

- for airplanes with swept wing (x = 30⋯60°), distance from the center of mass to the nose of the wing MAC.

L_{HS}=3.5*b_A=3.5*8.188=28.658 m - the distance form one-fourth of the SAX horizontal tail to the center of mass.

1.1.9. Determination of landing gear parameters there are following parameters to three strut landing gear

- landing gear wheel base b;

- landing gear wheel track B;

- offset e;

- height of landing gear h;

- height of the airplane center of mass H.

Derivatives from these parameters will be:

- angle offset for wheels of main struts ɣ; Angle of overturning φ (angle of a touch down of a fuselage tail section with runway surface);

- angle of main wheels setoff ɣ should be higher than angle of a touch down by a tail part.

$$ɣ\ \gamma = \varphi + (1\ldots2) \tag{1.30}$$

φ is angle of touchdown by the tail part:

$$\varphi = \alpha_{max} - \alpha_{wi} - \Psi \tag{1.31}$$

α_{wi}= (0…4) = 0 (angle between a wing chord and longitudinal axis of fuselage) Ψ=0 (static ground (parking angle) in zero approximation it is Ψ=0)

$$\varphi = 14 - 0 - 0 = 14.$$

$$\gamma = 14 + 2 = 16.$$

Regarding the center of mass e with angle ɣ the greater the value e the greater the front tail support loads and more difficult to take off a front support during take-off.

But the lesser the e reduce ɣ.

Wheelbase of the landing gear b it depends of fuselage length:

$$b = (0.30 \dots 0.40)L_F = 0.37 * 74.4 = 27.53\ m \quad (1.32)$$

Distance between a nose strut and center of mass a is chosen so that during airplane parking loading on nose strut would be equal (6…12%) of airplane mass:

$$a = (0.88 \dots 0.94)b = 0.91 * 27.53 = 25.05\ m. \quad (1.33)$$

$$e = (0.12 \dots 0.06)b = 0.09 * 27.53 = 2.48\ m. \quad (1.34)$$

h– height of loading gear is determined from the condition providing the minimum gap 200…250mm between the runway surface and the airplane structure.

B– the maximum size of track should be up to 12m.

On the basis of track of landing gear should be in such limits: $2h < B < 16\ m$

Calculation of H: $H = \frac{e}{\tan ɣ} = \frac{2.18}{tan16} = 8.65\ m.$

1.1.10. Conclusions

We could build an airplane with a bigger cargo capacity, longer range, and greater safety with the aid of modern technologies. The reduced mass of my design is owing to the use of composite materials in the fuselage, the wing tips contribute to a 5% fuel savings, and the new generation of engine that takes use of the air mass due to the large fan that is installed.

In a zero approximation, we were able to determine and compute the parameters of an airplane. We also discovered that the settings for airplane parameters and attributes cannot be picked at random. Changes in the quantitative values of some factors and features will result in changes in other parameters. The theoretical system

of plane vision was created after the geometrical characteristics of the airplane major nits were calculated. Following the specification of airplane parameters, the overall view of the airplane was drawn in three projections on the theoretical design.

1.2. Analysis of optimized aircraft design parameters influence on its aerodynamic and mass characteristics

1.2.1. Study of wing geometrical parameters to take off characteristics

In this lab work I am analysing the take-off characteristic of my plane with respect to the wing geometrical parameters. The main parameter for analysis which I have considered is Wing aspect ratio.

The second Characteristic that we are analysing for the required aircraft is the wing loading.

The next important parameter that we analyse in this lab is the lift to drag ratio.

The last parameter that we are analysing is the Cofficient of lift.

The lift coefficient at take-off is determined by the formula (1.35):

$$C_{y_{t.off}} = C_{y_w}^{t.off}\left(1 + \Delta\bar{C}_y \frac{\delta_{flap.t.off}}{\delta_{flap.tab}} \cdot \frac{\bar{b}_{flap}}{\bar{b}_{flap.tab}} \cdot \bar{S}_{mech}^{t.off} \cdot cos^2 X_{0.75}\right) + \Delta C_{y_{land}} + \Delta C_{y_{obd'}} \quad (1.35)$$

Where $C_{y_w}^{t.off}$ - the lift coefficient of the wing during take-off without use of mechanization;

$\Delta\bar{C}_y$ - increase in lift factor due to use mechanization of the wing;

$\delta_{flap.t.off}$ - angle of deviation of flap at take-off;

$\delta_{flap.tab}$ - flap deflection angle;

$\bar{b}_{flap.tab}$ - relative chord of flap from table;

$\bar{b}_{flap}$ - relative chord of flap;

$\bar{S}_{mech}^{t.off}$ - the relative area of the console serviced by mechanization;

$X_{0.75}$ - sweep of 0.75 chords in the area of mechanization;

$\Delta C_{y_{land}}$ - an increase in the lift coefficient due to the impact of the earth.

The increase in lift due to the impact of the earth can be estimated by the formula (1.36):

$$\Delta C_{yland} = 0.313 - 0.237\bar{h} + 0.0572(\bar{h})^2 \quad (1.36)$$

The derivative of the lift coefficient for the angle of attack for the aircraft in the flight configuration is determined by the formula (1.37):

$$C_y^{\alpha} = \frac{0.11 - 0.029\sqrt[4]{\bar{c}}}{\frac{0.0775}{\cos x_{0.5}} + \frac{1.5}{\lambda}} \quad (1.37)$$

Where $\bar{c}$ - relative thickness of the profile;

$x_{0.5}$ - wing sweep angle of 50% chord;

λ - aspect ratio of the wing.

The initial data and results are shown in the Figure1.7 (a), (b).

According to the results of the calculation, the graphs of the dependences of the lift coefficient and the lift-to-drag ratio on the aspect ratio of the wing are constructed for specific loading of the wings 250, 350, 450 and 550 daN/m^2, which are the most suitable according to the collected statistics of analog aircraft.

As the wing lengthens, the lift coefficient increases, and as the wing load increases, the lift-to-drag ratio decreases. But with higher aspect ratio, the lift-to-drag ratio is relatively higher.

Training Centre
CAD/CAM/CAE

Choose language ↓
Greetings **Guest**
Registration
Sign In

Wing and high-lift devices parameters influence on Cy_{TO} and K_{TO} values study

Calculation results

НАУ им.Жуковского ("ХАИ")
Кафедра №103
Факультет самолёто-вертолёто строения
Главная
Расчет характеристик ЛА
Airplane Take-off Mass

Short list | Detailed list

Initial data:

Airplane type = Passenger $n_{pass.} = 450$(itm.); $m_{pass.} = 120$(kg);

Engine type = Turbo-fan/jet;

Wing high-lift devices type = Slat and double sloted retractable flap
$\Delta\overline{C}_{y\,1.dev} = 2.2$; $\overline{l}_{sl.} = 0.8$; $k_{sl.} = 0.15$; $\overline{l}_{fl.} = 0.6$; $\overline{b}_{fl.} = 0.3$;
$\delta_{fl.TO} = 25$(deg.); $k_{fl.} = 0.25$;

$\overline{C} = 12$(%); $\lambda_w = 8.67$; $\eta = 5.846$; $\chi_{le} = 31.64$(deg.);
$\alpha_{TO} = 10$(deg.); $M_{TO} = 0.2$; $d_{fus.} = 6.2$(m); $\lambda_{fus.} = 12$;
$k_{mid.} = 4000$(daN/m^2); $k_{int.w} = 0.85$; $k_{stab.} = 1.35$; $k_{pl.} = 0.2$;
$\overline{h} = 0.641$; $\overline{l} = 11.589$; $\overline{l}_{slots.} = 0.75$;

Calculation results:

Wing aspect ratio influence on take-off lift coefficient and lift-to-drag ratio.

λ_w	6	6,5	7	7,5	8	8,5	8,67	9	9,5	10
Cy	1,733	1,742	1,749	1,754	1,759	1,762	1,763	1,765	1,768	1,77
p, daN/m^2	$K_{lift.off}$									
100.0	10,732	11,182	11,601	11,993	12,36	12,703	12,814	13,024	13,327	13,611
150.0	10,547	10,991	11,405	11,792	12,153	12,492	12,602	12,809	13,107	13,387
200.0	10,384	10,823	11,232	11,614	11,97	12,304	12,412	12,616	12,91	13,185
250.0	10,237	10,67	11,074	11,451	11,802	12,131	12,238	12,439	12,728	13
300.0	10,101	10,529	10,927	11,299	11,645	11,97	12,075	12,273	12,558	12,825
350.0	9,973	10,396	10,789	11,156	11,497	11,817	11,921	12,116	12,397	12,66
400.0	9,852	10,27	10,658	11,02	11,357	11,672	11,774	11,967	12,243	12,502
450.0	9,738	10,15	10,533	10,89	11,222	11,533	11,634	11,823	12,095	12,351
500.0	9,628	10,035	10,413	10,765	11,093	11,399	11,499	11,686	11,954	12,205
550.0	9,523	9,925	10,298	10,645	10,969	11,271	11,369	11,553	11,817	12,065
600.0	9,421	9,818	10,187	10,53	10,849	11,147	11,244	11,425	11,685	11,929
650.0	9,324	9,716	10,08	10,418	10,733	11,027	11,122	11,301	11,557	11,798
700.0	9,229	9,617	9,976	10,31	10,621	10,91	11,004	11,181	11,434	11,67

(a)

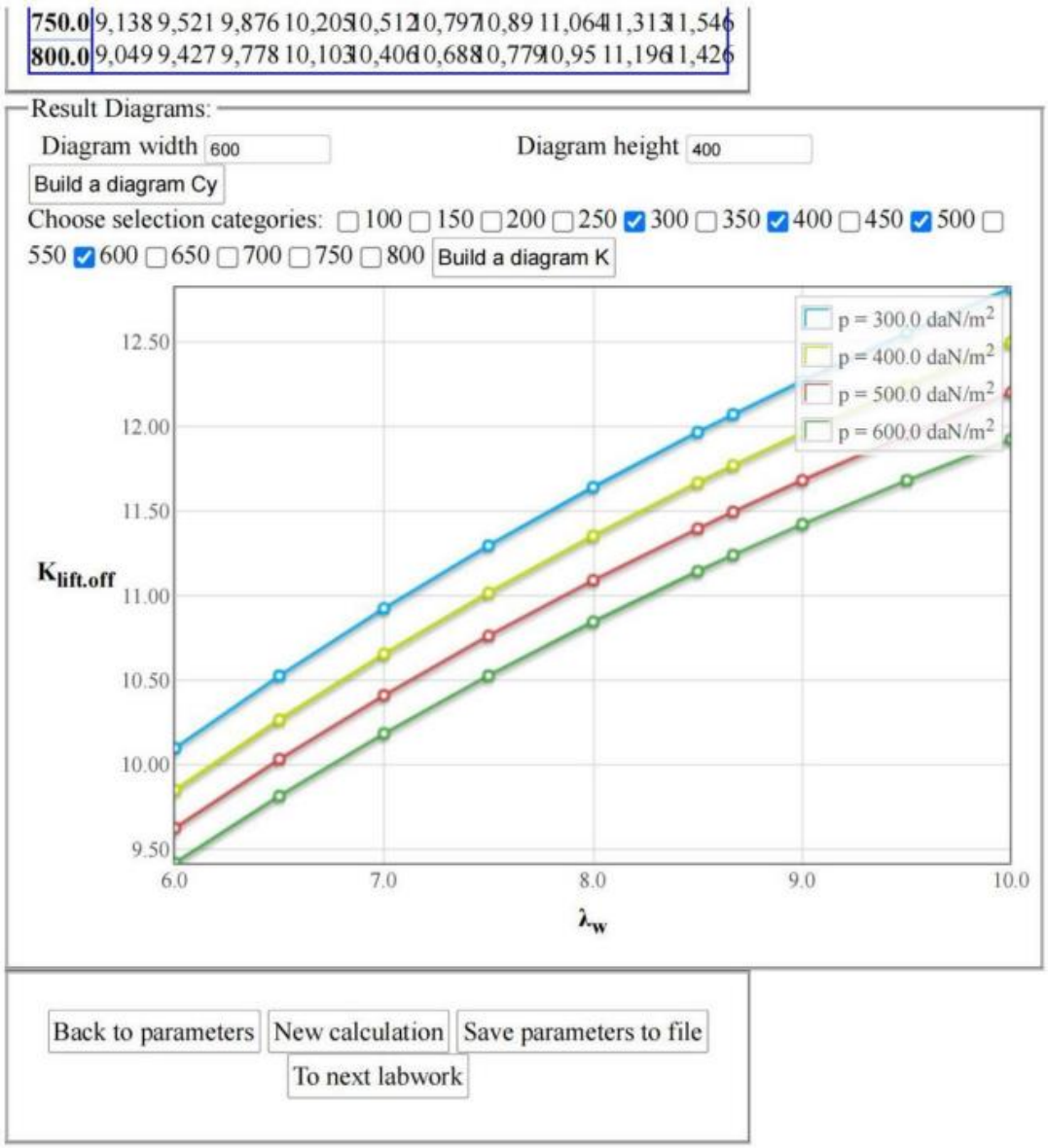

(b)

Figure 1.7 – The initial data and the results

1.2.2. Analysis of aircraft geometrical parameters influence to thrust to weight ratio

In this lab we need to determine the mass of the equipment, control system, operational item and crew members.

To study the effect of wing aspect ratio on thrust-to-weight ratio in cruise and at takeoff, the following formulas (1.38) are used:

$$t_{0cruise} = \frac{0.933 p_H M_{cruise}^2}{\xi_{cruise}} \left(\frac{F_1}{p} + F_2\right)$$

$$t_{0t.off} = \frac{1}{\xi_{t.off}} \left(\frac{0.832p}{C_{yt.off} L_{rol}} + \frac{1}{3}\left(\frac{1}{K_{t.off}} + 2f\right)\right) \quad (1.38)$$

$$t_0 = \frac{n_{eng}}{\xi_{t.off}(n_{eng} - 1)} \left(\frac{1}{K_{t.off}} + tg(\theta_{flap})\right)$$

Where p_H - pressure at cruise altitude;

F_1, F_2 - coefficient changes in traction, windshield resistance and tail unit, fuselage windshield.

As the specific load on the wing increases, the starting thrust-to-weight ratio is provided, which provides the lifting capacity, the runway length, the given angle of climb, and the energy due to the cruise speed of flight – decreases. As the wing lengthens, the starting thrust determined by the cruise speed, increases in all other modes.

The initial data and results are shown in the Figure1.8 (a), (b),(c).

Training Centre
CAD/CAM/CAE

Choose language ↓
Greetings **Guest**
Registration
Sign In

Wing and high-lift devices parameters influence on required starting thrust (power) to weight ratio values study

Calculation results

НАУ им.Жуковского ("ХАИ")
Кафедра №103
Факультет самолёто-вертолёто строения
Главная
Расчет характеристик ЛА
Airplane Take-off Mass

Short list | Detailed list

Initial data:

Airplane type = Passenger $n_{pass.} = 450$(itm.); $m_{pass.} = 120$(kg);

Engine type = Turbo-fan/jet;
$\xi_{int.} = 0.98$; $\xi_{tr.cr.} = 0.7$; $\xi_{tr.TO.} = 0.95$; $y = 8$; $M_{cr.} = 0.8$;
$H_{init.} = 10$(km); $H_{fin.} = 13$(km); $n_{eng.} = 2$(itm.);

Wing high-lift devices type = Slat and double sloted retractable flap
$\Delta\overline{C}_{y\,1.dev} = 2.2$; $\overline{l}_{sl.} = 0.8$; $k_{sl.} = 0.15$; $\overline{l}_{fl.} = 0.6$; $\overline{b}_{fl.} = 0.3$;
$\delta_{fl.TO} = 25$(deg.); $k_{fl.} = 0.25$;

$\overline{C} = 12$(%); $\lambda_w = 9.7$; $\eta = 5.846$; $\chi_{le} = 31.64$(deg.);
$\alpha_{TO} = 10$(deg.); $M_{TO} = 0.2$; $d_{fus.} = 6.2$(m); $\lambda_{fus.} = 12$;
$k_{mid.} = 4000$(daN/m^2); $k_{int.w} = 0.85$; $k_{stab.} = 1.35$; $k_{pl.} = 0.2$;
$\overline{h} = 0.641$; $\overline{l} = 11.589$; $\overline{l}_{slots.} = 0.8$; $\lambda_{n.} = 2.1$; $L_{TO} = 3000$(m);
$f_{tr.} = 0.02$; $\tan(\Theta) = 0.024$;

Calculation results:

Table №1: Starting thrust-to-weight ratio,defined by take-off distance

λ_w	6	6,5	7	7,5	8	8,5	9	9,5	9,7	10
p, daN/m^2					$t_{0\,to}$					
100.0	0,1170	0,1286	0,1261	0,1239	0,1221	0,1204	0,1189	0,1176	0,1171	0,1164
150.0	0,1350	0,1471	0,1444	0,1422	0,1402	0,1385	0,1370	0,1356	0,1351	0,1344
200.0	0,1530	0,1654	0,1627	0,1603	0,1583	0,1565	0,1549	0,1535	0,1530	0,1523
250.0	0,1709	0,1836	0,1808	0,1784	0,1763	0,1745	0,1728	0,1714	0,1709	0,1701
300.0	0,1887	0,2019	0,1990	0,1965	0,1943	0,1924	0,1907	0,1892	0,1887	0,1879
350.0	0,2065	0,2201	0,2171	0,2145	0,2122	0,2103	0,2086	0,2070	0,2065	0,2057
400.0	0,2243	0,2383	0,2351	0,2325	0,2302	0,2282	0,2264	0,2249	0,2243	0,2235
450.0	0,2421	0,2564	0,2532	0,2505	0,2481	0,2461	0,2442	0,2426	0,2421	0,2412
500.0	0,2598	0,2746	0,2713	0,2684	0,2660	0,2639	0,2621	0,2604	0,2598	0,2590
	0,2776	0,2927	0,2893	0,2864	0,2839	0,2818	0,2799	0,2782	0,2776	0,2767

(a)

550.0										
600.0	0,2953	0,3108	0,3073	0,3043	0,3018	0,2996	0,2977	0,296	0,2953	0,2944
650.0	0,3131	0,3289	0,3253	0,3223	0,3197	0,3174	0,3154	0,3137	0,3131	0,3122
700.0	0,3308	0,347	0,3433	0,3402	0,3376	0,3352	0,3332	0,3315	0,3308	0,3299
750.0	0,3485	0,3651	0,3613	0,3581	0,3554	0,3531	0,351	0,3492	0,3485	0,3476
800.0	0,3663	0,3832	0,3793	0,3761	0,3733	0,3709	0,3688	0,3669	0,3663	0,3653

Table №2: Starting thrust-to-weight ratio,defined by take-off safety

λ_w	6	6,5	7	7,5	8	8,5	9	9,5	9,7	10
p, da	**N/m²**				$t_{0\,\Theta}$					
100.0	0,2009	0,2316	0,225	0,2193	0,2142	0,2098	0,2058	0,2023	0,2009	0,1991
150.0	0,2035	0,2348	0,228	0,2222	0,217	0,2125	0,2085	0,2048	0,2035	0,2016
200.0	0,2058	0,2377	0,2308	0,2249	0,2196	0,215	0,2109	0,2072	0,2058	0,2039
250.0	0,2081	0,2404	0,2334	0,2274	0,222	0,2174	0,2132	0,2095	0,2081	0,2061
300.0	0,2102	0,243	0,2359	0,2298	0,2244	0,2196	0,2154	0,2116	0,2102	0,2083
350.0	0,2123	0,2454	0,2383	0,2321	0,2266	0,2218	0,2176	0,2138	0,2123	0,2103
400.0	0,2144	0,2478	0,2406	0,2343	0,2288	0,224	0,2197	0,2158	0,2144	0,2124
450.0	0,2164	0,2502	0,2429	0,2365	0,231	0,2261	0,2217	0,2179	0,2164	0,2144
500.0	0,2184	0,2525	0,2451	0,2387	0,2331	0,2282	0,2238	0,2198	0,2184	0,2163
550.0	0,2204	0,2548	0,2473	0,2408	0,2352	0,2302	0,2258	0,2218	0,2204	0,2183
600.0	0,2223	0,257	0,2495	0,2429	0,2372	0,2322	0,2278	0,2238	0,2223	0,2202
650.0	0,2242	0,2592	0,2516	0,245	0,2393	0,2342	0,2297	0,2257	0,2242	0,2221
700.0	0,2261	0,2613	0,2537	0,2471	0,2413	0,2362	0,2317	0,2276	0,2261	0,224
750.0	0,228	0,2635	0,2558	0,2491	0,2433	0,2381	0,2336	0,2295	0,228	0,2259
800.0	0,2299	0,2656	0,2578	0,2511	0,2452	0,2401	0,2355	0,2314	0,2299	0,2277

Table №3: Starting thrust-to-weight ratio,defined by cruising speed

λ_w	6	6,5	7	7,5	8	8,5	9	9,5	9,7	10
p, da	**N/m²**				$t_{0\,cr.}$					
100.0	0,6293	0,6328	0,6361	0,6391	0,6419	0,6446	0,6471	0,6494	0,6503	0,6517
150.0	0,4708	0,4734	0,4758	0,478	0,4801	0,4821	0,4839	0,4856	0,4863	0,4872
200.0	0,3905	0,3926	0,3945	0,3963	0,398	0,3995	0,401	0,4024	0,4029	0,4037
250.0	0,3418	0,3436	0,3452	0,3467	0,3482	0,3495	0,3507	0,3519	0,3523	0,353
300.0	0,3091	0,3107	0,3121	0,3135	0,3147	0,3158	0,3169	0,3179	0,3183	0,3189
350.0	0,2857	0,2871	0,2883	0,2895	0,2906	0,2917	0,2926	0,2935	0,2939	0,2944
400.0	0,268	0,2692	0,2704	0,2715	0,2725	0,2734	0,2743	0,2751	0,2754	0,2759
450.0	0,2542	0,2553	0,2564	0,2574	0,2583	0,25920,26		0,2607	0,261	0,2614
500.0	0,2431	0,2442	0,2452	0,2461	0,2469	0,2477	0,2485	0,2492	0,2494	0,2498
550.0	0,234	0,235	0,2359	0,2368	0,2376	0,2383	0,239	0,2397	0,2399	0,2403
600.0	0,2264	0,2274	0,2282	0,229	0,2298	0,2305	0,2312	0,2318	0,232	0,2323
650.0	0,22	0,2209	0,2217	0,2225	0,2232	0,2238	0,2245	0,225	0,2253	0,2256
700.0	0,2145	0,2153	0,2161	0,2168	0,2175	0,2181	0,2187	0,2193	0,2195	0,2198
750.0	0,2097	0,2105	0,2112	0,2119	0,2126	0,2132	0,2137	0,2142	0,2144	0,2147
800.0	0,2055	0,2063	0,207	0,2076	0,2082	0,2088	0,2093	0,2098	0,21	0,2103

Result Diagrams:

Diagram width 600 Diagram height 400

(b)

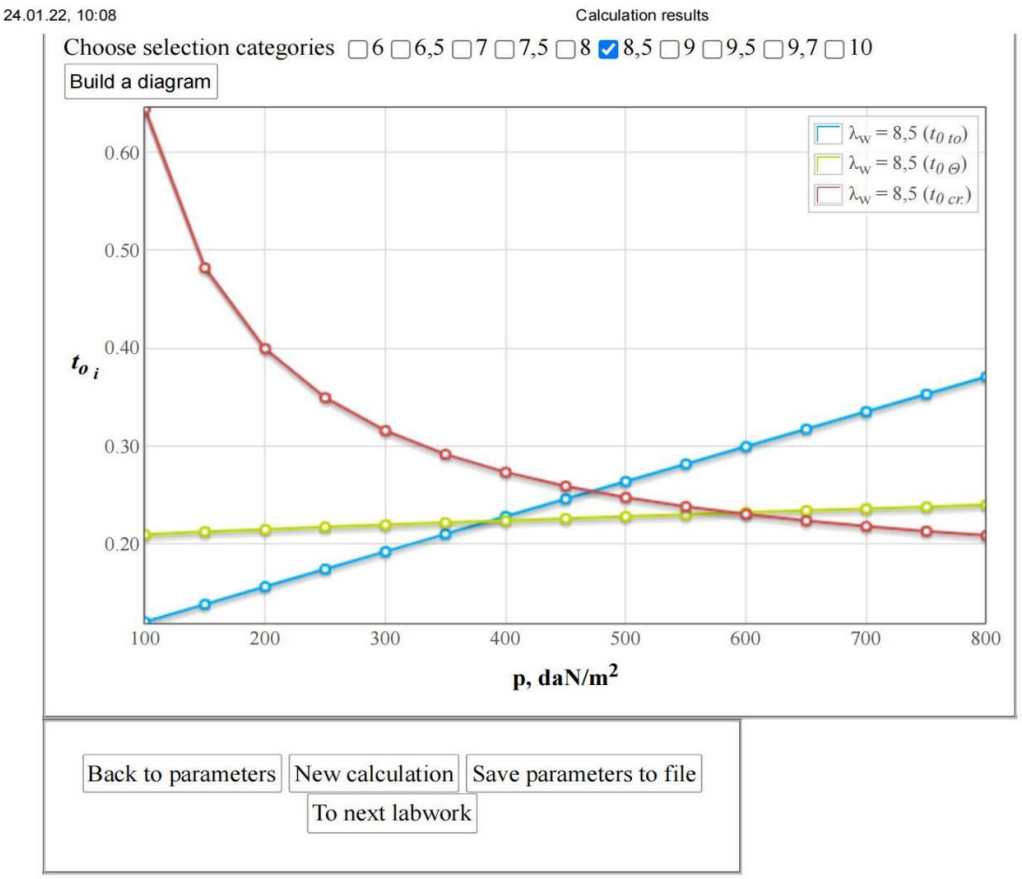

(c)

Figure 1.8 – The initial data and the results

1.2.3. Analysis of aircraft geometrical parameters influence to relative mass of power plant

The relative mass of the power plant determined by the formula (1.39):

$$\bar{m}_{p.pl} = R\gamma_{eng}t_{max} \quad (1.39)$$

Where R - coefficient taking into account the increase in the mass of the power plant compared to the weight of the engine;

γ_{eng} - specific weight of the engine;

t_{max} - the highest starting value thrust-to-weight ratio.

The initial data and results are shown in the Figure1.9 (a), (b), (c).

The figures show that the most favorable values of the specific load on the wing are within 400-600 daN/m^2, beyond which both the specific weight of power plant and the maximum required thrust-to weight ratio increase.

Training Centre
CAD/CAM/CAE

Choose language ↓
Greetings **Guest**
Registration
Sign In

Airplane parameters influence on power unit relative mass value study

Calculation results

НАУ им.Жуковского ("ХАИ")
Кафедра №103
Факультет самолёто-вертолёто строения
Главная
Расчет характеристик ЛА
Airplane Take-off Mass

Short list | Detailed list

Initial data:

Airplane type = Passenger $n_{pass.} = 450$(itm.); $m_{pass.} = 120$(kg);

Engine type = Turbo-fan/jet;
$\xi_{int.} = 0.98$; $\xi_{tr.cr.} = 0.7$; $\xi_{tr.TO.} = 0.95$; $y = 8$; $M_{cr.} = 0.8$;
$H_{init.} = 10$(km); $H_{fin.} = 13$(km); $k_1 = 0.26$; $n_{rev.eng} = 2$(itm.);
$n_{eng.} = 2$(itm.); $\gamma_{en.} = 0.3$(daN/kWt);

Wing high-lift devices type = Slat and double sloted retractable flap
$\Delta\overline{C}_{y\ l.dev} = 2.2$; $\bar{l}_{sl.} = 0.8$; $k_{sl.} = 0.15$; $\bar{l}_{fl.} = 0.6$; $\bar{b}_{fl.} = 0.3$;
$\delta_{fl.TO} = 25$(deg.); $k_{fl.} = 0.25$;

$\overline{C} = 12$(%); $\lambda_w = 9.7$; $\eta = 5.846$; $\chi_{le} = 31.64$(deg.);
$\alpha_{TO} = 10$(deg.); $M_{TO} = 0.2$; $d_{fus.} = 6.2$(m); $\lambda_{fus.} = 12$;
$k_{mid.} = 4000$(daN/m^2); $k_{int.w} = 0.65$; $k_{stab.} = 1.35$; $k_{pl.} = 0.2$;
$\bar{h} = 0.641$; $\bar{l} = 11.589$; $\bar{l}_{slots.} = 0.8$; $\lambda_{n.} = 2.1$; $L_{TO} = 3000$(m);
$f_{tr.} = 0.02$; $\tan(\Theta) = 0.024$;

Calculation results:

Table №1: Starting thrust-to-weight ratio (maximum) depending from specific wing load

λ_w	6	6,5	7	7,5	8	8,5	9	9,5	9,7	10
p, daN/m^2					$t_{0\ max}$					
100.0	0,637	0,64	0,643	0,646	0,649	0,651	0,653	0,656	0,656	0,658
150.0	0,477	0,479	0,482	0,484	0,486	0,487	0,489	0,491	0,491	0,492
200.0	0,396	0,398	0,4	0,401	0,403	0,404	0,406	0,407	0,407	0,408
250.0	0,347	0,348	0,35	0,351	0,353	0,354	0,355	0,356	0,356	0,357
300.0	0,314	0,315	0,316	0,318	0,319	0,32	0,321	0,322	0,322	0,323
350.0	0,29	0,291	0,292	0,293	0,294	0,295	0,296	0,297	0,297	0,298
400.0	0,272	0,273	0,274	0,275	0,276	0,277	0,278	0,278	0,279	0,279
450.0	0,258	0,259	0,26	0,261	0,262	0,262	0,263	0,264	0,264	0,265
500.0	0,26	0,275	0,271	0,269	0,266	0,264	0,262	0,261	0,26	0,259
550.0	0,278	0,293	0,289	0,287	0,284	0,282	0,28	0,278	0,278	0,277

(a)

600.0	0,295	0,311	0,307	0,304	0,302	0,3	0,298	0,296	0,295	0,295
650.0	0,313	0,329	0,325	0,322	0,32	0,318	0,316	0,314	0,313	0,312
700.0	0,331	0,347	0,343	0,34	0,338	0,335	0,333	0,332	0,331	0,33
750.0	0,349	0,365	0,361	0,358	0,356	0,353	0,351	0,349	0,349	0,348
800.0	0,366	0,383	0,379	0,376	0,373	0,371	0,369	0,367	0,366	0,365

Table №2: Power unit relative mass from specific wing load dependency

λ_w	6	6,5	7	7,5	8	8,5	9	9,5	9,7	10
p, daN/m^2					$\overline{m}_{0\ pu}$					
100.0	0,089	0,089	0,089	0,09	0,09	0,091	0,091	0,091	0,091	0,091
150.0	0,066	0,067	0,067	0,067	0,068	0,068	0,068	0,068	0,068	0,068
200.0	0,055	0,055	0,056	0,056	0,056	0,056	0,056	0,057	0,057	0,057
250.0	0,048	0,048	0,049	0,049	0,049	0,049	0,049	0,049	0,05	0,05
300.0	0,044	0,044	0,044	0,044	0,044	0,044	0,045	0,045	0,045	0,045
350.0	0,04	0,04	0,041	0,041	0,041	0,041	0,041	0,041	0,041	0,041
400.0	0,038	0,038	0,038	0,038	0,038	0,038	0,039	0,039	0,039	0,039
450.0	0,036	0,036	0,036	0,036	0,036	0,036	0,037	0,037	0,037	0,037
500.0	0,036	0,038	0,038	0,037	0,037	0,037	0,036	0,036	0,036	0,036
550.0	0,039	0,041	0,04	0,04	0,039	0,039	0,039	0,039	0,039	0,038
600.0	0,041	0,043	0,043	0,042	0,042	0,042	0,041	0,041	0,041	0,041
650.0	0,044	0,046	0,045	0,045	0,044	0,044	0,044	0,044	0,044	0,043
700.0	0,046	0,048	0,048	0,047	0,047	0,047	0,046	0,046	0,046	0,046
750.0	0,048	0,051	0,05	0,05	0,049	0,049	0,049	0,049	0,048	0,048
800.0	0,051	0,053	0,053	0,052	0,052	0,052	0,051	0,051	0,051	0,051

Result Diagrams:

Diagram width 600 Diagram height 400

Choose a table Table №1

Choose selection categories: ☐ 6 ☐ 6,5 ☐ 7 ☐ 7,5 ☑ 8 ☐ 8,5 ☑ 9 ☐ 9,5 ☐ 9,7 ☑ 10

Build a diagram

(b)

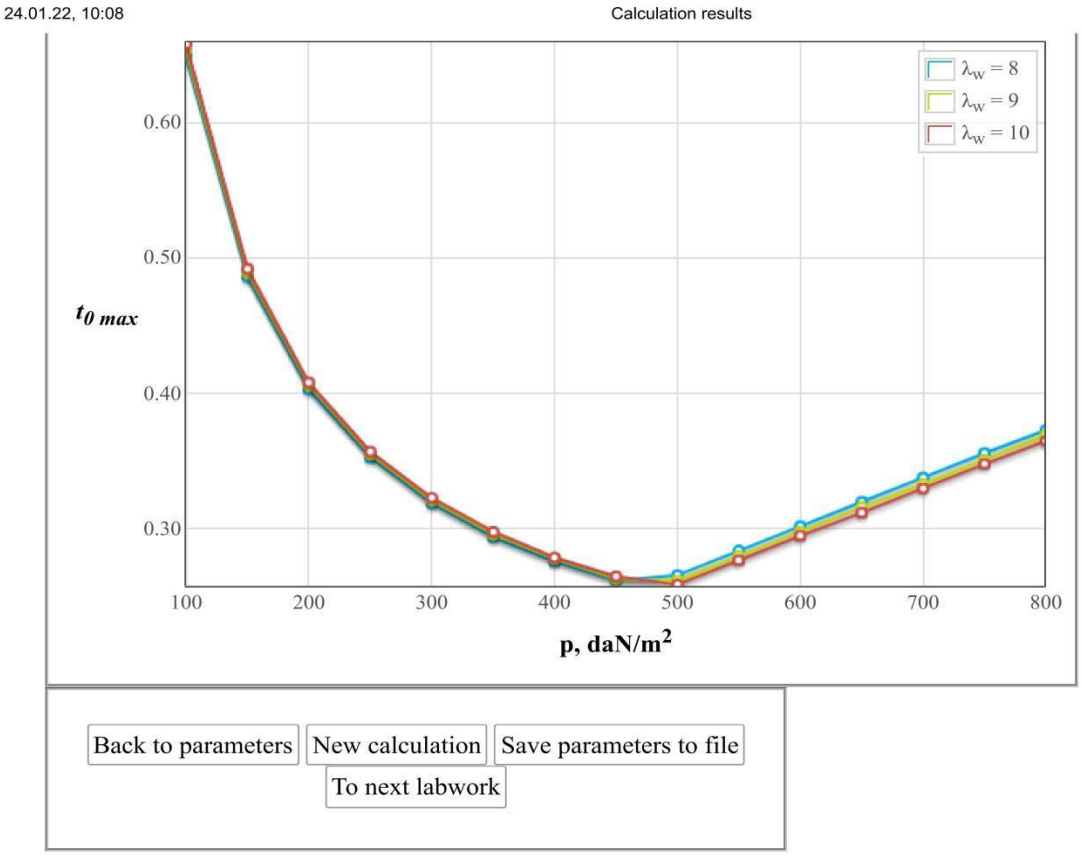

(c)

Figure 1.9 – The initial data and the results

1.2.4. Analysis of Aircraft Geometrical Parameters influence to relative mass of Fuel

The initial data and results are shown in the Figure1.10 (a), (b).

Relative mass of the fuel increases with the increase in the specific load on the wing. As the wing aspect ratio increases, the relative weight of the fuel decreases.

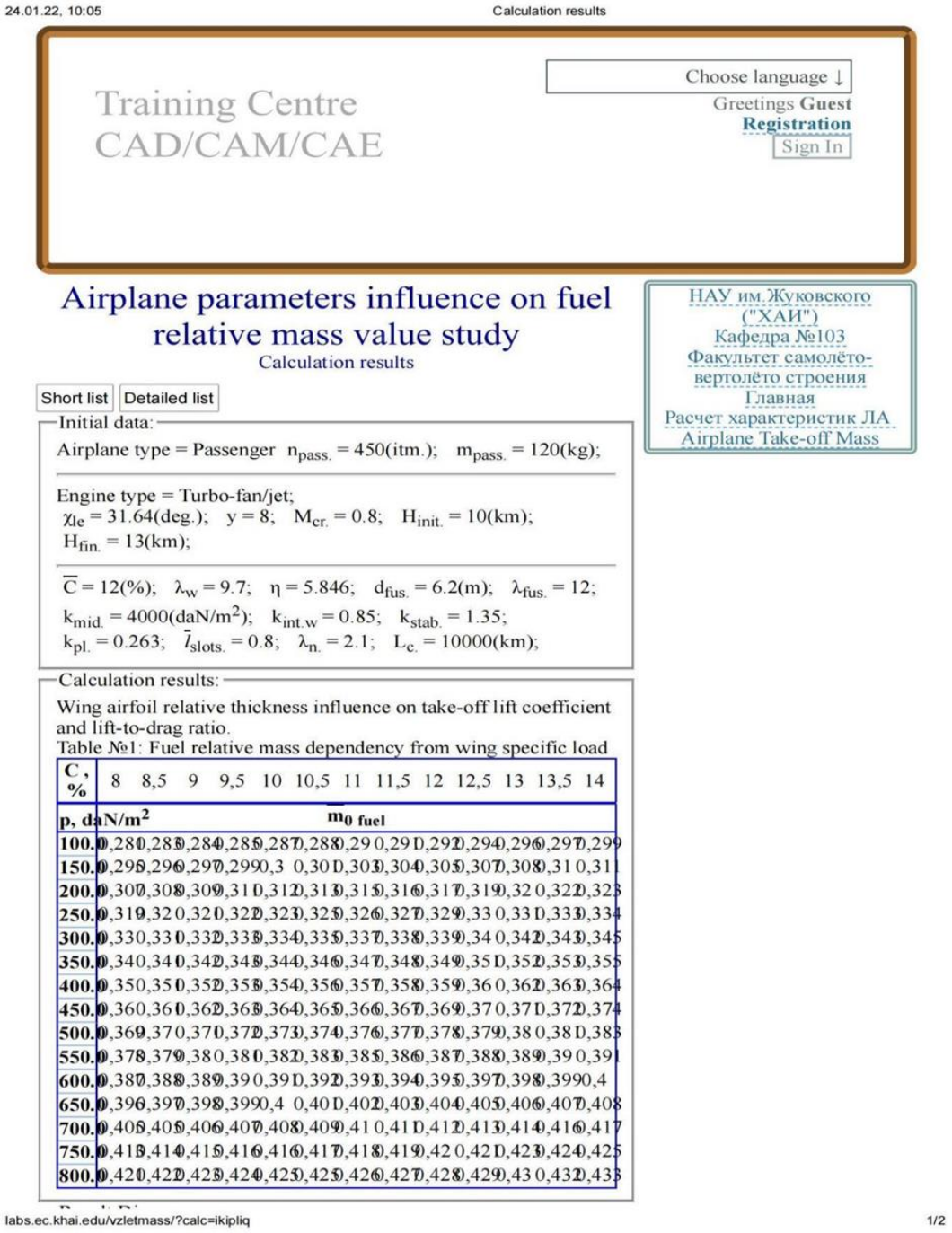

24.01.22, 10:05 Calculation results

Training Centre CAD/CAM/CAE

Choose language ↓
Greetings **Guest**
Registration
Sign In

НАУ им.Жуковского ("ХАИ")
Кафедра №103
Факультет самолёто-вертолёто строения
Главная
Расчет характеристик ЛА
Airplane Take-off Mass

Airplane parameters influence on fuel relative mass value study

Calculation results

Short list | Detailed list

Initial data:

Airplane type = Passenger $n_{pass.} = 450$(itm.); $m_{pass.} = 120$(kg);

Engine type = Turbo-fan/jet;
$\chi_{le} = 31.64$(deg.); $y = 8$; $M_{cr.} = 0.8$; $H_{init.} = 10$(km);
$H_{fin.} = 13$(km);

$\overline{C} = 12$(%); $\lambda_w = 9.7$; $\eta = 5.846$; $d_{fus.} = 6.2$(m); $\lambda_{fus.} = 12$;
$k_{mid.} = 4000$(daN/m^2); $k_{int.w} = 0.85$; $k_{stab.} = 1.35$;
$k_{pl.} = 0.263$; $\bar{l}_{slots.} = 0.8$; $\lambda_{n.} = 2.1$; $L_{c.} = 10000$(km);

Calculation results:

Wing airfoil relative thickness influence on take-off lift coefficient and lift-to-drag ratio.
Table №1: Fuel relative mass dependency from wing specific load

C, %	8	8,5	9	9,5	10	10,5	11	11,5	12	12,5	13	13,5	14
p, daN/m^2	$\overline{m}_{0\ fuel}$												
100.0	0,280	0,285	0,284	0,285	0,287	0,288	0,290	0,291	0,292	0,294	0,296	0,297	0,299
150.0	0,296	0,296	0,297	0,299	0,3	0,301	0,303	0,304	0,305	0,307	0,308	0,310	0,311
200.0	0,307	0,308	0,309	0,311	0,312	0,313	0,315	0,316	0,317	0,319	0,320	0,322	0,323
250.0	0,319	0,320	0,321	0,322	0,323	0,325	0,326	0,327	0,329	0,330	0,331	0,333	0,334
300.0	0,330	0,331	0,332	0,333	0,334	0,335	0,337	0,338	0,339	0,340	0,342	0,343	0,345
350.0	0,340	0,341	0,342	0,343	0,344	0,346	0,347	0,348	0,349	0,351	0,352	0,353	0,355
400.0	0,350	0,351	0,352	0,353	0,354	0,356	0,357	0,358	0,359	0,360	0,362	0,363	0,364
450.0	0,360	0,361	0,362	0,363	0,364	0,365	0,366	0,367	0,369	0,370	0,371	0,372	0,374
500.0	0,369	0,370	0,371	0,372	0,373	0,374	0,376	0,377	0,378	0,379	0,380	0,381	0,383
550.0	0,378	0,379	0,380	0,381	0,382	0,383	0,385	0,386	0,387	0,388	0,389	0,390	0,391
600.0	0,387	0,388	0,389	0,390	0,391	0,392	0,393	0,394	0,395	0,397	0,398	0,399	0,4
650.0	0,396	0,397	0,398	0,399	0,4	0,401	0,402	0,403	0,404	0,405	0,406	0,407	0,408
700.0	0,405	0,405	0,406	0,407	0,408	0,409	0,410	0,411	0,412	0,413	0,414	0,416	0,417
750.0	0,415	0,414	0,415	0,416	0,416	0,417	0,418	0,419	0,420	0,421	0,423	0,424	0,425
800.0	0,420	0,422	0,423	0,424	0,425	0,425	0,426	0,427	0,428	0,429	0,430	0,432	0,433

labs.ec.khai.edu/vzletmass/?calc=ikipliq 1/2

(a)

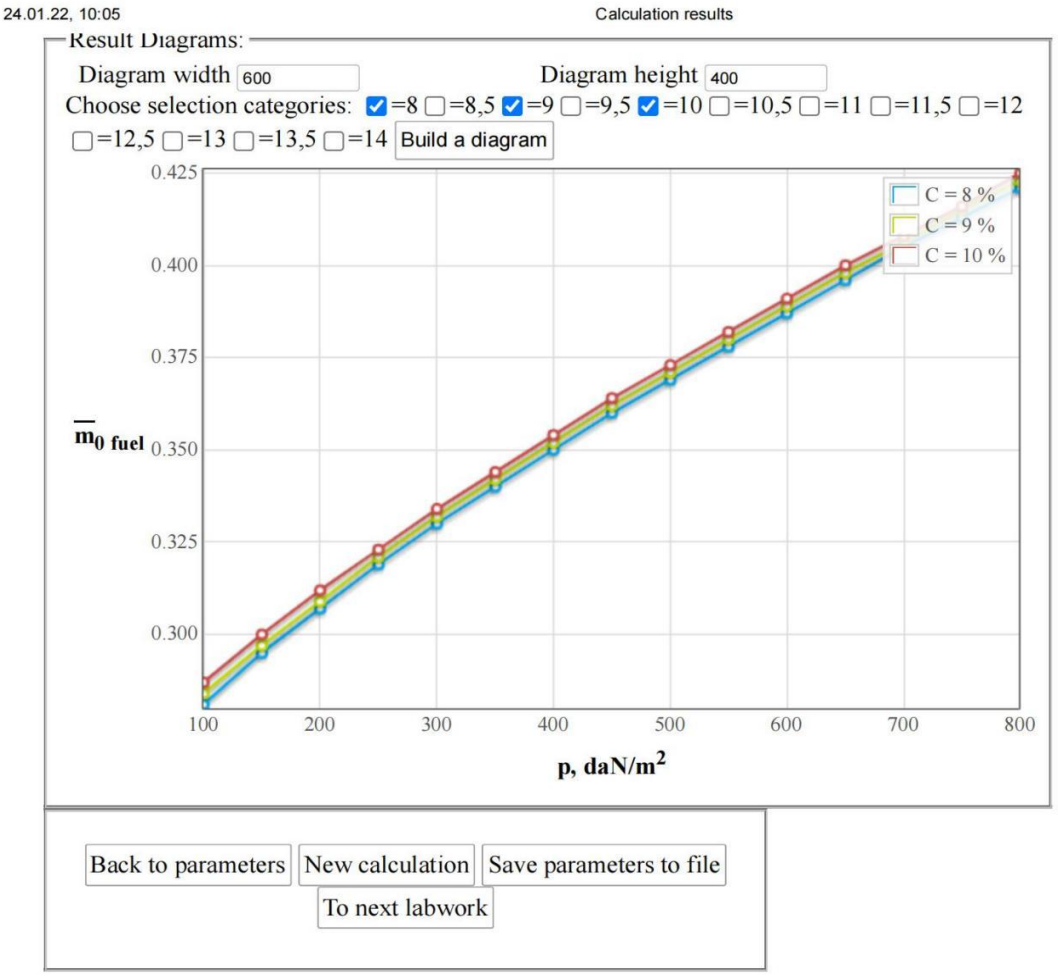

(b)

Figure 1.10 – The initial data and the results

1.2.5. Analysis of Aircraft Geometrical Parameters Influence to relative mass of Structures

The initial data and results are shown in the Figure1.11 (a), (b), (c).

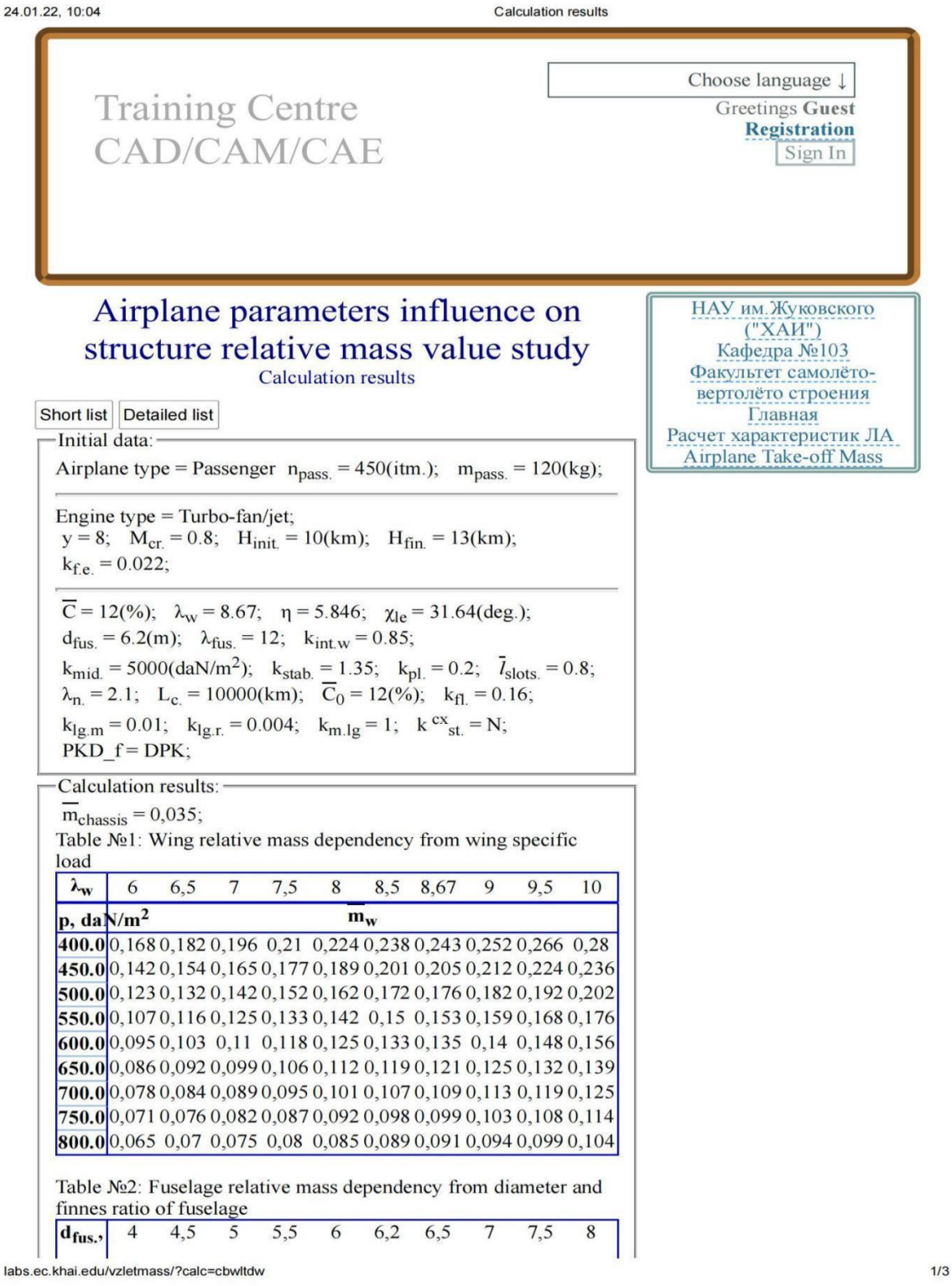

24.01.22, 10:04 Calculation results

Training Centre CAD/CAM/CAE

Choose language ↓
Greetings **Guest**
Registration
Sign In

НАУ им.Жуковского ("ХАИ")
Кафедра №103
Факультет самолёто-вертолёто строения
Главная
Расчет характеристик ЛА
Airplane Take-off Mass

Airplane parameters influence on structure relative mass value study

Calculation results

Short list | Detailed list

Initial data:

Airplane type = Passenger $n_{pass.} = 450$(itm.); $m_{pass.} = 120$(kg);

Engine type = Turbo-fan/jet;
$y = 8$; $M_{cr.} = 0.8$; $H_{init.} = 10$(km); $H_{fin.} = 13$(km);
$k_{f.e.} = 0.022$;

$\overline{C} = 12$(%); $\lambda_w = 8.67$; $\eta = 5.846$; $\chi_{le} = 31.64$(deg.);
$d_{fus.} = 6.2$(m); $\lambda_{fus.} = 12$; $k_{int.w} = 0.85$;
$k_{mid.} = 5000$(daN/m^2); $k_{stab.} = 1.35$; $k_{pl.} = 0.2$; $\overline{l}_{slots.} = 0.8$;
$\lambda_{n.} = 2.1$; $L_{c.} = 10000$(km); $\overline{C}_0 = 12$(%); $k_{fl.} = 0.16$;
$k_{lg.m} = 0.01$; $k_{lg.r.} = 0.004$; $k_{m.lg} = 1$; $k^{cx}_{st.} = N$;
PKD_f = DPK;

Calculation results:

$\overline{m}_{chassis} = 0,035$;

Table №1: Wing relative mass dependency from wing specific load

λ_w	6	6,5	7	7,5	8	8,5	8,67	9	9,5	10
p, daN/m^2	$\overline{m}_w$									
400.0	0,168	0,182	0,196	0,21	0,224	0,238	0,243	0,252	0,266	0,28
450.0	0,142	0,154	0,165	0,177	0,189	0,201	0,205	0,212	0,224	0,236
500.0	0,123	0,132	0,142	0,152	0,162	0,172	0,176	0,182	0,192	0,202
550.0	0,107	0,116	0,125	0,133	0,142	0,15	0,153	0,159	0,168	0,176
600.0	0,095	0,103	0,11	0,118	0,125	0,133	0,135	0,14	0,148	0,156
650.0	0,086	0,092	0,099	0,106	0,112	0,119	0,121	0,125	0,132	0,139
700.0	0,078	0,084	0,089	0,095	0,101	0,107	0,109	0,113	0,119	0,125
750.0	0,071	0,076	0,082	0,087	0,092	0,098	0,099	0,103	0,108	0,114
800.0	0,065	0,07	0,075	0,08	0,085	0,089	0,091	0,094	0,099	0,104

Table №2: Fuselage relative mass dependency from diameter and finnes ratio of fuselage

$d_{fus.}$,	4	4,5	5	5,5	6	6,2	6,5	7	7,5	8

labs.ec.khai.edu/vzletmass/?calc=cbwltdw 1/3

(a)

m										
$\lambda_{fus.}$	$\overline{m}_{fus.}$									
8.0	0,05	0,059	0,069	0,079	0,091	0,095	0,103	0,115	0,127	0,138
8.5	0,052	0,061	0,072	0,083	0,095	0,1	0,108	0,121	0,133	0,145
9.0	0,054	0,064	0,075	0,087	0,1	0,105	0,113	0,127	0,14	0,153
9.5	0,056	0,067	0,078	0,091	0,105	0,11	0,119	0,133	0,147	0,16
10.0	0,058	0,069	0,082	0,095	0,109	0,115	0,124	0,139	0,154	0,168
10.5	0,06	0,072	0,085	0,099	0,114	0,12	0,129	0,145	0,161	0,176
11.0	0,062	0,074	0,088	0,103	0,118	0,125	0,135	0,151	0,168	0,183
11.5	0,064	0,077	0,091	0,107	0,123	0,13	0,14	0,157	0,175	0,191
12.0	0,066	0,08	0,094	0,111	0,128	0,135	0,145	0,164	0,181	0,198
12.5	0,068	0,082	0,098	0,114	0,132	0,14	0,151	0,17	0,188	0,206
13.0	0,07	0,085	0,101	0,118	0,137	0,145	0,156	0,176	0,195	0,213
13.5	0,072	0,087	0,104	0,122	0,142	0,149	0,162	0,182	0,202	0,221
14.0	0,074	0,09	0,107	0,126	0,146	0,154	0,167	0,188	0,209	0,228
14.5	0,076	0,093	0,111	0,13	0,151	0,159	0,172	0,194	0,216	0,236
15.0	0,078	0,095	0,114	0,134	0,155	0,164	0,178	0,2	0,222	0,244
15.5	0,08	0,098	0,117	0,138	0,16	0,169	0,183	0,206	0,229	0,251
16.0	0,083	0,1	0,12	0,142	0,165	0,174	0,188	0,212	0,236	0,259

Table №3: Stabilisers relative mass dependency from wing specific load

p, daN/m²	400	450	500	550	600	650	700	750	800
$\overline{m}_{st.}$	0,0189	0,0174	0,0135	0,0125	0,0116	0,0108	0,0101	0,0095	0,0089

Table №4: Airplane structure relative mass dependency from wing specific load

λ_w	6	6,5	7	7,5	8	8,5	8,67	9	9,5	10
p, daN/m²	$\overline{m}_{stuct.}$									
400.0	0,356	0,37	0,384	0,398	0,412	0,426	0,431	0,441	0,455	0,469
450.0	0,329	0,341	0,352	0,364	0,376	0,388	0,392	0,399	0,411	0,423
500.0	0,306	0,315	0,325	0,335	0,345	0,355	0,359	0,365	0,375	0,385
550.0	0,29	0,298	0,307	0,315	0,324	0,332	0,335	0,341	0,35	0,358
600.0	0,277	0,284	0,292	0,299	0,307	0,314	0,317	0,322	0,329	0,337
650.0	0,266	0,273	0,279	0,286	0,293	0,299	0,302	0,306	0,313	0,319
700.0	0,257	0,263	0,269	0,275	0,281	0,287	0,289	0,293	0,299	0,305
750.0	0,25	0,255	0,261	0,266	0,271	0,277	0,278	0,282	0,287	0,293
800.0	0,244	0,249	0,254	0,258	0,263	0,268	0,27	0,273	0,278	0,282

Result Diagrams:

Diagram width 600 Diagram height 400

Choose a table Table №4

☐ λ_w=6 ☐ λ_w=6,5 ☐ λ_w=7 ☐ λ_w=7,5 ☐ λ_w=8 ☑ λ_w=8,5 ☐ λ_w=8,67 ☑ λ_w=9 ☐ λ_w=9,5 ☑ λ_w=10

Build a diagram

(b)

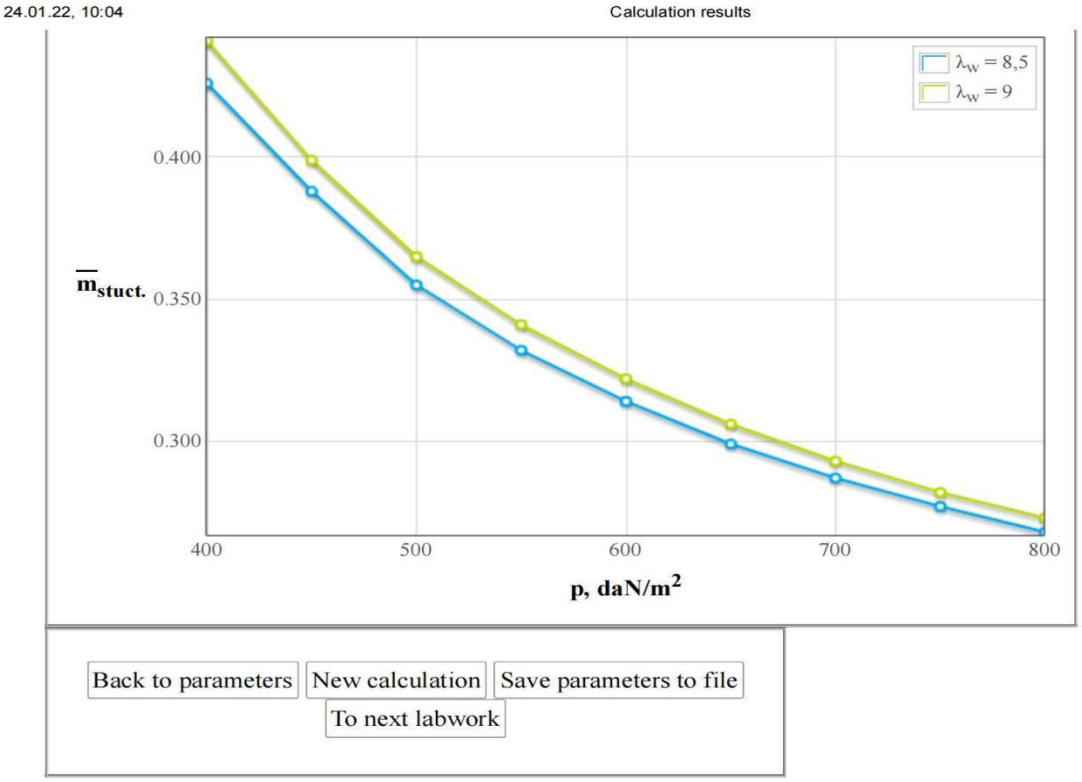

(c)

Figure 1.11 – The initial data and the results

With an increase in the specific load on the wing, the relative wing weight decreases. With an increase in aspect ratio, the relative mass of the wing increases.

1.2.6. Calculation of mass of equipment, control system and operational items

In this lab we need to determine the mass of the equipment, control system, operational item and crew members.

The initial data and results are shown in the Figure1.12.

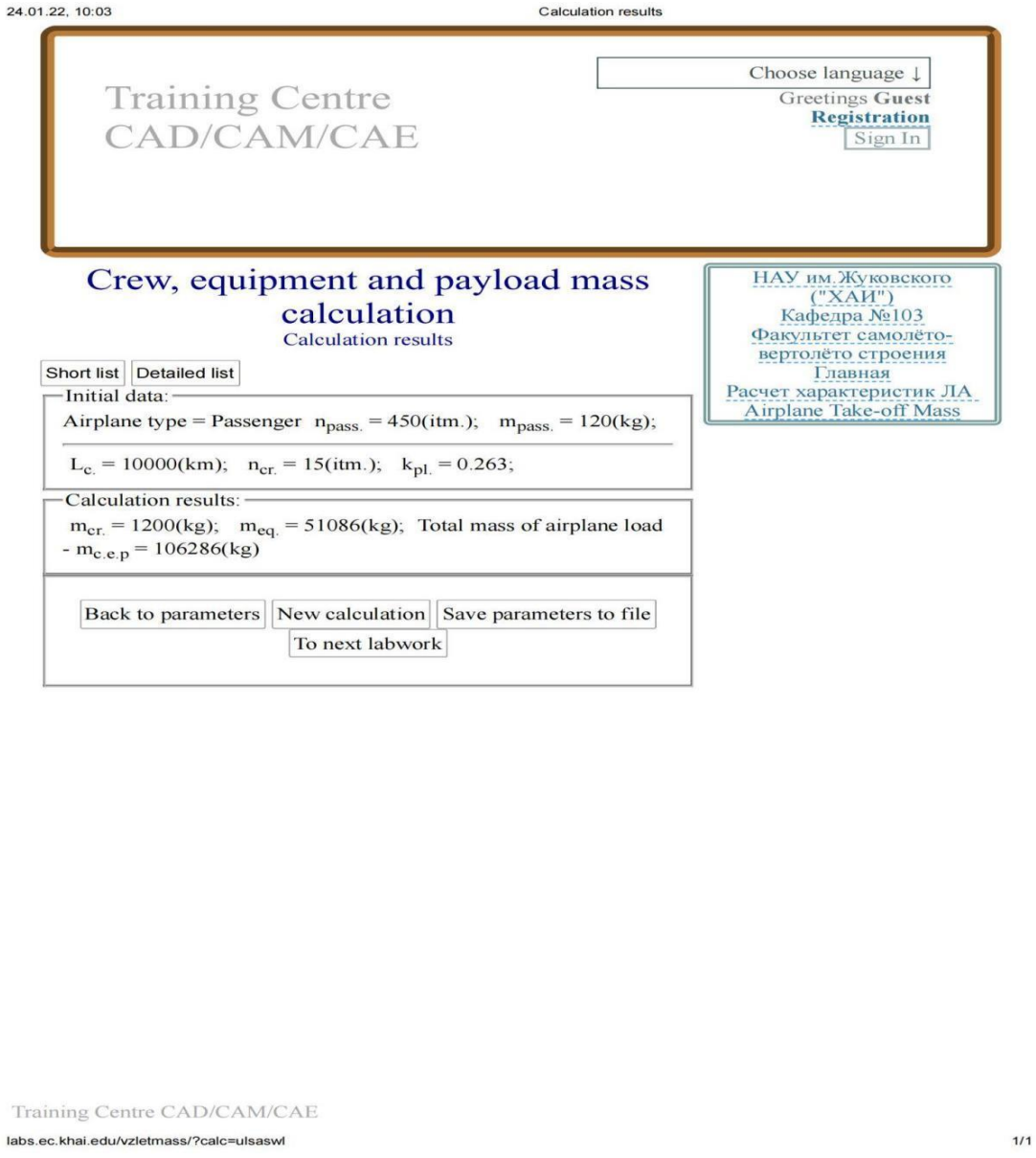

Figure 1.12 – The initial data and the results

1.2.7. Analysis of the total aircraft mass with respect to wing loading and Wing respect ratio

The initial data and results are shown in the Figure1.13 (a), (b).

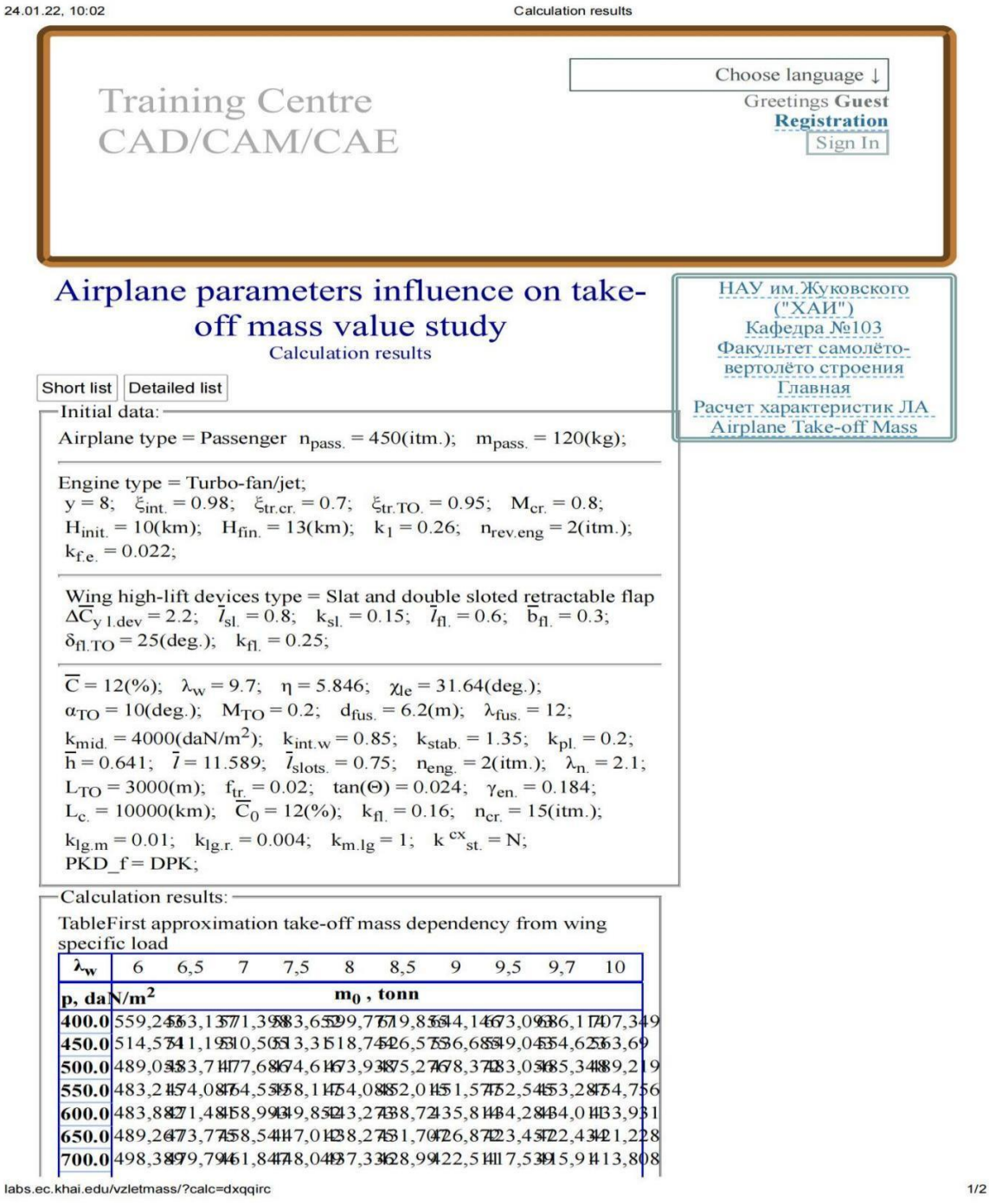

24.01.22, 10:02 Calculation results

Training Centre CAD/CAM/CAE

Choose language ↓
Greetings **Guest**
Registration
Sign In

НАУ им.Жуковского ("ХАИ")
Кафедра №103
Факультет самолёто-вертолёто строения
Главная
Расчет характеристик ЛА
Airplane Take-off Mass

Airplane parameters influence on take-off mass value study

Calculation results

Short list | Detailed list

Initial data:

Airplane type = Passenger $n_{pass.} = 450$(itm.); $m_{pass.} = 120$(kg);

Engine type = Turbo-fan/jet;
$y = 8$; $\xi_{int.} = 0.98$; $\xi_{tr.cr.} = 0.7$; $\xi_{tr.TO.} = 0.95$; $M_{cr.} = 0.8$;
$H_{init.} = 10$(km); $H_{fin.} = 13$(km); $k_1 = 0.26$; $n_{rev.eng} = 2$(itm.);
$k_{f.e.} = 0.022$;

Wing high-lift devices type = Slat and double sloted retractable flap
$\Delta\overline{C}_{y\ l.dev} = 2.2$; $\overline{l}_{sl.} = 0.8$; $k_{sl.} = 0.15$; $\overline{l}_{fl.} = 0.6$; $\overline{b}_{fl.} = 0.3$;
$\delta_{fl.TO} = 25$(deg.); $k_{fl.} = 0.25$;

$\overline{C} = 12$(%); $\lambda_w = 9.7$; $\eta = 5.846$; $\chi_{le} = 31.64$(deg.);
$\alpha_{TO} = 10$(deg.); $M_{TO} = 0.2$; $d_{fus.} = 6.2$(m); $\lambda_{fus.} = 12$;
$k_{mid.} = 4000$(daN/m^2); $k_{int.w} = 0.85$; $k_{stab.} = 1.35$; $k_{pl.} = 0.2$;
$\overline{h} = 0.641$; $\overline{l} = 11.589$; $\overline{l}_{slots.} = 0.75$; $n_{eng.} = 2$(itm.); $\lambda_{n.} = 2.1$;
$L_{TO} = 3000$(m); $f_{tr.} = 0.02$; $\tan(\Theta) = 0.024$; $\gamma_{en.} = 0.184$;
$L_{c.} = 10000$(km); $\overline{C}_0 = 12$(%); $k_{fl.} = 0.16$; $n_{cr.} = 15$(itm.);
$k_{lg.m} = 0.01$; $k_{lg.r.} = 0.004$; $k_{m.lg} = 1$; $k^{cx}_{st.} = N$;
PKD_f = DPK;

Calculation results:

TableFirst approximation take-off mass dependency from wing specific load

λ_w	6	6,5	7	7,5	8	8,5	9	9,5	9,7	10
p, daN/m^2	m_0 , tonn									
400.0	559,24	563,13	571,39	583,65	599,77	619,85	644,14	673,09	686,11	707,34
450.0	514,57	541,19	550,50	563,31	579,74	600,26	625,57	656,68	669,04	689,63
500.0	489,05	513,71	527,68	546,74	571,46	602,93	640,75	685,27	702,78	729,37
550.0	483,21	504,08	524,55	548,11	577,54	614,08	658,52	710,04	730,15	760,57
600.0	483,88	502,71	524,15	548,99	579,85	624,32	676,38	735,81	758,42	791,93
650.0	489,26	503,77	524,58	549,11	581,02	628,27	681,70	742,68	765,23	799,34
700.0	498,38	509,79	529,46	551,84	584,78	630,04	683,73	744,62	767,22	801,51

labs.ec.khai.edu/vzletmass/?calc=dxqqirc 1/2

(a)

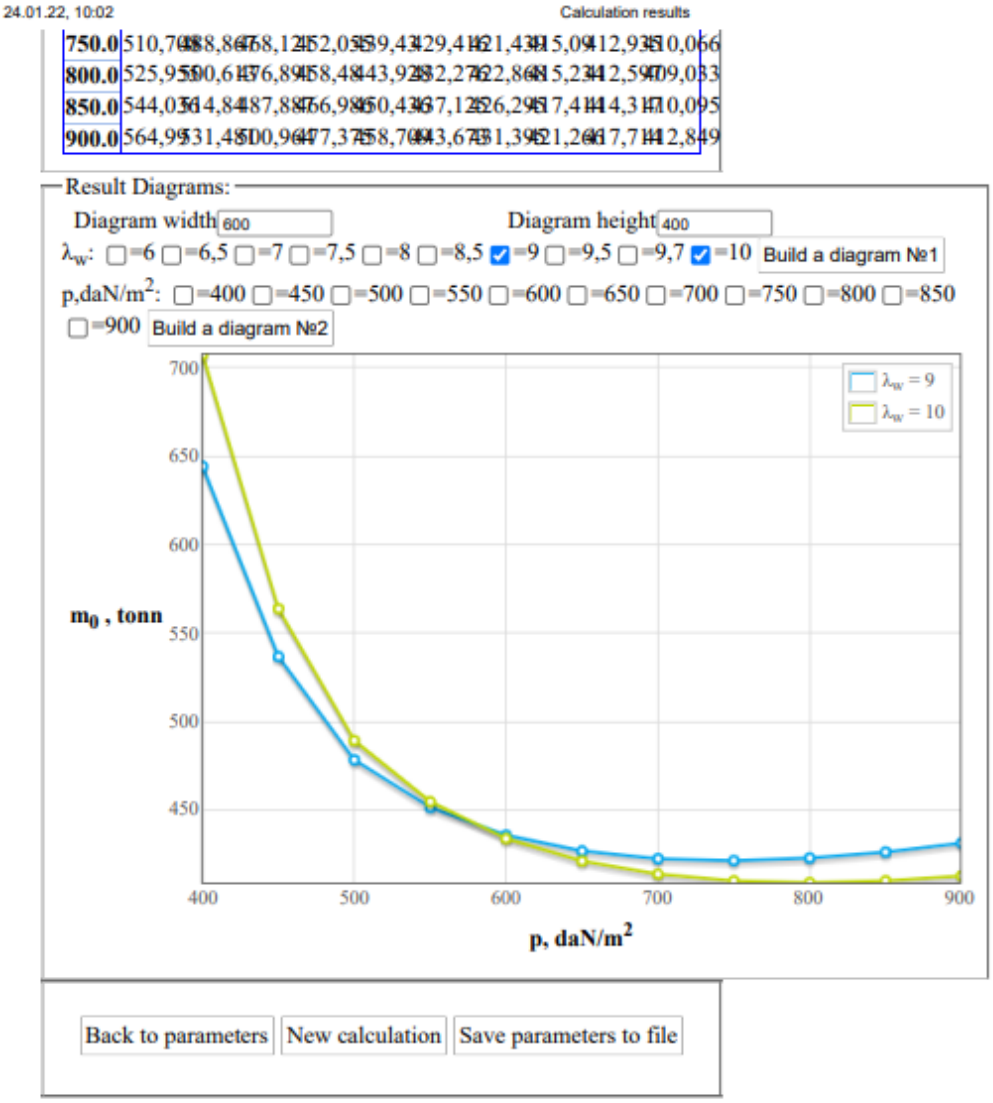

(b)

Figure 1.13 – The initial data and the results

2. ECONOMIC SECTION

2.1. Calculation of aircraft and engine operation cost and transportation cost of one cargo ton per kilometer

The operating costs of this type of aircraft per 1:00 flight (flight hour) consist of direct and indirect (airport) expenses (formula (2.1)):

$$C_{OP} = A + B \quad (2.1)$$

Where A - direct costs per flight hour, dollars;

B - indirect costs per flight hour, dollars.

Direct costs include expenses for depreciation and overhaul and maintenance of an airplane (glider) and engines for fuel and flight personnel wages with accruals.

Indirect costs include depreciation, maintenance and maintenance of all aerodrome and airport facilities (bus stations, hotels, taxiways, parking lots, weather services, hangars, warehouses, roads, utilities, garages, etc.), excluding expenses for repair factories and linear workshops, as well as salary expenses for the payroll of GA units.

The total cost of operating the aircraft for the transport of passengers or commercial cargo per kilometer (CTKM) is determined by (formula (2.2)):

$$C_{TKM} = \frac{A+B}{m_{ld} \cdot k \cdot V_c} \quad (2.2)$$

Where m_{ld} = 54000kg, is the maximum payload of the aircraft;

Vc= 880 km / h - airspeed;

K = 0.65 - utilization factor of the aircraft load.

The size of the speed of the aircraft is determined on the basis of its cruising speed.

Flight (technical) speed is the average speed of a non-stop flight in calm, calculated taking into account the time spent at all stages of the flight from the start of acceleration at the landing airport. calculated speed by (formula (2.3)):

$$V_c = \frac{L \times V_{cr}}{L + (V_{cr} \times \Delta t)} \quad (2.3)$$

where Vcr = 880 km / h - cruising speed of the aircraft;

L = 10000 km - non-stop flight range;

t = 0.25 - loss of time for evolution or maneuvering in the airport area after take-off and before landing, as well as climb and decrease, which corresponds to a speed equal to cruising (in hours).

The magnitude of these losses depends on the altitude of the aircraft.

$$V_c = \frac{10000 \cdot 880}{10000 + (880 \times 0{,}25)} = 861\ km/h$$

Direct expenses per one hour of flight, consist of the following expenses (formula (2.4)):

$$A = \sum_{i=1}^{7} A_i \quad (2.4)$$

where A_1 is the cost of depreciation and overhaul of the aircraft (glider)

A_2 - expenses for depreciation and overhaul of engines;

A_3 - maintenance and current repair costs for the airframe;

A_4 - maintenance and current repair costs of power plants;

A_5 - salary of flight personnel with accruals;

A_6 - fuel cost;

A_7 - other direct costs.

All A_i, we take per one flight hour.

The cost of depreciation and overhaul for one hour of aircraft operation, we define

by (formula (2.5)):

$$A_1 = K_1 \times P_C \times \frac{1 + K_{RA} \times \left(\frac{T_C}{t_C} - 1\right)}{T_C} \tag{2.5}$$

where K_1 = 1.065 - coefficient taking into account non-productive raid (instruction, training, flight test, etc.).

P_C- price of an airplane without engines, dollars (formula (2.6)):

$$P_C = 0{,}015 \cdot K_{HBO} \cdot K_{CEP} \cdot K_V \cdot m_{ep} \cdot \left(3340 + 0{,}077 \cdot m_{ep} - 1{,}05 \cdot 10^{-5} \cdot m_{ep}^{1,5}\right) \tag{2.6}$$

Where K_{HBO} = 1.61;

$m_{ep} = m_{af} - \left(m_1 + m_{pp}\right)$ - mass of an empty plane;

m_{af} = 60000 kg - mass of the airframe;

m_1 = 1200 kg - weight of the service load of the aircraft taking into account the weight of the crew;

m_{pp} = 19200 kg - mass of power plants;

So $m_{ep} = m_{af} - \left(m_1 + m_{pp}\right)$ = 60000 – (1200 + 19200) = 39600 kg.

Coefficient taking into account the seriality of the designed aircraft (formula (2.7)):

$$K_{cep} = \left(\frac{35 \cdot 10^5}{m_{ep} \cdot \sum n_C}\right)^{0.4} \tag{2.7}$$

Where $\sum n_C = 100$ – number of aircraft in a series, so $K_{cep} = \left(\frac{35 \cdot 10^5}{39600 \cdot 100}\right)^{0.4}$ = 0.61.

Coefficient taking into account the estimated flight speed of the designed aircraft (formula (2.8)):

$$K_V = \frac{1}{2} \cdot \left(1 + \frac{Vcr}{800}\right) \tag{2.8}$$

Where Vcr = 880 km/h – aircraft cruising speed, so $K_V = \frac{1}{2} \cdot \left(1 + \frac{880}{800}\right)$ = 1.05.

P_c = 0.015 × 1.61 × 0.61 × 1.05 × 39600 × (3340+0.077 × 39600-1.05 × 10^{-5} × $39600^{1.5}$)=3406782.118 Dollars.

K_{RA} - coefficient showing the ratio of the cost of major repairs of the aircraft to the price of the aircraft (formula (2.9)):

$$K_{RA} = 0.11 + (3 \cdot 10^4 / P_c) \quad (2.9)$$

So K_{RA} = 0.11+30000/3406782.118 = 0.118.

For main aircraft on average:

$T_c = 30000h$;

$t_c = 5000h$;

$A_1 = 1.065 \times 3406782.118 \times \frac{1+0.118\times\left(\frac{30000}{5000}-1\right)}{30000}$ 192.3 dollars/h.

Depreciation and overhaul expenses at 1:00 of engine operation, dollars / h, are determined by (formula (2.10)):

$$A_2 = K_2 \cdot n_{en} \cdot P_{en} \cdot \frac{1 + K_{REN} \cdot \left(\frac{T_{en}}{t_{en}} - 1\right)}{T_{en}} \quad (2.10)$$

K_2 = 1.07 - coefficient taking into account non-production raid;

n_{en} = 2 - the number of engines installed on the plane;

P_{en} - price of one engine, dollars (formula (2.11)):

$$P_{EN} = 61.183 \cdot K_{\text{HBO}} \cdot N_{\text{E}max} \quad (2.11)$$

Where $N_{\text{E}max}$ = 11335kW - maximum engine power;

K_{HBO} = 1.61;

$P_{EN} = 61.183 \times 1.61 \times 11335 = 1116549.98$ dollars;

T_{en} = 6000 h;

t_{en} = 3000 h;

K_{REN} = 0.6;

$$A_2 = 1.07 \times 2 \times 1116549.98 \times \frac{1+0.6\times\left(\frac{6000}{3000}-1\right)}{6000} = 637.18 \text{ dollars/h}$$

The costs of current repairs and maintenance of the airframe (A_3) and engines (A_4), dollars / h, consist of the costs of materials and spare parts, the wages of technical workers directly involved in the maintenance and repair of aircraft and engines, and are determined as follows (formula (2.12)):

$$A_3 = 0.024 \cdot K_3 \cdot K_4 \cdot \left(0{,}39 - 0{,}121 \cdot 10^{-5} \cdot m_{ep}\right) \cdot m_{ep} \qquad (2.12)$$

Where K_3 = 0.61 - coefficient taking into account the maintenance method;

K_4 = 1 - for aircraft with turbojet engine and turbofan engine;

m_{ep} = 39600 kg;

$$A_3 = 0.024 \times 0.61 \times 1 \times (0.39 - 0.121 \times 10^{-5} \times 39600) \times 39600$$

= 198.32dollars/h

$$A_4 = \frac{0.024\times16\times K_2\times K_5\times n_{en}\times\sqrt{R_{max}}}{1+7\times10^{-5}\times T_{en}} \qquad (2.12)$$

Where K_2= 1.07 - coefficient taking into account non-production plaque;

K_5 = 1;

$R_{max} = N_{Emax}$ = 11335kW;

T_{en} = 6000g.

$$A_4 = \frac{0.024\times16\times1.07\times1\times2\times\sqrt{11335}}{1+7\times10^{-5}\times6000} = 61.61 \text{ dollars/h}$$

The wage costs of flight personnel for one flight hour (A_5), dollars / h, we consider, based on the number of passenger seats (formula (2.13)):

$$A_5 = 1.5 \times \left(0.9 \times n_{pass} - 0.00237 \times n_{pass}^2 - 2.9 \times 10^{-6} \times n_{pass}^3\right) \quad (2.13)$$

Where n_{pass} = 450 people - the maximum possible number of passenger seats on this aircraft;

$A_5 = 1.5 \times (0.9 \times 450 - 0.00237 \times 450^2 - 2.9 \times 10^{-6} \times 450^3) = 508.781$ dollars/h

The fuel costs attributable to 1:00 flight (A_6), dollars / h, we calculate by (formula (2.15)).

$$A_6 = 1.5 \times b \times P_k \times m_T \times n_{en} = \frac{\overline{m_T} \times m_0}{t_\Sigma \times n_{en}} \times P_k \quad (2.15)$$

Where $\overline{m_T}$ = 0.28 - relative mass of fuel;

m_0= 240000 kg - take-off mass of the aircraft;

t_Σ = 11 h - total flight time;

P_k = $ 1.5 / kg - the price of kerosene;

b = 1.045 - coefficient taking into account productive fuel consumption.

$A_6 = \frac{0.28 \times 240000}{11 \times 2} \times 1.5$ = 4581.81 dollars / h.

Other expenses for the aircraft (formula (2.16)):

$$A_7 = 0.07 \times \sum_{i=1}^{6} A_i \quad (2.16)$$

A_7 = 0.07*(192.3+637.18+198.32+61.61+508.781+4581.81) = 432.6 dollars / h.

A_{Σ} = 192.3 + 637.18 + 198.32 + 61.61 + 508.781 + 4581.81 + 432.6 =6612.6 dollars / h.

Indirect costs (B) include depreciation, maintenance and maintenance of all aerodrome and airport facilities and the salaries of ground personnel (except the salaries of technical workers engaged in the maintenance and repair of the aircraft fleet).

Indirect costs depend on the class of the airfield and the number of take-offs and landings per hour of flight.

So, for this aircraft indirect costs will be (formula (2.17)).

$$B = 0.4 \times A_{\Sigma} \tag{2.17}$$

B = 0.4×6612.6 = 2645.04 dollars / h.

The operating costs of this aircraft per 1:00 flight (flight hour) are (formula (2.1)).

$C_{OP} = 6612.6 + 2645.04$ = 9257.64 dollars / h.

The total cost of operating the aircraft for the transport of passengers and commercial cargo per kilometer is calculated by (formula (2.18)):

$$C_{\text{TKM}} = \frac{\text{A} + B}{m_{ld} \cdot k \cdot V_c} = \frac{9257.64}{14.25 \times 0.61 \times 880} = 1.21 \text{ dollars / h} \tag{2.18}$$

The revenue received by the aviation company from operating a fleet of aircraft of this type falls on one ton-kilometer, determined by (formula (2.19)):

$$\text{R} = \frac{P_{B \times n_{pass} \times K_3}}{m_{ld} \times V_c \times \tau} = \frac{830 \times 450 \times 0.61}{14.25 \times 880 \times 10} = 1.81 \text{ dollars / h.} \tag{2.19}$$

The profit earned by an aviation company from operating a fleet of aircraft of this type falls on one ton-kilometer, calculated by (formula (2.20)):

$$P_{rf} = R - C_{TKM} = 1.81 - 1.21 = 0.6 \text{ dollars/TKM} \tag{2.20}$$

To determine the price of a ticket, provided that the operation of an aircraft of this

class is break-even. We write the formula in the form (formula (2.21)).

$$R = \mathrm{C_{TKM}} + P_{rf} \tag{2.21}$$

where $P_{rf} = 0$ (break-even condition), and putting the unknown price of the ticket (CB) in revenue, we get:

$$P_B = \frac{m_{ld} \times V_c \times \tau \times \mathrm{C_{TKM}}}{n_{pas} \times \mathrm{K_3}} = \frac{14.25 \times 880 \times 10 \times 1.21}{450 \times 0.61} = 553 \text{ dollars}$$

$$\frac{P_B \times 450 \times 0.61}{14.25 \times 880 \times 10} = 1.21$$

P_B = 553 dollars.

With a margin of 25%, ticket price:

P_B = 692 dollars.

2.2. Conclusions

In this section, we calculated the costs of operating the aircraft and the engine at $ 897.11 / h and determined the price of the ticket, which amounted to $ 692. The indirect costs for one hour of flight are $ 2645.04 / h.

3. SPECIAL TASK

3.1. Introduction

3.1.1. Source and basis of topic selection

With the rapid development of aviation science and technology, the structure of aircraft has put forward the requirements of light weight, high reliability, high maintenance, high survivability. In order to meet these requirements, we must increase the intelligence of the structure and develop smart structure. For example the wing of the aircraft will change in terms of geometric structure dimensions such as wingspan, chord length and area[6] [7].

Smart structure technology could lead to a revolution in engineering concepts and ethics. In the 21st century it might be quite unacceptable engineering to build any structure or vehicle (that could endanger the lives of people or the environment) without including an integrated sensor system to warn of impending mechanical failure. For pipelines, pressure vessels, storage tanks, etc., simple built-in fiber-optic structural monitoring systems could provide an early warning of structural weaknesses and prevent many of the failures that today are responsible for a number of environmental problems. In major structures such as dams, nuclear reactors, or large buildings, this kind of system could warn of the development of structural faults or, after events like earthquakes, provide important information regarding structural soundness.

In aircraft, where composite materials are finding increasing application, structurally integrating fiber-optic sensor systems capable of detecting damage and

assessing its growth in time could find acceptance as part of the new fly-by-light technology. Through the use of artificial intelligence such a system might also determine the effect of this damage in terms of limiting flight maneuvers or evaluating the reduction in the useful life of duly instrumented components. This could also greatly improve maintenance efficiency and effectiveness[8].

Since the two guiding principles of designing smart materials are multifunctional composite of materials and biomimetic design of materials, smart material system has or part of the following smart functions and life characteristics:

i) Sensing function: It can sense the intensity and change of the external environment or its own environmental conditions, such as load, stress, strain, vibration, heat, light, electricity, magnetism, chemistry, nuclear radiation, etc.
ii) Feedback function: Through the sensor network, the system input and output information is compared, and the results are provided to the control system.
iii) Information recognition and accumulation function: The ability to recognize and accumulate all kinds of information obtained from the sensor network.
iv) Response function: According to the external environment and internal conditions change, timely and dynamic response, and take necessary actions.
v) Self-diagnostic capability: By analyzing and comparing the current situation and the past situation of the system, it can self-diagnose and correct the problems such as system failure and judgment error.
vi) Self-healing ability: It can repair some local damage or destruction through regenerative mechanisms such as self-propagation, self-growth and in-situ recombination.

vii) Self-regulating capacity: To the constantly changing external environment and conditions, it can automatically adjust its structure and function in time, and change its own state and behavior accordingly, so that the material system always makes an appropriate response to the external changes in an optimized way.

A wingtip, also known as a winglet or wingtip device, is an aerodynamic component attached to the outermost section of an aircraft wing. Wingtips are designed to reduce drag and increase fuel efficiency by modifying the airflow around the wingtip.

There are several different types of wingtips, including blended winglets, raked wingtips, and split scimitar winglets. Each design has its own unique shape and size, but they all serve the same basic function of improving the aerodynamics of the aircraft.

Wingtips can also improve the aircraft's handling characteristics by reducing the size of the wingtip vortices, which are turbulent air currents that form at the end of the wing. By reducing the size of these vortices, wingtips can improve the aircraft's stability and reduce the amount of turbulence experienced by other aircraft flying in close proximity[9].

3.1.2. Purpose

The ultimate purpose of this topic is to change the shape of the wing by smart structure control with wingtip winglets to adapt to changes in the external flight environment. Specific requirements are as follows:

1) Deepen the understanding of smart structure driving and control function through the research of this subject;
2) Have a certain understanding and grasp of the technical points of wingtip

winglet in installation through the specific operation control link;

3) Through the complete grasp of this topic will learn the theory of the practice, to reach a new level, and do at the same time to domestic and foreign hot topics of research results and development direction have a certain understanding.

3.1.3. Significance

Modern aircraft design is a set of high-tech, multidisciplinary, highly comprehensive fine optimization design technology, in its layout design constantly appear a variety of technical innovation. The aerodynamic design of the wing is one of the most important technologies in aircraft layout design. Modern large medium and long-range passenger and cargo aircraft have supercritical wings with high aerodynamic efficiency and complex shape. In addition to its own parameters, the design includes comprehensive analysis and fine optimization of power plant types and installation characteristics, wing, fuselage and landing gear rectification, wing tip wing fusion, different characteristics of each control surface at high and low speeds and deformation influence under load. In order to get satisfactory results, to achieve the requirements of multiple objectives.

In recent years, the emergence of fine designs such as blended winglets is a good example. It effectively reduces drag, increases lift, and thus increases the range (such as the Boeing 737-800 aircraft increasing the range by 240-350 km) or effective load, and reduces direct operating costs. For large passenger and cargo aircraft, the effect is even more significant. It has very important economic benefits. Of course, winglets must be matched to different aircraft configurations.

Winglets have been widely used on modern aircraft. Different types of winglets are installed on the Boeing 747, Boeing 767, and Airbus aircraft. Their main function is to improve the vortex distribution at the wingtip and reduce induced drag during flight. The blended winglets used on the Boeing 737-700/-800 aircraft were developed by APB (Aviation Partner Boeing), a joint venture between Boeing and API. These blended winglets differ significantly from traditional winglets. The blended winglets provide a smooth transition between the wingtip and winglet, with a larger transition radius and smooth chord variation. This can optimize the load distribution on the wingspan, minimize the effects of aerodynamic interference and flow separation, and achieve higher aerodynamic efficiency compared to traditional winglets with abrupt transition angles. The effect on reducing drag is more significant.

The research of this project is based on an example of a variable winglet structure design to implement the application of smart structures in wing control. If the research progresses smoothly, we will design a smart control system that can perceive and adapt to the external environment of the aircraft while ensuring reliability and quality. The success of the research will make a significant breakthrough in the application of smart structures in aircraft, and pave the way for further developments.

Changing the shape of the wing to get the right aerodynamic force has already been used[10] [11]. Frenchman Clement Ader designed the wing to be a foldable structure like the wings of a bat or bird[12]. The wing area can be reduced by a third or even a half. Since 1995, NASA/DARPA/AFRL has jointly launched the Smart Wing Program, which focuses on wing torsion and hingeless control surface technology to achieve seamless, smooth and continuous deformation of wings with multiple degrees of

freedom, so as to achieve optimal aerodynamic performance under any operating conditions[13] [14]. NASA has formulated the "Flexible high-aspect ratio wing" plan for civil aircraft development between 2030 and 2035. The goal is to reduce the structural weight of the wing by 25 percent and increase the aspect ratio by 30 to 40 percent[15] [16].

3.1.4. The present situation and development of smart structure

The smart structure technology first gained attention in the late 1970s when the United States embedded fibers into composite materials, resulting in significant improvements in structural functionality. Since then, smart structure technology has been widely recognized and developed in many advanced countries. In recent years, it has received even higher levels of attention, especially in the United States, where the military and government agencies are directly involved in its development. In 1995, the White House Office of Science and Technology Policy and the National Critical Technologies Review Panel included smart materials and structure technology in the "National Critical Technology Report." In 1997, smart structures were listed as one of six strategic research tasks under the "Basic Research Program." Various branches of the US military, the Ballistic Missile Defense Agency, NASA, and large companies such as Boeing, McDonnell Douglas, TRW, and United Technologies have each developed research and development plans. These plans include the Ballistic Missile Defense Agency's "Adaptive Structures Program," the Army Research Laboratory's "Smart Metal Structure Program," and the Air Force's Aerospace Laboratory's "Smart Structure Skin Program."

In Europe, the main countries researching smart structures are Germany, the UK,

France, and Italy. From 1989 to 1991, seven companies from the UK, France, and Italy completed the first collaborative research program in this field supported by the European Union, called the "Composite Material Photochemical Sensing Program." The program experimentally validated the use of implanted optical fibers to measure strain, temperature, and curing monitoring in composite materials. In the early 1990s, the UK established the first dedicated research institution for smart materials and structures in Europe, the "Strathclyde University Institute for Smart Materials and Structures." The German Aerospace Research Institute is the main institution in Europe conducting research in this field, currently researching the use of implanted optical fibers in self-diagnosing smart structures for damage detection and evaluation in reusable launch vehicles and in the "Future European Space Transportation System Program."

Japan started researching functional structures in space since 1984, and the Japan Aerospace Exploration Agency, Tokyo Institute of Technology, and some large corporations are involved in this work. The main research focuses on using functional structures to achieve active vibration control, precise control of adaptive static shape, and adaptive variable trusses.

Due to the difficulty of researching self-repairing capabilities in smart composite materials structures, only countries such as the United States and Japan have invested heavily in laboratory research. To date, there are no mature research methods, and there are few practical research reports on self-repairing capabilities. Domestic research on self-repairing capabilities is also weak and still in the early stages.

3.1.5. General idea

- Select the straight wing as the research object. Determine the dimensions of the straight wing and the rotation angle of the winglet.
- Establish an effective wing calculation model by UG.
- Use CFD software to perform aerodynamic calculations on the wing model, find the data parameters of the drag coefficient, lift coefficient and lift-drag ratio of the model wing surface under different winglet angles and angles of attack, make their change curves, analyze the change rules and causes, and then find the reasonable rotation angle of the winglet tip under different angles of attack.

3.2. Modeling of the wing

3.2.1. The choice of the airfoil

Due to the large size of the wing studied in this paper, the airfoil of some large civil airliners can be selected by referring to a NACA airfoil. The NACA airfoil is a type of airfoil used in aircraft design that was developed by the National Advisory Committee for Aeronautics (NACA) in the early 20th century. The NACA airfoil is known for its precise mathematical definition and predictable aerodynamic characteristics, which made it a popular choice for aircraft designers.

The NACA airfoil is characterized by a series of four-digit numbers that describe the shape of the airfoil. The first digit represents the maximum camber (or curvature) of the airfoil as a percentage of the chord length. The second digit represents the position of the maximum camber as a fraction of the chord length. The last two digits represent the thickness of the airfoil as a percentage of the chord length.

For example, a NACA 2412 airfoil has a maximum camber of 2%, located 40% of the chord length from the leading edge, and a thickness of 12% of the chord length.

One of the key advantages of the NACA airfoil is its ability to generate lift at low angles of attack, making it well-suited for low-speed applications such as general aviation and wind turbines. In addition, the NACA airfoil can be easily modified to meet specific design requirements by adjusting the camber and thickness parameters.

So I choosed NACA2217. Its shape is shown in Figure 3.1 below.

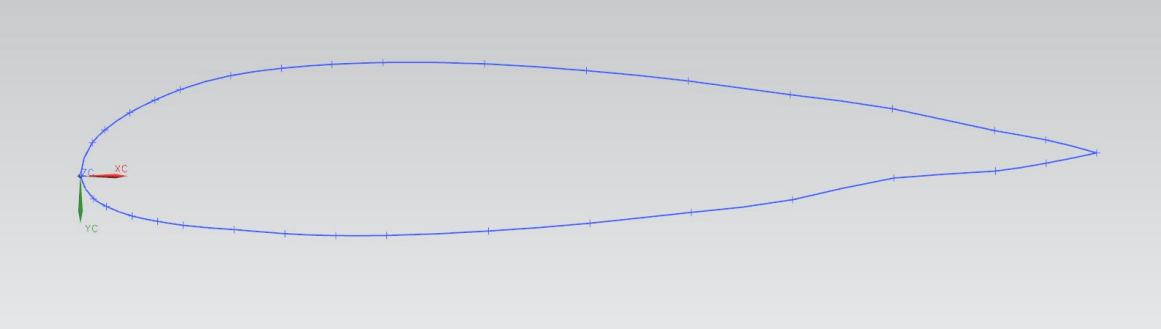

Figure 3.1 – NACA 2217

3.2.2. The choice of the wing

The main purpose of this design is to study the influence of the wingtip winglets on the aerodynamic performance of the wing surface. The requirements for the model are relatively low, so we only need to choose a relatively simple half-wing model and ignore the influence of aircraft components such as the fuselage. Therefore, a straight wing model is selected. After the model is selected, the size of the flat wing model is given, and the half wing length is guaranteed to be 10 times of its airfoil chord line. If the half wing span is 33m, the airfoil chord length is 3.3m.

3.2.3. The choice of the winglet

In order to better study the influence of wingtip winglets on the wing, the interference of strength, stiffness and force at the joint of the wing and fuselage is

ignored in the study, and the winglets and wings are regarded as a whole, and the winglets rotate around the airfoil string. Since the airfoil is asymmetrical, the rotation Angle of the wing tip should correspond to the top and the bottom for reference and comparison in data analysis. The selected states are as follows: winglets do not deflect, that is, the wing model with Angle of 0°; When the small wing is tilted upward, select rotation angles of 90 degrees, 75 degrees, 60 degrees, 45 degrees, 30 degrees and 15 degrees. Since the winglet model selected has a long span, the winglet length can be set as 1/10 of the half-span length, so the winglet length is set as 3.3m. The following figure shows a magnified diagram of the winglet model and its winglet.

3.2.4. Establishment of wing model

Based on the above model size data, the theoretical shape of the wing to be studied was established by UG.

First of all, the data points of the airfoil NASA2217 were used as sketch data points to form (Insert→Curve→Spline→Through points) a line.

Then, the guide line needed to generate the wing model by sweeping method is established, so that the change of winglet Angle can be changed through the guide line, so as to achieve the winglet rotation effect.

Finally, the auxiliary plane and lines of the drawing are hidden, and the wing model is left and saved as a prt file for the calculation of aerodynamic performance later.

The wing model of each movable wing tip to be studied is shown in the Figure (3.2), (3.3), (3.4), (3.5), (3.6), (3.7), (3.8) below.

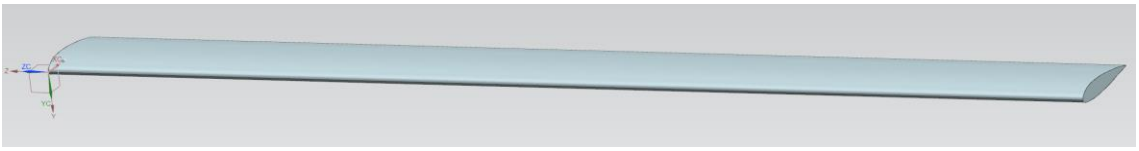

Figure 3.2 - Flat wing model

Figure 3.3 - Wing model with winglet Angle of 15°

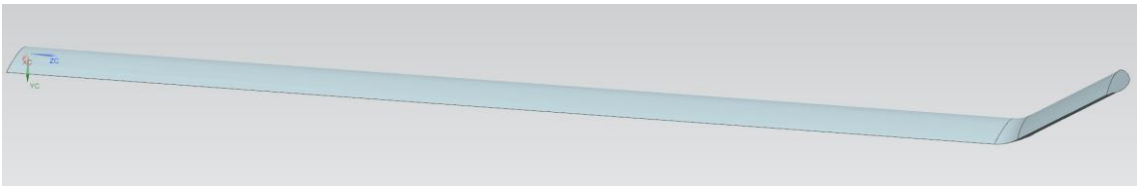

Figure 3.4 - Wing model with winglet Angle of 30°

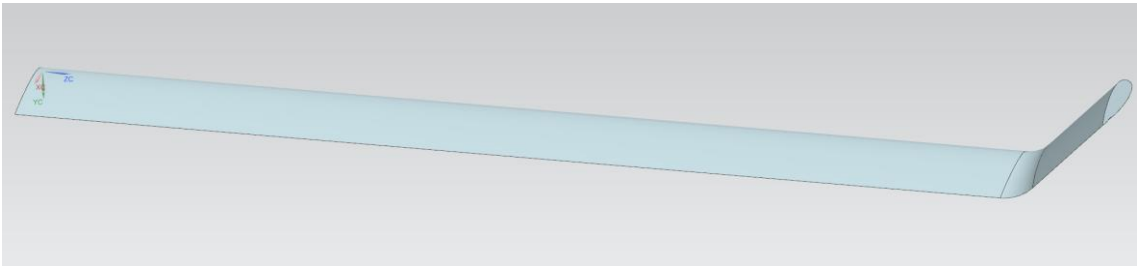

Figure 3.5 - Wing model with winglet Angle of 45°

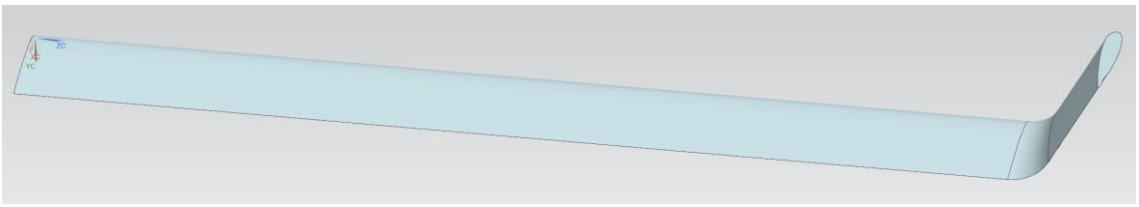

Figure 3.6 - Wing model with winglet Angle of 60°

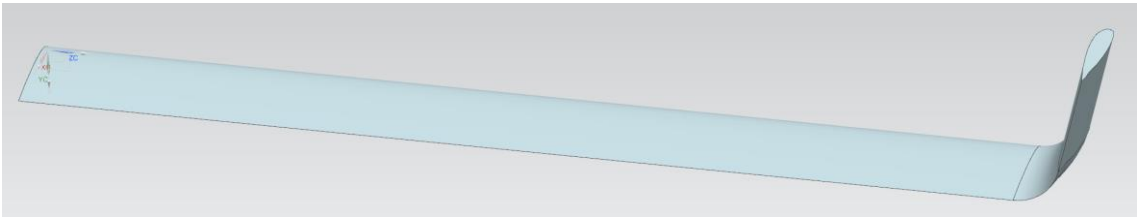

Figure 3.7 - Wing model with winglet Angle of 75°

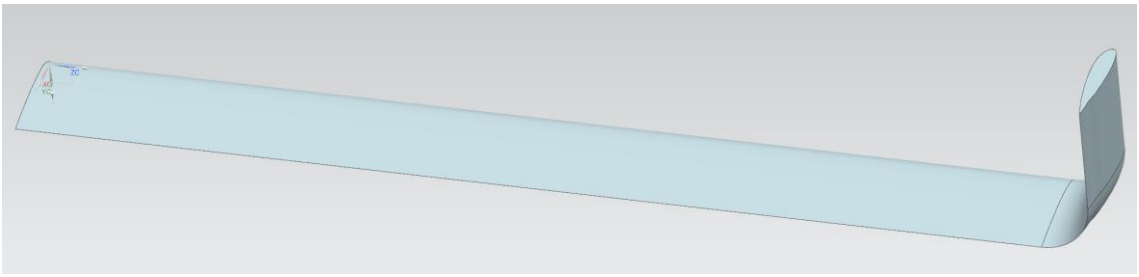

Figure 3.8 - Wing model with winglet Angle of 90°

3.3. Calculation of aerodynamic characteristics of movable winglet

3.3.1. CFD solution technique

The simulation stages of CFD for calculating flow problems is shown in Figure (3.8).

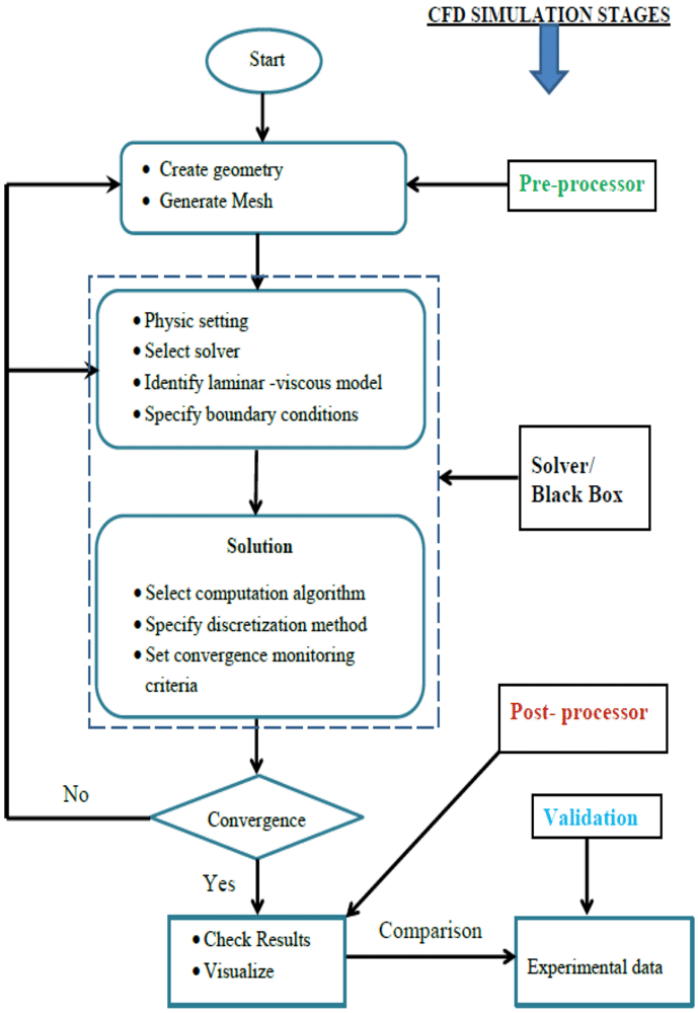

Figure 3.8 – CFD simulation stages

Computational fluid dynamics (CFD) is a branch of fluid mechanics that uses computer simulations to obtain information about a fluid under certain conditions, enabling "computational experiments" to be carried out using a computer instead of an experimental device. It has been widely used in aerospace, thermal power, civil water conservancy, automotive engineering, railway, shipbuilding industry, chemical engineering, fluid machinery, environmental engineering and other fields.

The aerodynamic calculation of aircraft is a very common problem in the field of aerodynamics. In this design, mainly aiming at an aircraft wing model, CFD software is used to simulate the flight flow field of the wing, and the aerodynamic calculation

and analysis of the model are carried out.

3.3.2. Design of wingtip rotation mechanism

In order to realize the rotation of the winglet, a simple rotation mechanism can be designed at the connection between the main wing and the winglet. The selection of the scheme is based on the successful addition of the winglet aircraft today. The mechanism is through the lug hinged to achieve the transmission of the connection, and the hydraulic drive way to make the rod with sleeve action, then at the hinged will produce a moment of rotation, under the action of the moment of rotation, can realize the wing tip rotation. The schematic diagram of the rotating mechanism is shown in Figure (3.9). Through flight control, the winglets can be rotated at the required Angle. The aerodynamic characteristics of the wing model with the movable wingtip will be calculated below.

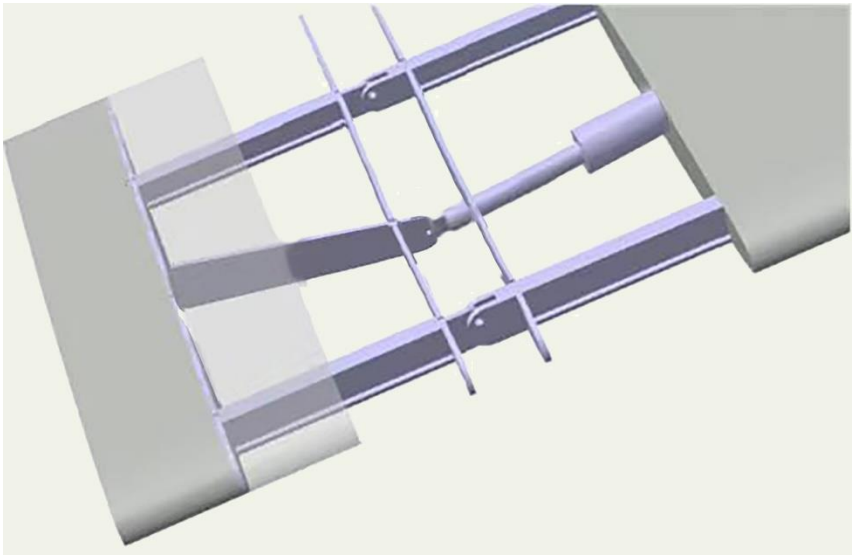

Figure 3.9 - Wingtip rotation mechanism

3.4. Calculation of flow field in each deformation condition

The application of CFD software to the aerodynamic analysis of aircraft needs to

calculate the external flow field around the flow under different working conditions (Angle of attack, incoming flow Mach number, etc.). The flow is generally assumed to be steady and compressible, and the software acts as a numerical wind tunnel. After obtaining the pressure distribution of the flow field, the software will automatically integrate the shear stress and pressure on the surface of the aircraft. The aerodynamic force of the aircraft wing surface is obtained, so as to obtain the lift, drag, side force, pitch, yaw and roll moment of the whole aircraft under this working condition.

In this graduation design, the airfoil has been selected as NACA airfoil, so the Mach number of the flow field is 0.8. In order to study the influence of winglets' changes on the aerodynamic characteristics of the wing surface and the markings of the outflow field, it is necessary to study the relationship between multiple groups of Angle of attack and winglets' Angle. However, considering the limited time, only one range of Angle of attack can be selected in this graduation design, that is, when the Angle of attack of the incoming flow changes from 0° to 8° (with an interval of 4°). Effect of winglets on aerodynamic characteristics of airfoil surface.

3.4.1. Aerodynamic characteristics of a flat wing model

The straight wing is the wing model when the winglet Angle is 0°. Its model diagram is shown in Figure (3.2).

The specific calculation model is treated as follows:

- The calculation domain model is established. According to the shape of the wing model determined above, Designer Modeler is applied to generate a cuboid calculation domain to define fluid inlet and fluid outlet circumference.

- Mesh. If you want to get more accurate data, you need to divide the grid more finely.
- Output the Mesh file for FLUENT calculations, then save and exit the program.

The generated flat wing model grid is shown in Figure (3.10).

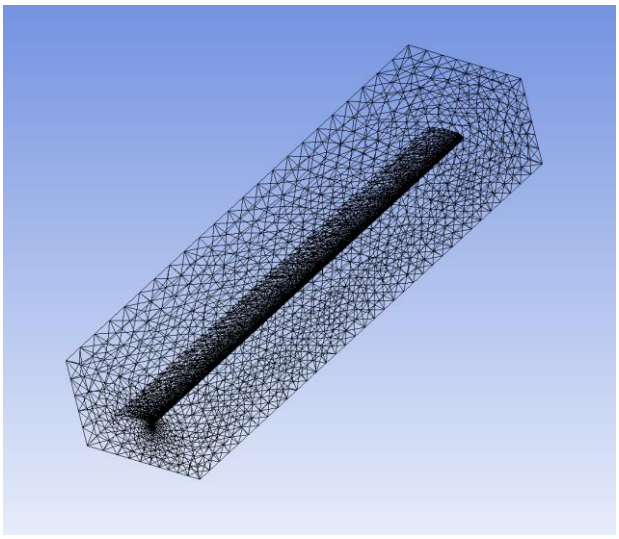

Figure 3.10 - Flat wing calculation model grid

- Using FLUENT solver to solve the problem

  Select calculation model: Select k-epsilon in Viscous under Models.

  Physical property parameters: The fluid is selected as air.

  Boundary condition parameters: Set the inlet to velocity-inlet, speed to 980km/h, and outflow.

  Lift and drag monitoring Settings: When calculating lift and drag at each Angle of attack, it is important to set their direction. Generally speaking, lift and drag refer to the force in the coordinate system of wind axis, that is to say, the direction of drag is along the direction of incoming flow, and the direction of lift is perpendicular to the direction of incoming flow.

The monitoring figures of lift coefficient, drag coefficient and moment coefficient of the flat wing model at different angles of attack are shown in the Figure 3.11 (a), (b), (c). Figure (a), (b) and (c) in Figure 3.11 respectively show the variation curves of drag coefficients along with the iterative process when the Angle of attack α= 0°, α= 4° and α= 8°.

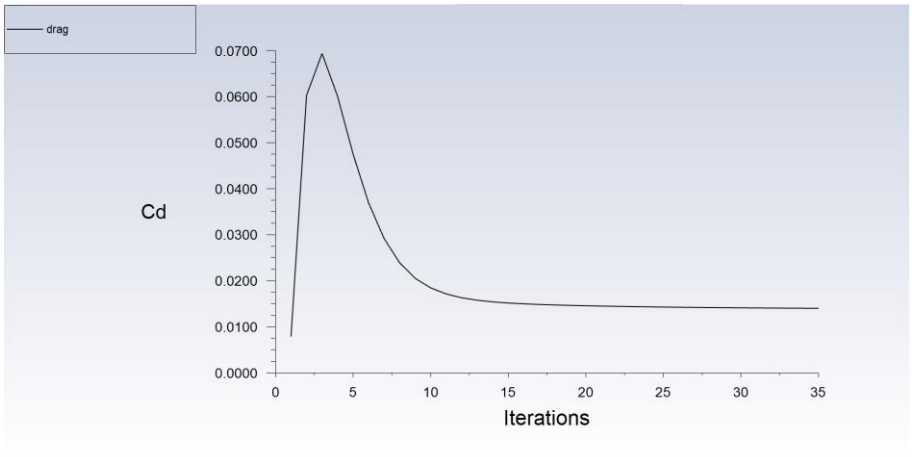

(a)

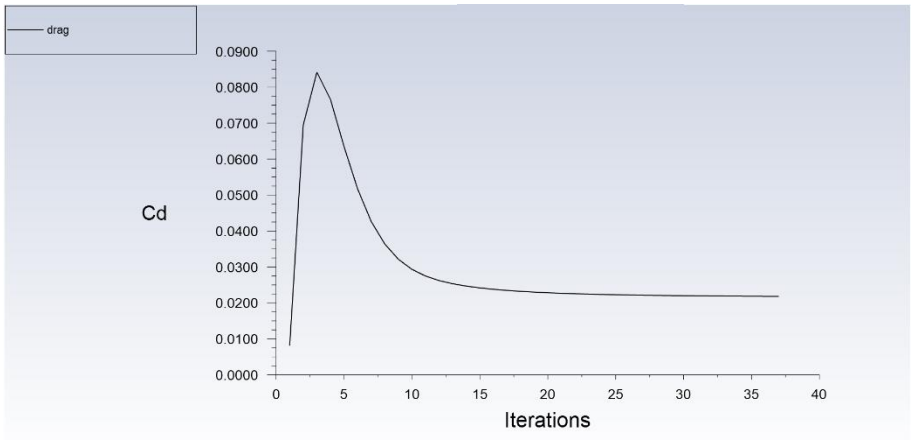

(b)

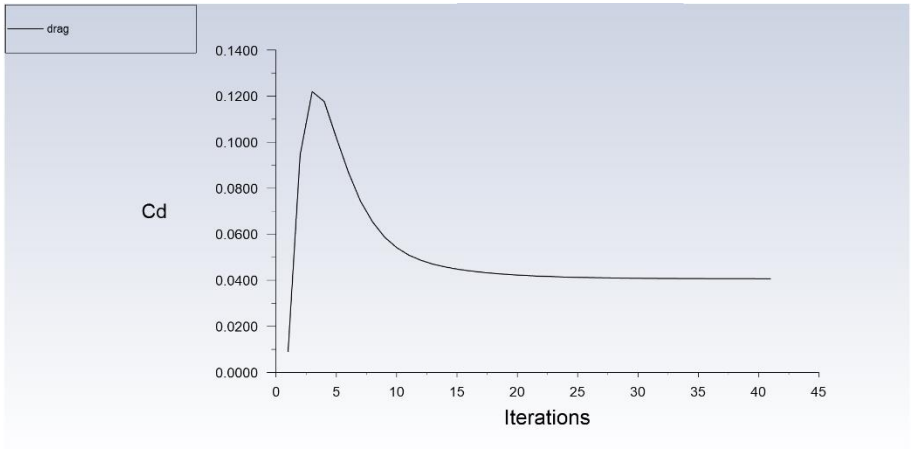

(c)

Figure 3.11 - Drag coefficient changes at different angles of attack

Figure (a), (b) and (c) in Figure 3.12 respectively show the variation curves of lift coefficients along with the iterative process when the Angle of attack α= 0°, α= 4° and α= 8°.

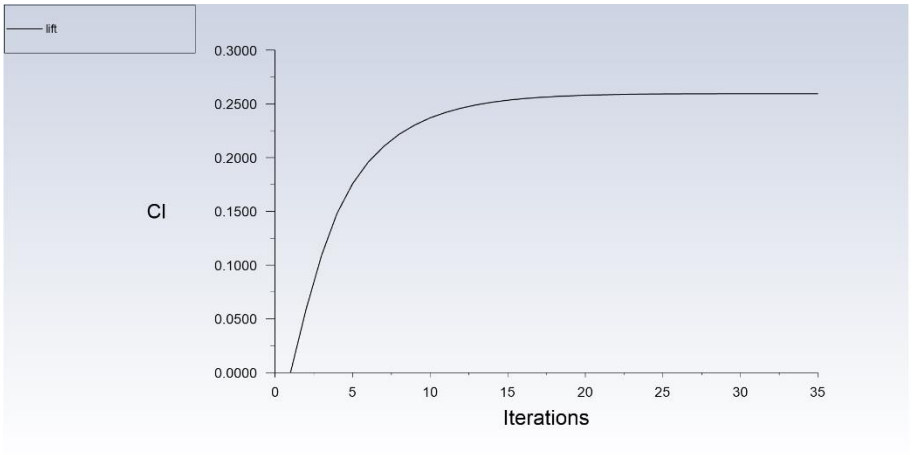

(a)

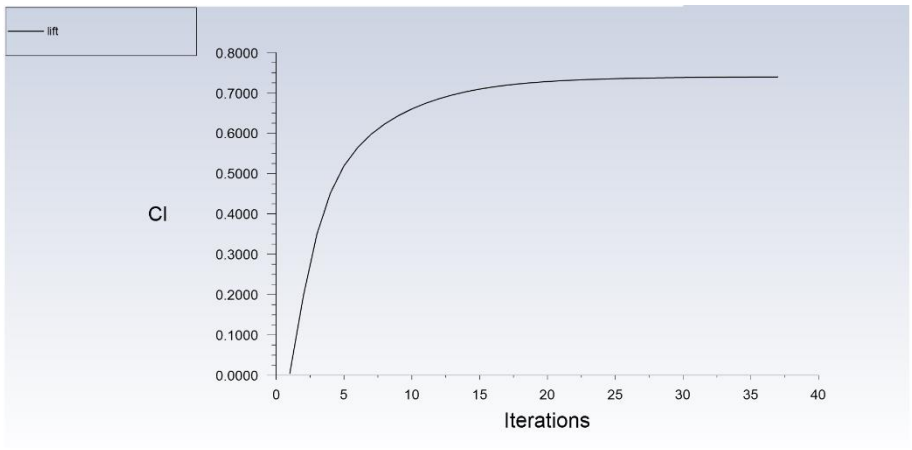

(b)

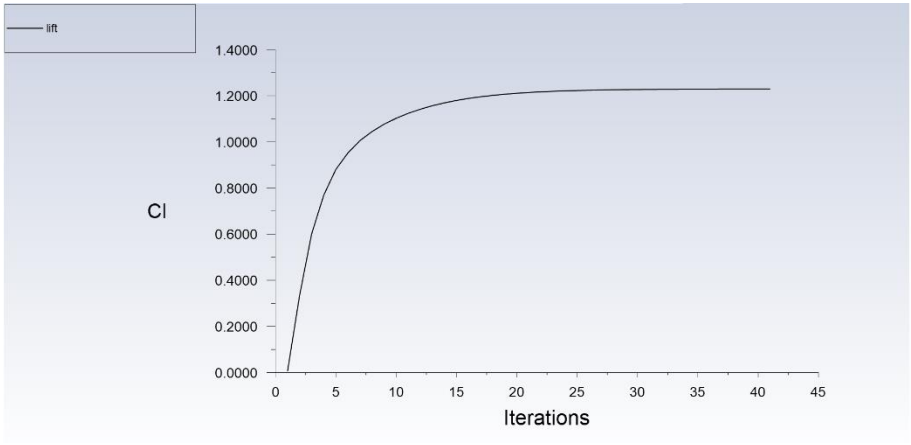

(c)

Figure 3.12 - Lift coefficient changes at different angles of attack

3.4.2. Aerodynamic characteristics of a wing model with a 15° winglet Angle

The straight wing is the wing model when the winglet Angle is 15°. Its model diagram is shown in Figure (3.3). The steps of computational model processing are the same as those of straight wing. The generated flat wing model grid is shown in Figure (3.13).

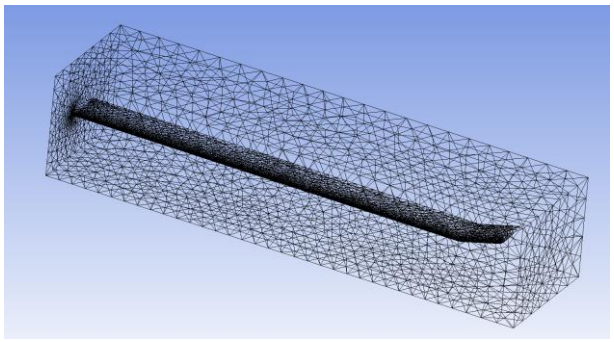

Figure 3.13 - Wing model grid at 15° winglet angle

The monitoring graphs of lift coefficient and drag coefficient of the wing model with 15° winglet Angle at different angles of attack are shown in Figure 3.14 (a), (b), (c).

Figure (a), (b) and (c) in Figure 3.14 respectively show the variation curves of

drag coefficients along with the iterative process when the Angle of attack α= 0°, α= 4° and α= 8°.

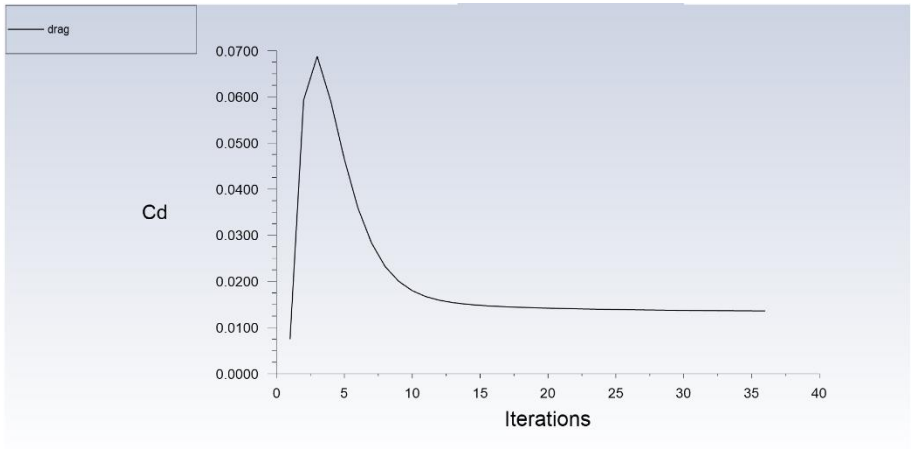

(a)

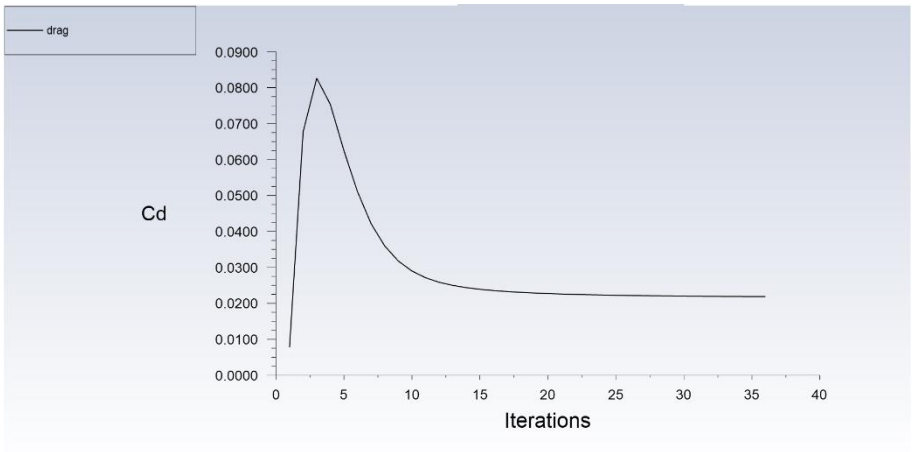

(b)

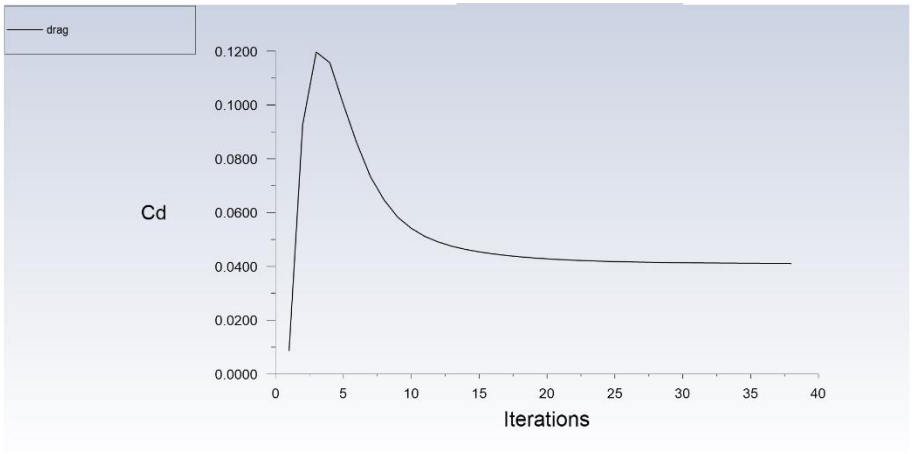

(c)

Figure 3.14 - Drag coefficient changes at different angles of attack

Figure (a), (b) and (c) in Figure 3.15 respectively show the variation curves of lift

coefficients along with the iterative process when the Angle of attack α= 0°, α= 4° and α= 8°.

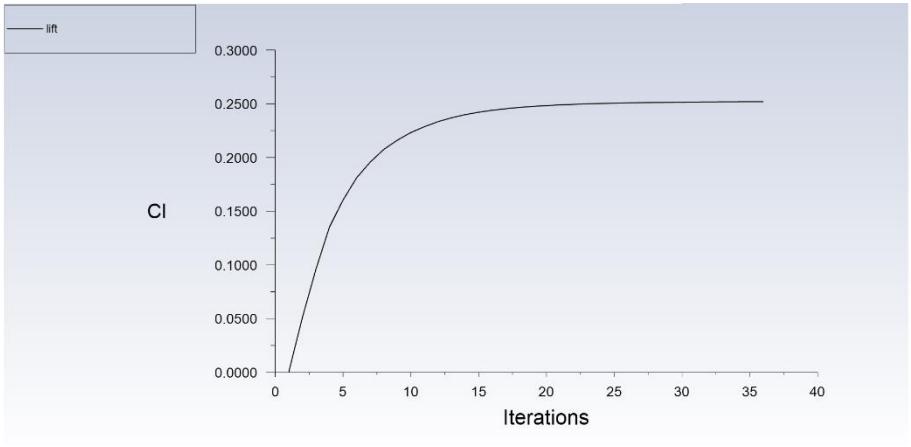

(a)

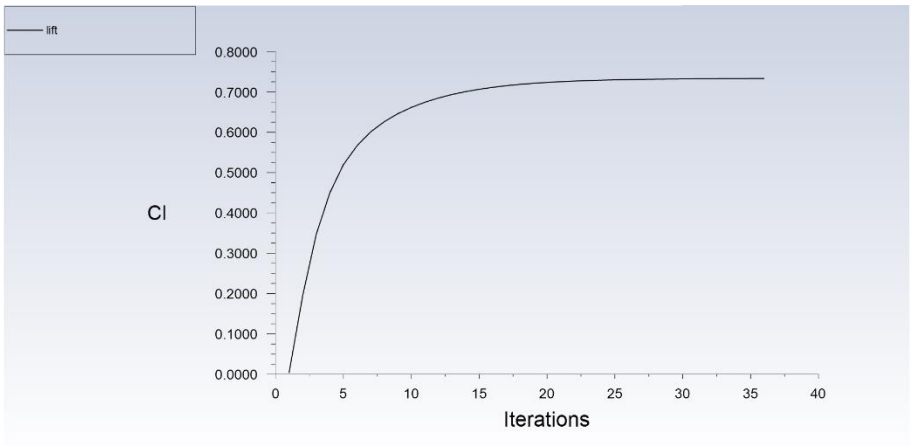

(b)

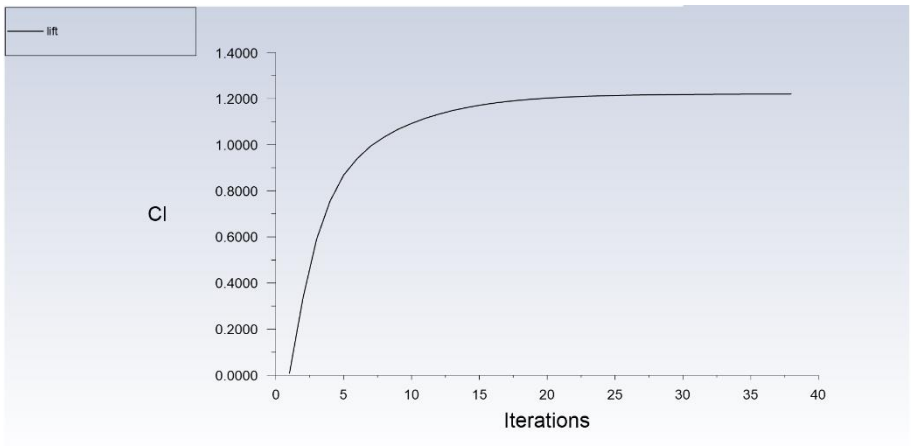

(c)

Figure 3.15 - Lift coefficient changes at different angles of attack

3.4.3. Aerodynamic characteristics of a wing model with a 30° winglet Angle

The straight wing is the wing model when the winglet Angle is 30°. Its model diagram is shown in Figure (3.4). The steps of computational model processing are the same as those of straight wing. The generated flat wing model grid is shown in Figure (3.16).

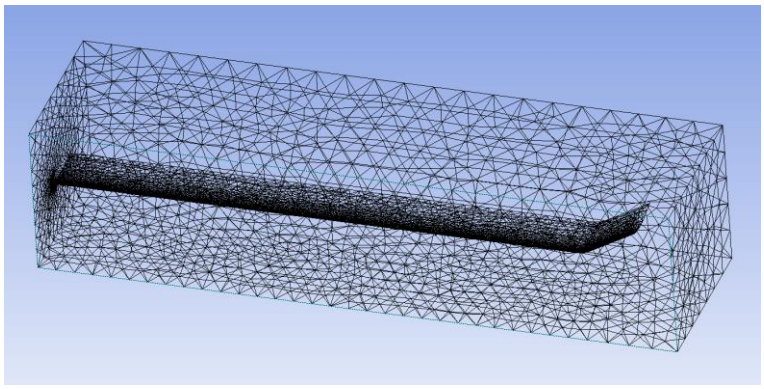

Figure 3.16 - Wing model grid at 30° winglet angle

The monitoring graphs of lift coefficient and drag coefficient of the wing model with 30° winglet Angle at different angles of attack are shown in Figure 3.17 (a), (b), (c).

Figure (a), (b) and (c) in Figure 3.17 respectively show the variation curves of drag coefficients along with the iterative process when the Angle of attack α= 0°, α= 4° and α= 8°.

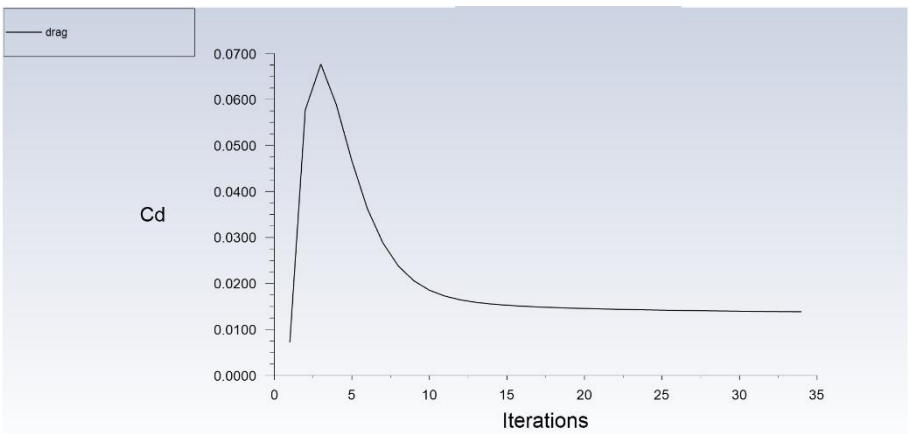

(a)

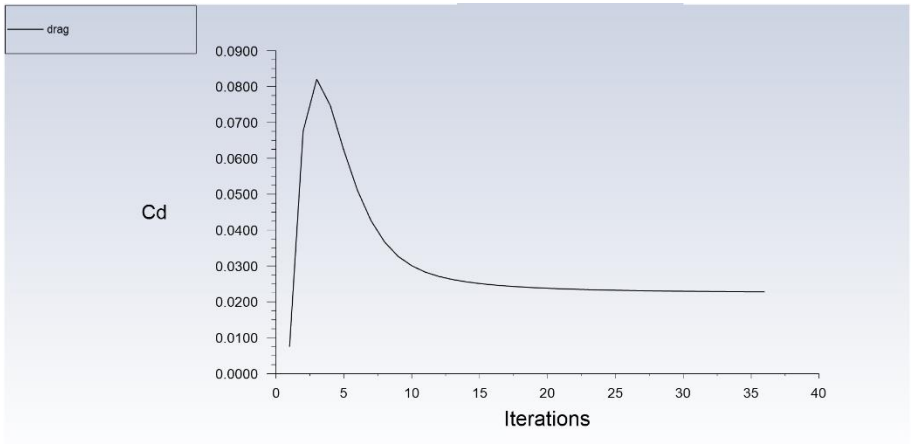

(b)

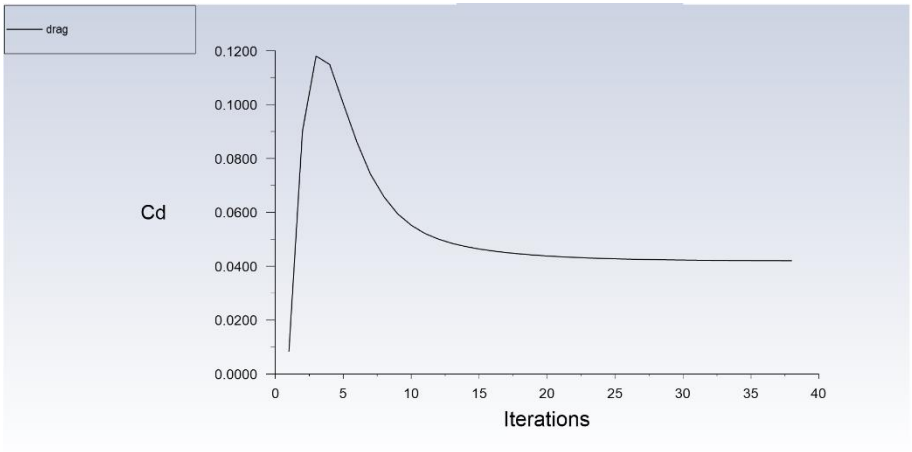

(c)

Figure 3.17 - Drag coefficient changes at different angles of attack

Figure (a), (b) and (c) in Figure 3.18 respectively show the variation curves of lift coefficients along with the iterative process when the Angle of attack α= 0°, α= 4° and α= 8°.

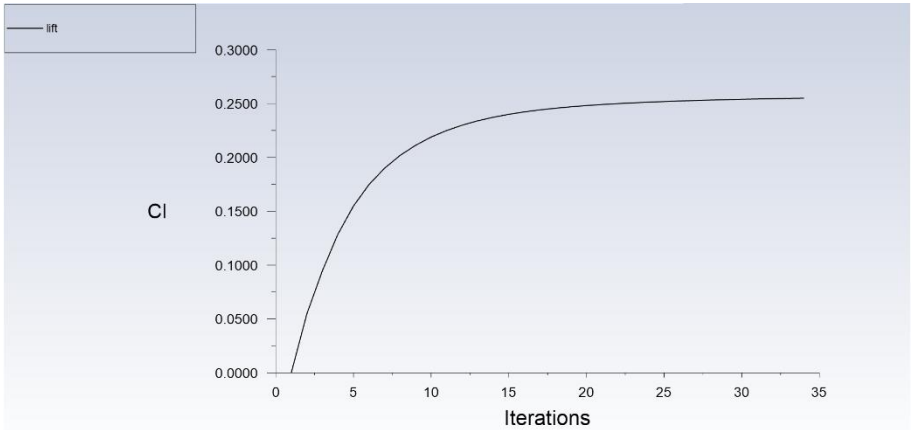

(a)

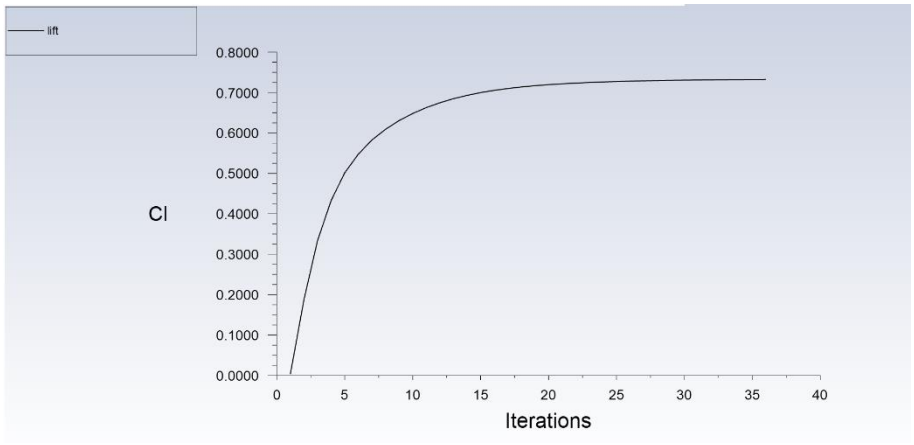

(b)

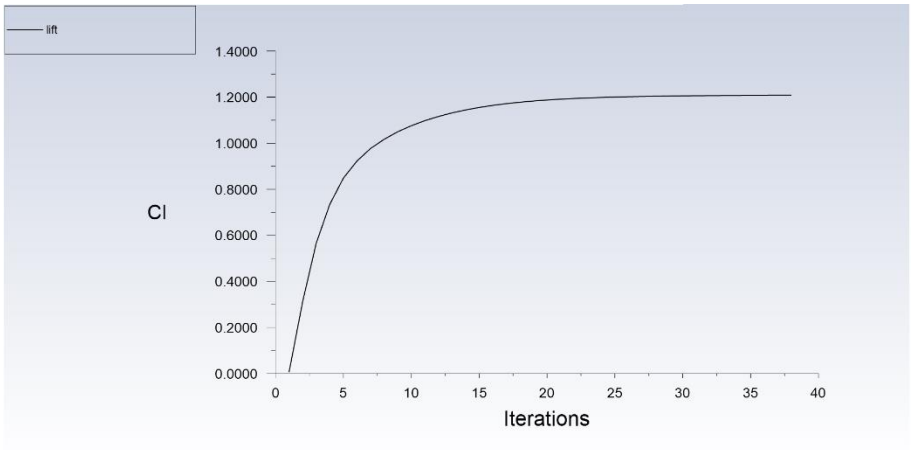

(c)

Figure 3.18 - Lift coefficient changes at different angles of attack

3.4.4. Aerodynamic characteristics of a wing model with a 45° winglet Angle

The straight wing is the wing model when the winglet Angle is 45°. Its model diagram is shown in Figure (3.5). The steps of computational model processing are the same as those of straight wing. The generated flat wing model grid is shown in Figure (3.19).

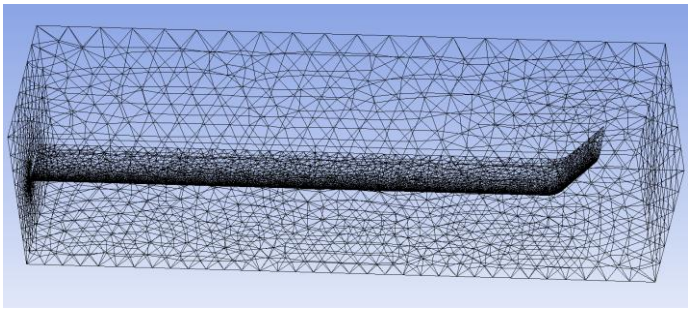

Figure 3.19 - Wing model grid at 45° winglet angle

The monitoring graphs of lift coefficient and drag coefficient of the wing model with 45° winglet Angle at different angles of attack are shown in Figure 3.20 (a), (b), (c).

Figure (a), (b) and (c) in Figure 3.20 respectively show the variation curves of drag coefficients along with the iterative process when the Angle of attack α= 0°, α= 4° and α= 8°.

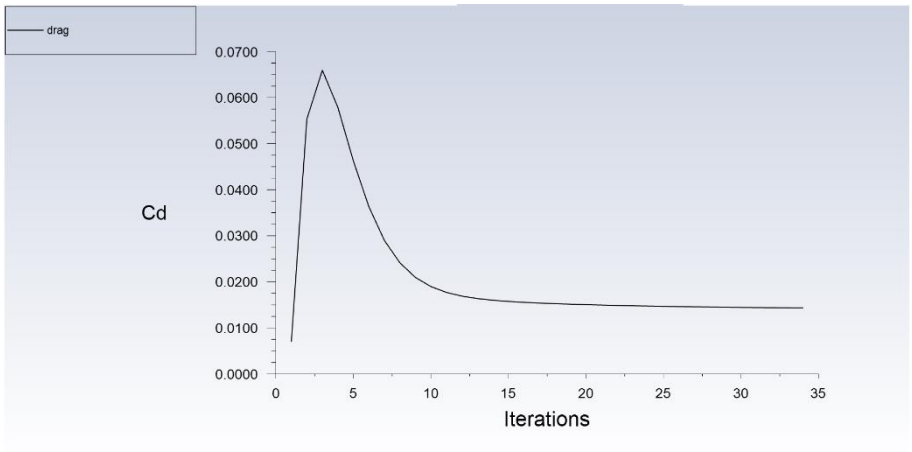

(a)

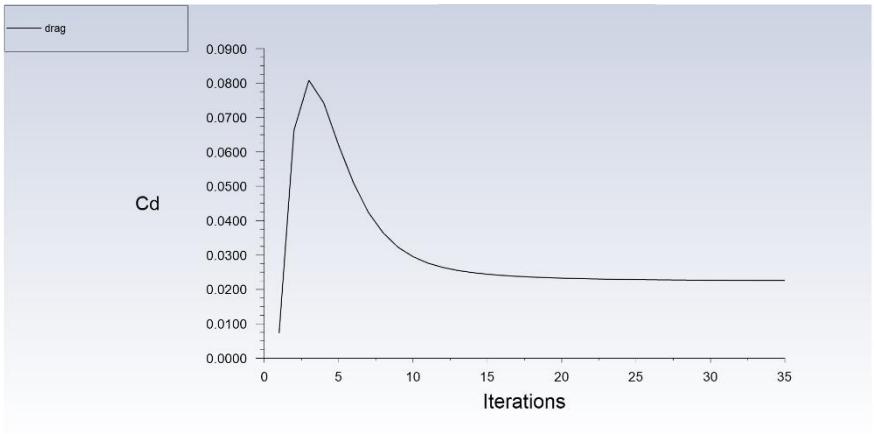

(b)

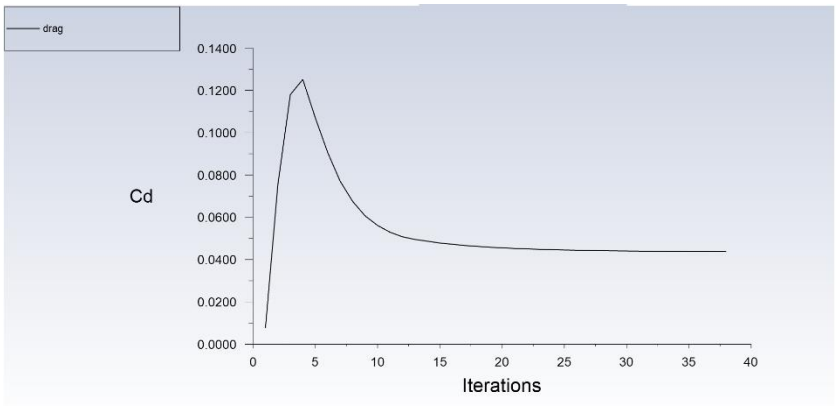

(c)

Figure 3.20 - Drag coefficient changes at different angles of attack

Figure (a), (b) and (c) in Figure 3.21 respectively show the variation curves of lift coefficients along with the iterative process when the Angle of attack α= 0°, α= 4° and α= 8°.

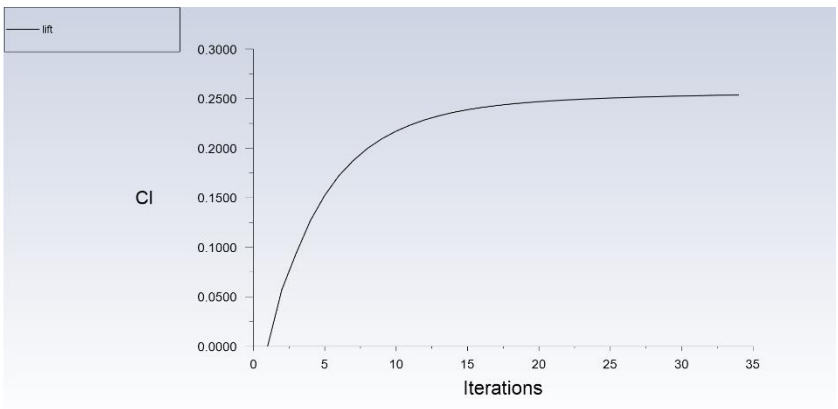

(a)

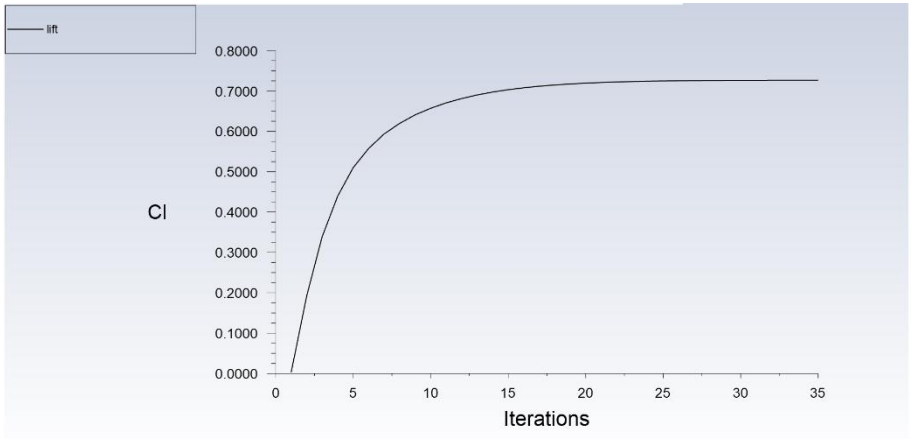

(b)

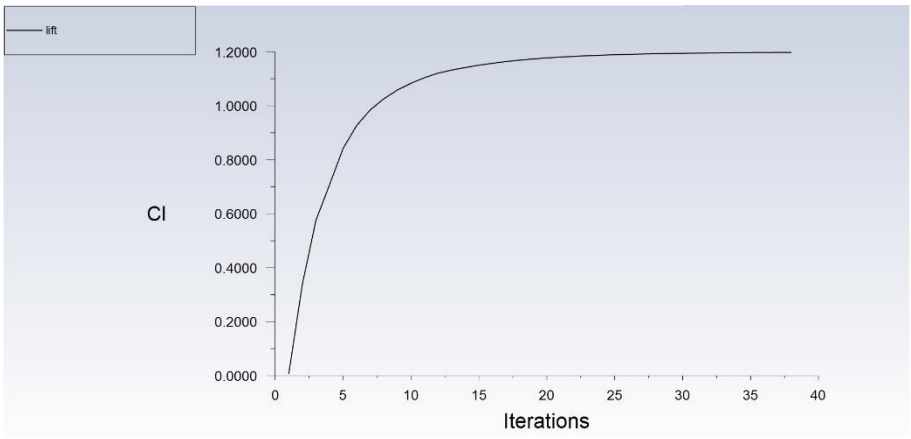

(c)

Figure 3.21 - Lift coefficient changes at different angles of attack

3.4.5. Aerodynamic characteristics of a wing model with a 60° winglet Angle

The straight wing is the wing model when the winglet Angle is 60°. Its model diagram is shown in Figure (3.6). The steps of computational model processing are the same as those of straight wing. The generated flat wing model grid is shown in Figure (3.22).

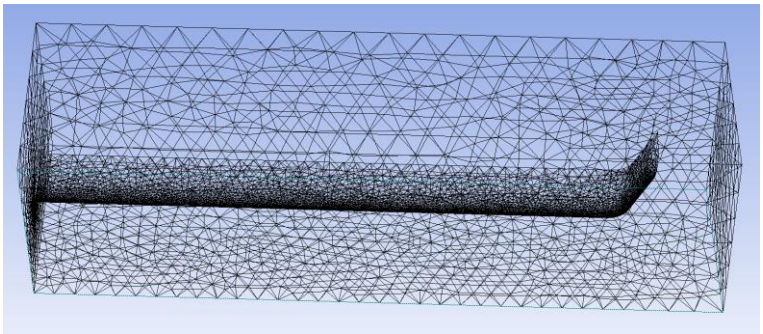

Figure 3.22 - Wing model grid at 60° winglet angle

The monitoring graphs of lift coefficient and drag coefficient of the wing model with 60° winglet Angle at different angles of attack are shown in Figure 3.23 (a), (b), (c).

Figure (a), (b) and (c) in Figure 3.23 respectively show the variation curves of drag coefficients along with the iterative process when the Angle of attack α= 0°, α= 4° and α= 8°.

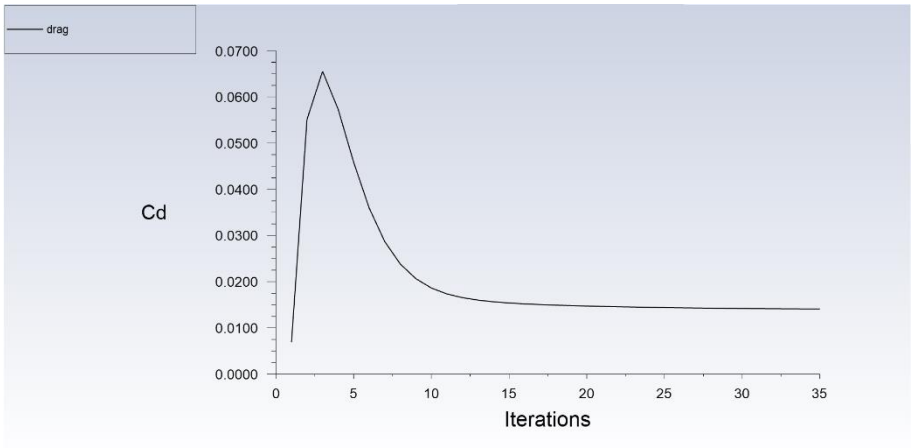

(a)

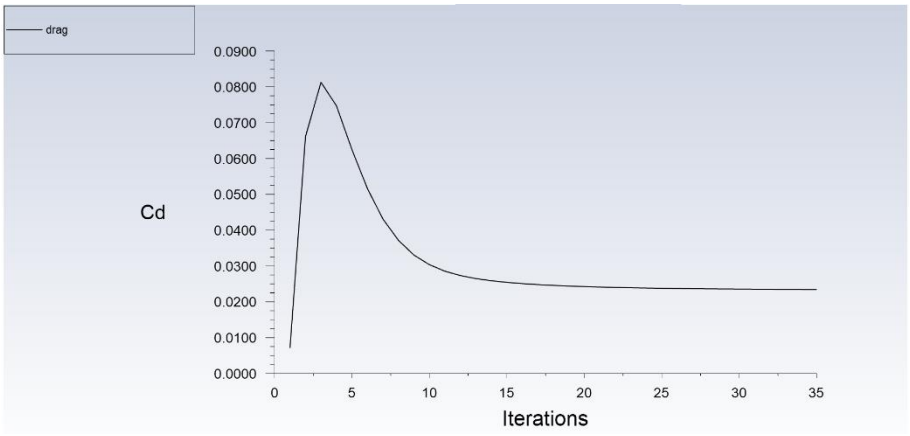

(b)

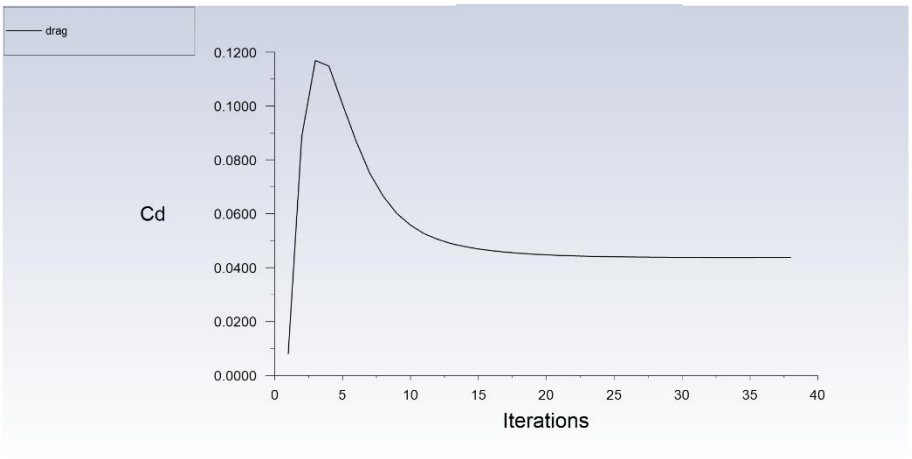

(c)

Figure 3.23 - Drag coefficient changes at different angles of attack

Figure (a), (b) and (c) in Figure 3.24 respectively show the variation curves of lift coefficients along with the iterative process when the Angle of attack α= 0°, α= 4° and α= 8°.

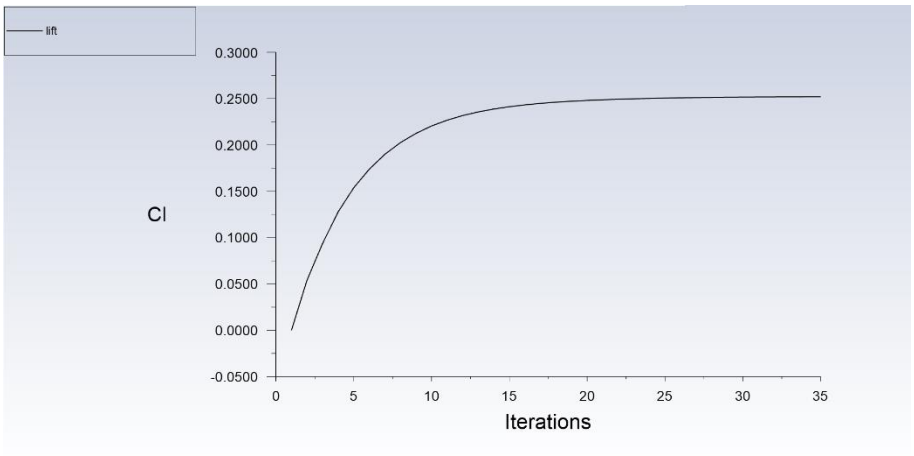

(a)

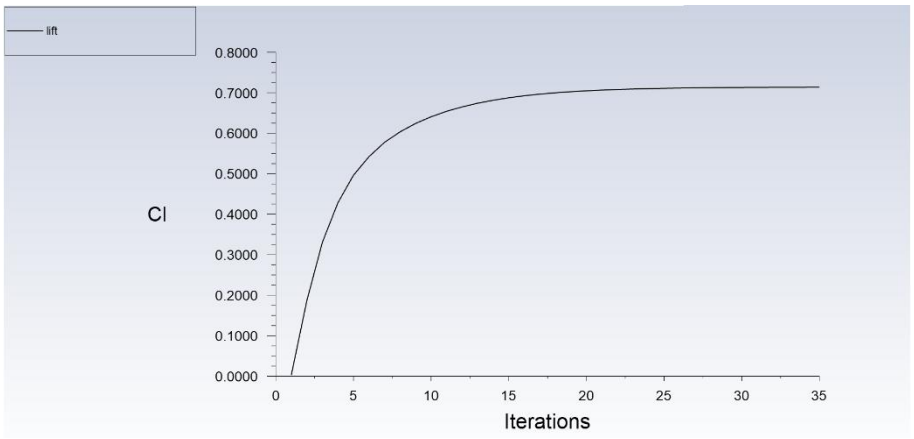

(b)

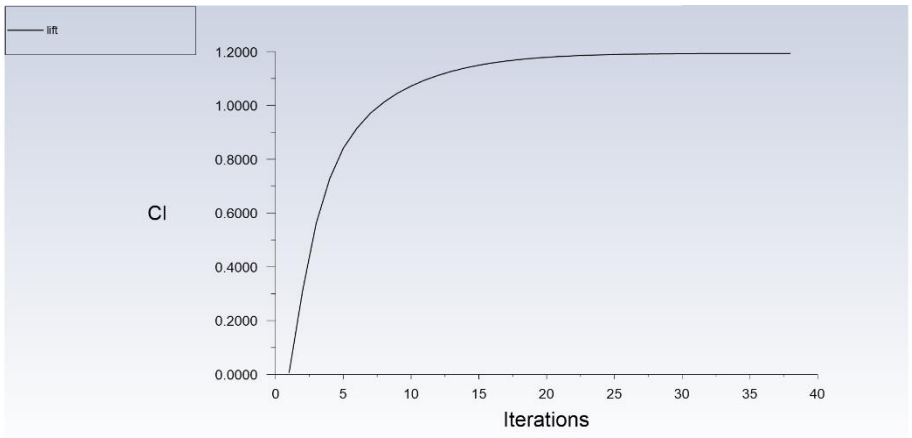

(c)

Figure 3.24 - Lift coefficient changes at different angles of attack

3.4.6. Aerodynamic characteristics of a wing model with a 75° winglet Angle

The straight wing is the wing model when the winglet Angle is 75°. Its model

diagram is shown in Figure (3.7). The steps of computational model processing are the same as those of straight wing. The generated flat wing model grid is shown in Figure (3.25).

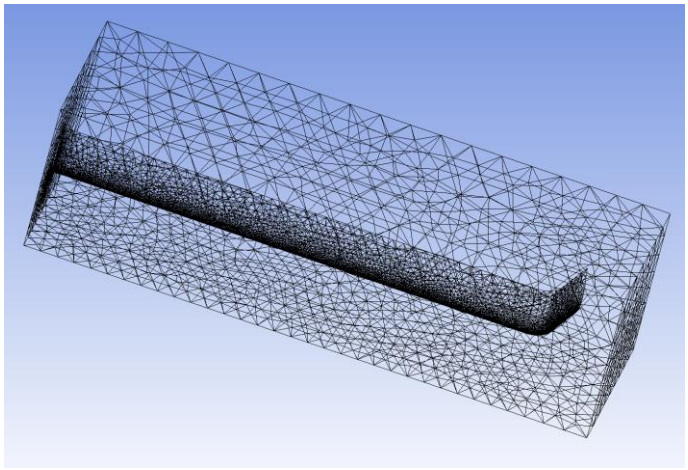

Figure 3.25 - Wing model grid at 75° winglet angle

The monitoring graphs of lift coefficient and drag coefficient of the wing model with 75° winglet Angle at different angles of attack are shown in Figure 3.26 (a), (b), (c).

Figure (a), (b) and (c) in Figure 3.26 respectively show the variation curves of drag coefficients along with the iterative process when the Angle of attack α= 0°, α= 4° and α= 8°.

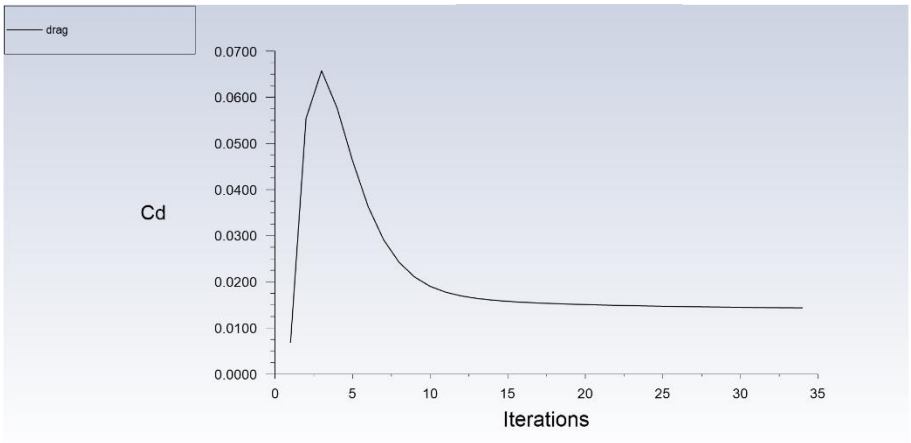

(a)

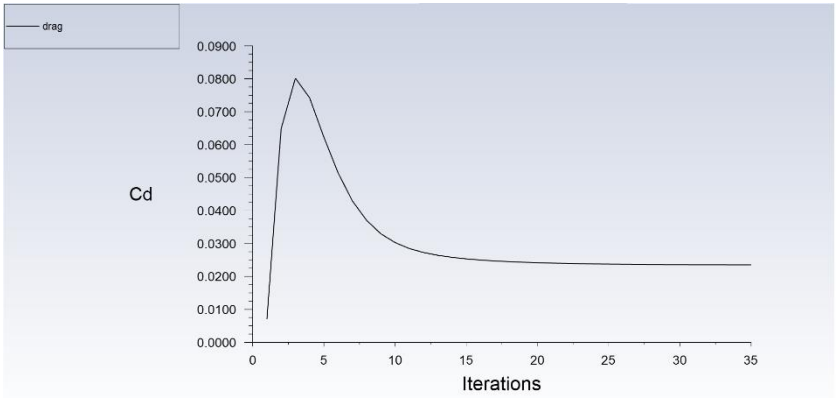

(b)

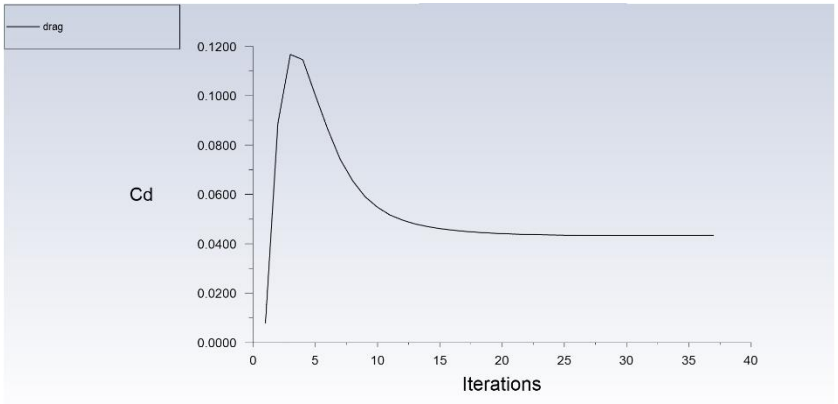

(c)

Figure 3.26 - Drag coefficient changes at different angles of attack

Figure (a), (b) and (c) in Figure 3.27 respectively show the variation curves of lift coefficients along with the iterative process when the Angle of attack α= 0°, α= 4° and α= 8°.

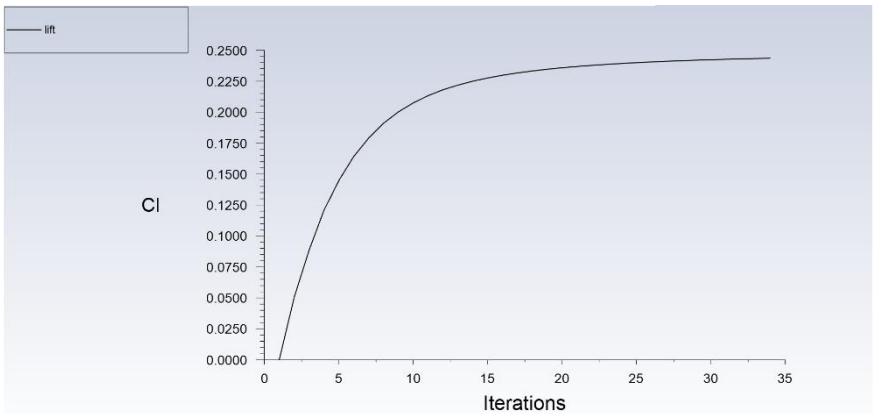

(a)

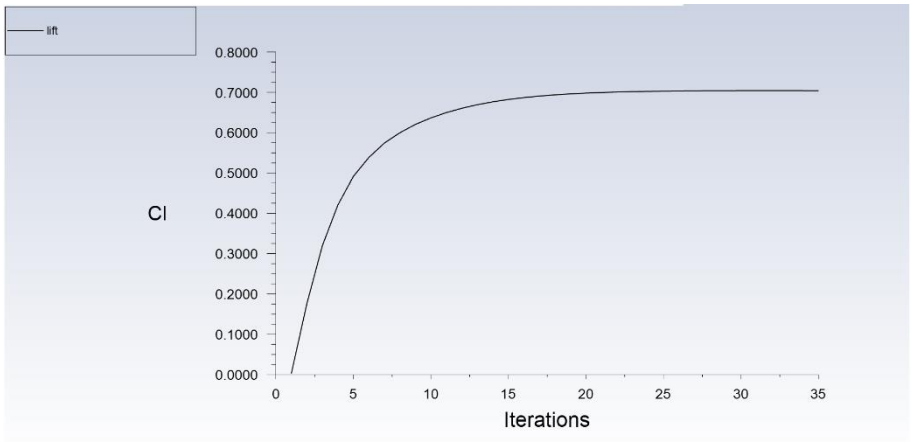

(b)

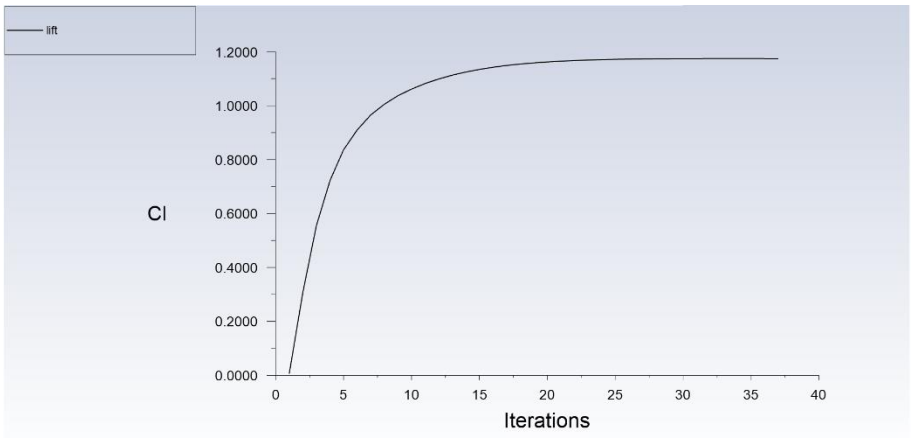

(c)

Figure 3.27 - Lift coefficient changes at different angles of attack

3.4.7. Aerodynamic characteristics of a wing model with a 90° winglet Angle

The straight wing is the wing model when the winglet Angle is 90°. Its model diagram is shown in Figure (3.8). The steps of computational model processing are the same as those of straight wing. The generated flat wing model grid is shown in Figure (3.28).

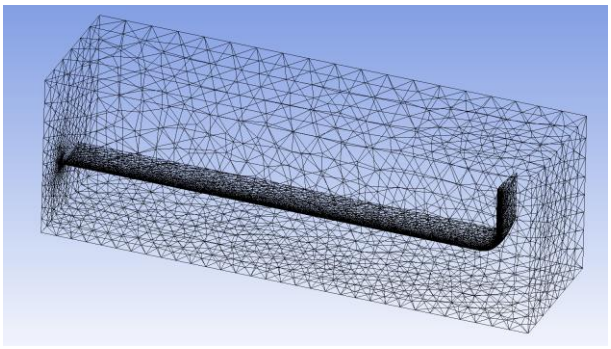

Figure 3.28 - Wing model grid at 90° winglet angle

The monitoring graphs of lift coefficient and drag coefficient of the wing model with 90° winglet Angle at different angles of attack are shown in Figure 3.29 (a), (b), (c).

Figure (a), (b) and (c) in Figure 3.29 respectively show the variation curves of drag coefficients along with the iterative process when the Angle of attack α= 0°, α= 4° and α= 8°.

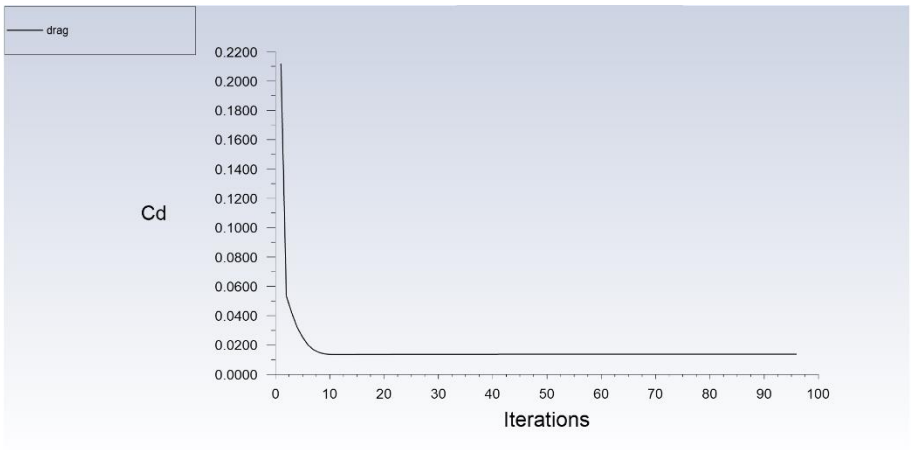

(a)

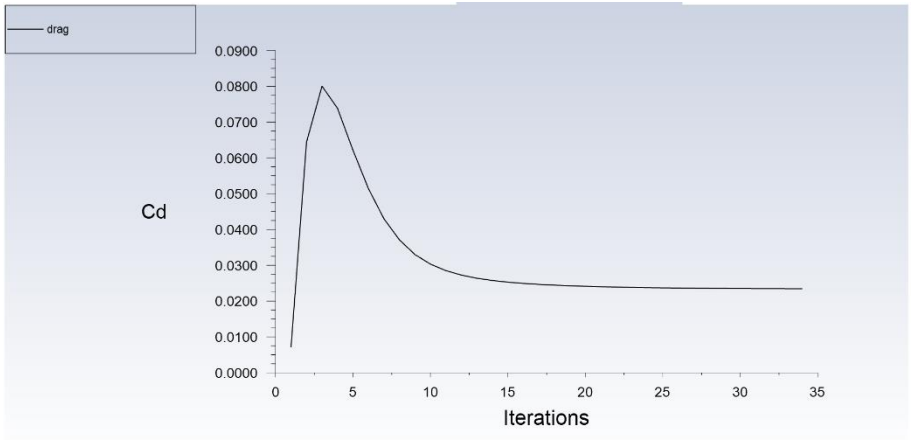

(b)

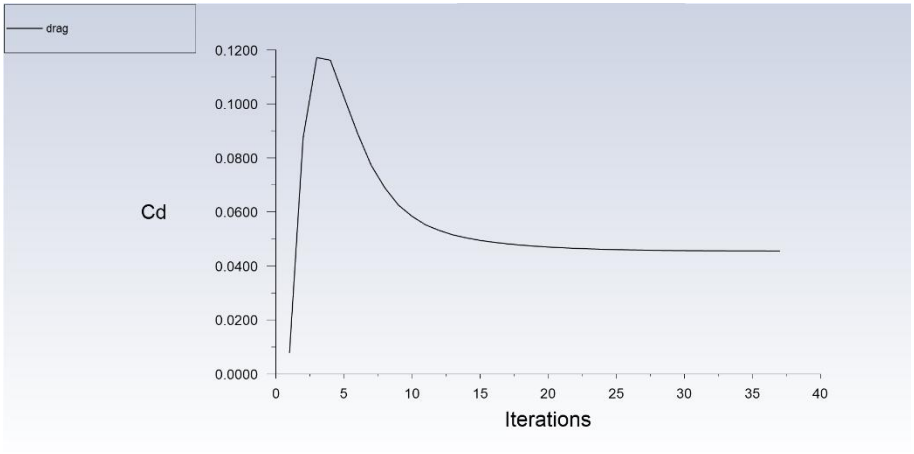

(c)

Figure 3.29 - Drag coefficient changes at different angles of attack

Figure (a), (b) and (c) in Figure 3.30 respectively show the variation curves of lift coefficients along with the iterative process when the Angle of attack α= 0°, α= 4° and α= 8°.

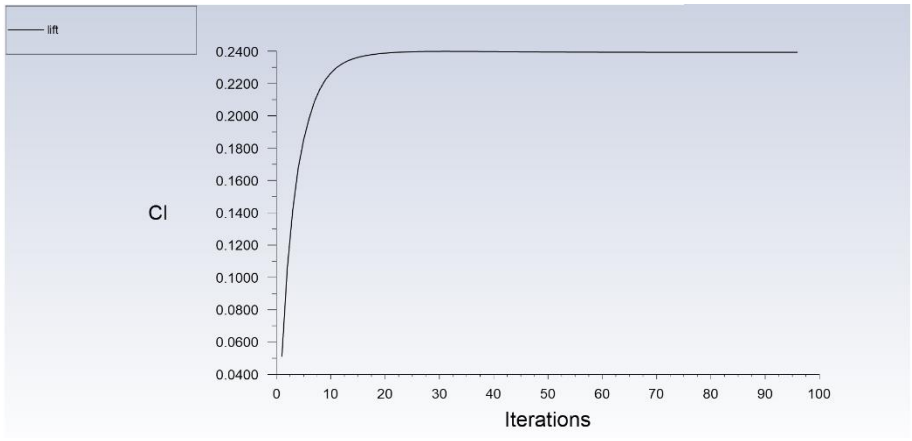

(a)

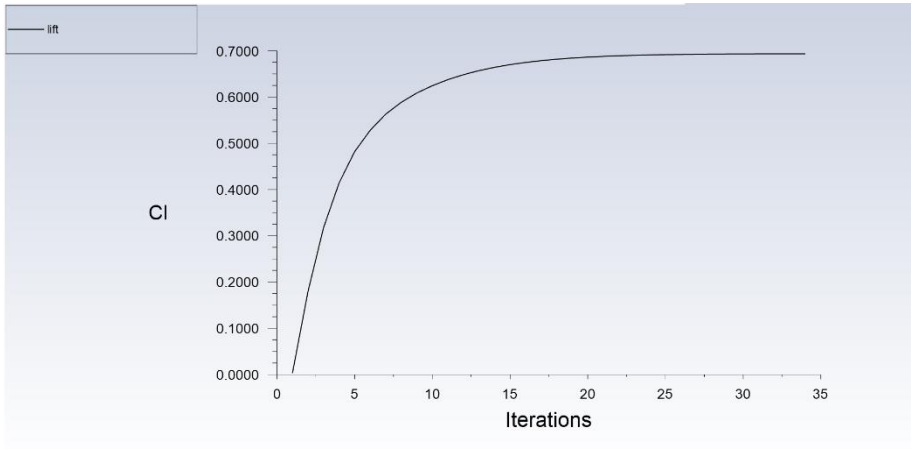

(b)

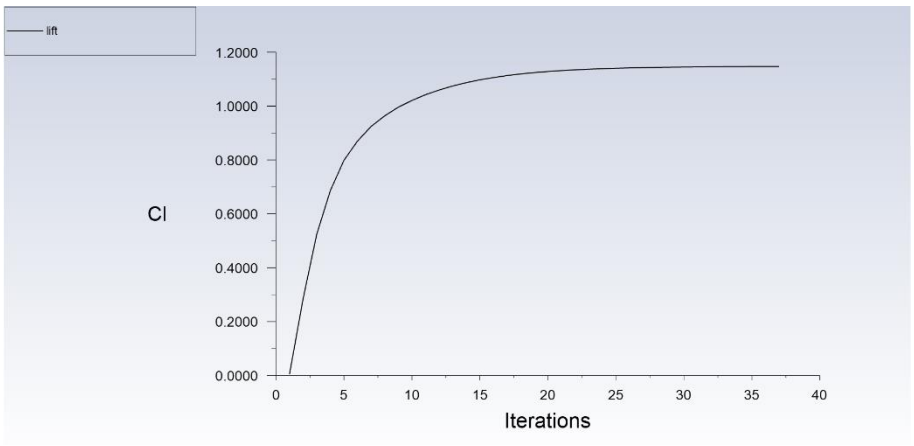

(c)

Figure 3.30 - Lift coefficient changes at different angles of attack

3.5. Data Analysis

Using CFD simulation calculation, the lift coefficient and drag coefficient of the wing model under different winglet angles and different Angle of attack of the incoming flow were obtained, and the corresponding data point text was obtained. Therefore, the convergence points of the curves can be judged by the monitoring charts of lift and drag, and the corresponding convergence values can be found from the output data points text, which can well reflect the aerodynamic characteristics of the wing model under various working conditions. Then the lift coefficient and drag coefficient of the wing models with different winglet angles can be found when the Angle of attack of the incoming flow changes. With the change law, the flight state of the wing model with different winglet angles can be further discussed by analyzing the changing trend of the curve and the causes of the change law.

3.5.1. The variation law of lift coefficient (Cl)

The convergent values of lift coefficients corresponding to each Angle of attack are listed in Table 3.1, and the variation rules of lift coefficients of wing models with different winglet angles varying with the Angle of attack of incoming flow can be obtained by using data coordinate points in the table.

Table 3.1 – Lift coefficients of each wing model at different angles of attack

	$\alpha = 0^o$	$\alpha = 4^o$	$\alpha = 8^o$
Cl at winglet angle 0°	0.25943733	0.73963854	1.2291348
Cl at winglet angle 15°	0.25193126	0.73309482	1.2199971
Cl at winglet angle 30°	0.25492924	0.73242909	1.2082083

End of Table 3.1

Cl at winglet angle 45°	0.25370182	0.72637917	1.1974449
Cl at winglet angle 60°	0.25202787	0.71377817	1.1927905
Cl at winglet angle 75°	0.24350535	0.70400654	1.1744561
Cl at winglet angle 90°	0.23923747	0.69321349	1.1469473

With the data in Table 3.1 as the horizontal and vertical coordinate points, the corresponding lift coefficient curve of the wing model under different winglet angles changing with the Angle of attack can be obtained. These are shown in Figure 3.31.

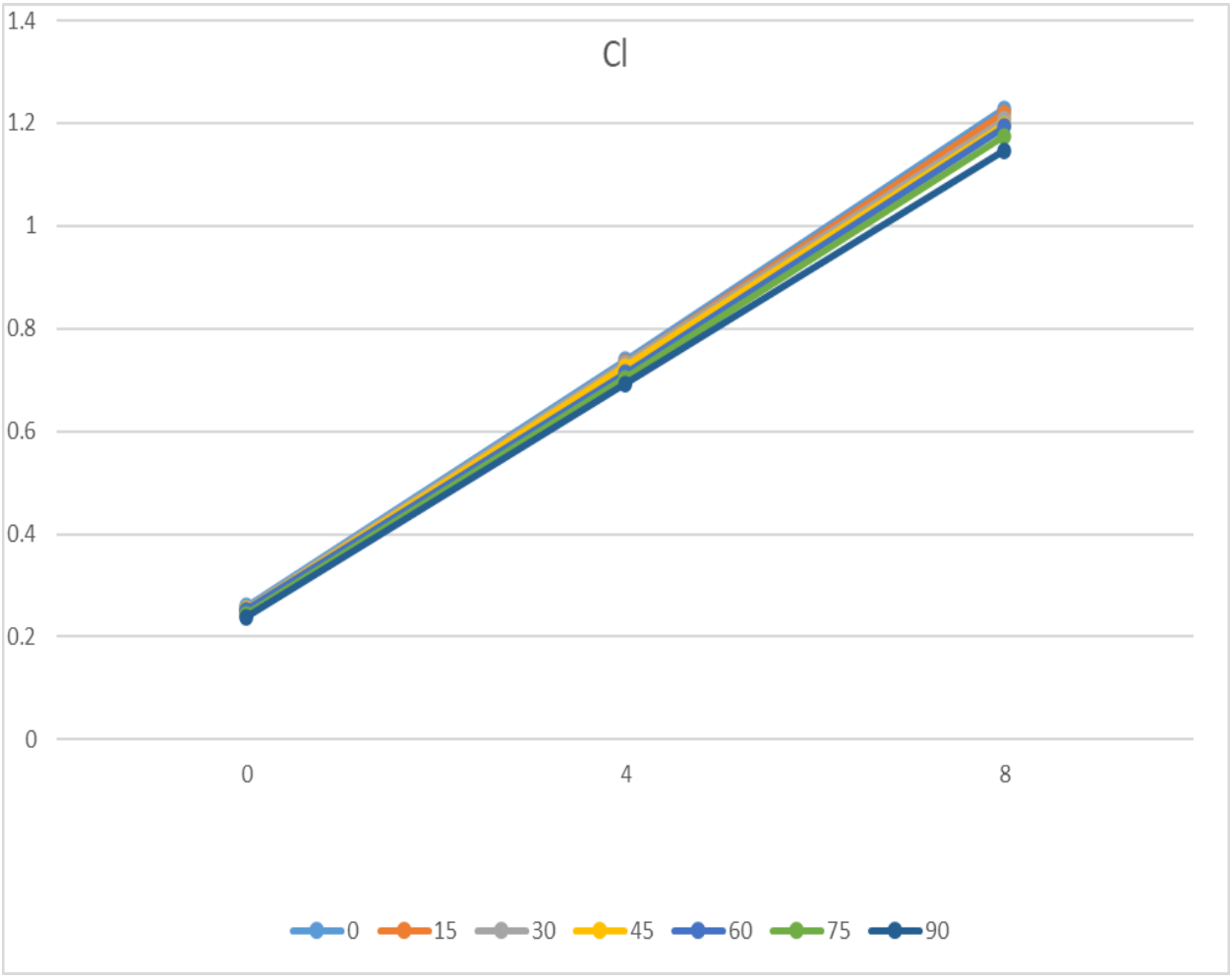

Figure 3.31 - Variation of lift coefficient corresponding to different angles of winglets

According to Figure 3.31, we can find the following changes:

- When the Angle of attack is the same, the lift coefficient of the wing models with different winglet angles changes.
- When the Angle of attack changes, the lift force coefficient of the wing model with winglet deflection also changes correspondingly. When the Angle of attack of the incoming flow is positive, the lift coefficient shows an upward trend.
- As for the lift coefficient curve of the model wing, when the rotation Angle of the winglet rotates from 0° to the maximum Angle of 90°, the lift coefficient of the model wing becomes smaller and smaller.

3.5.2. The variation law of drag coefficient (Cd)

The convergent values of lift coefficients corresponding to each Angle of attack are listed in Table 3.2, and the variation rules of lift coefficients of wing models with different winglet angles varying with the Angle of attack of incoming flow can be obtained by using data coordinate points in the table.

Table 3.2 – Drag coefficients of each wing model at different angles of attack

	$\alpha = 0^o$	$\alpha = 4^o$	$\alpha = 8^o$
Cd at winglet angle 0°	0.014014923	0.021816053	0.040660691
Cd at winglet angle 15°	0.013593926	0.021876903	0.041095949
Cd at winglet angle 30°	0.013857663	0.022790483	0.042033959
Cd at winglet angle 45°	0.014328466	0.02258951	0.043753382
Cd at winglet angle 60°	0.01408476	0.023451505	0.043832593

End of Table 3.2

Cd at winglet angle 75°	0.014358816	0.023520955	0.043418635
Cd at winglet angle 90°	0.013800586	0.023453628	0.045518955

With the data in Table 3.2 as the horizontal and vertical coordinate points, the corresponding drag coefficient curve of the wing model under different winglet angles changing with the Angle of attack can be obtained. These are shown in Figure 3.32.

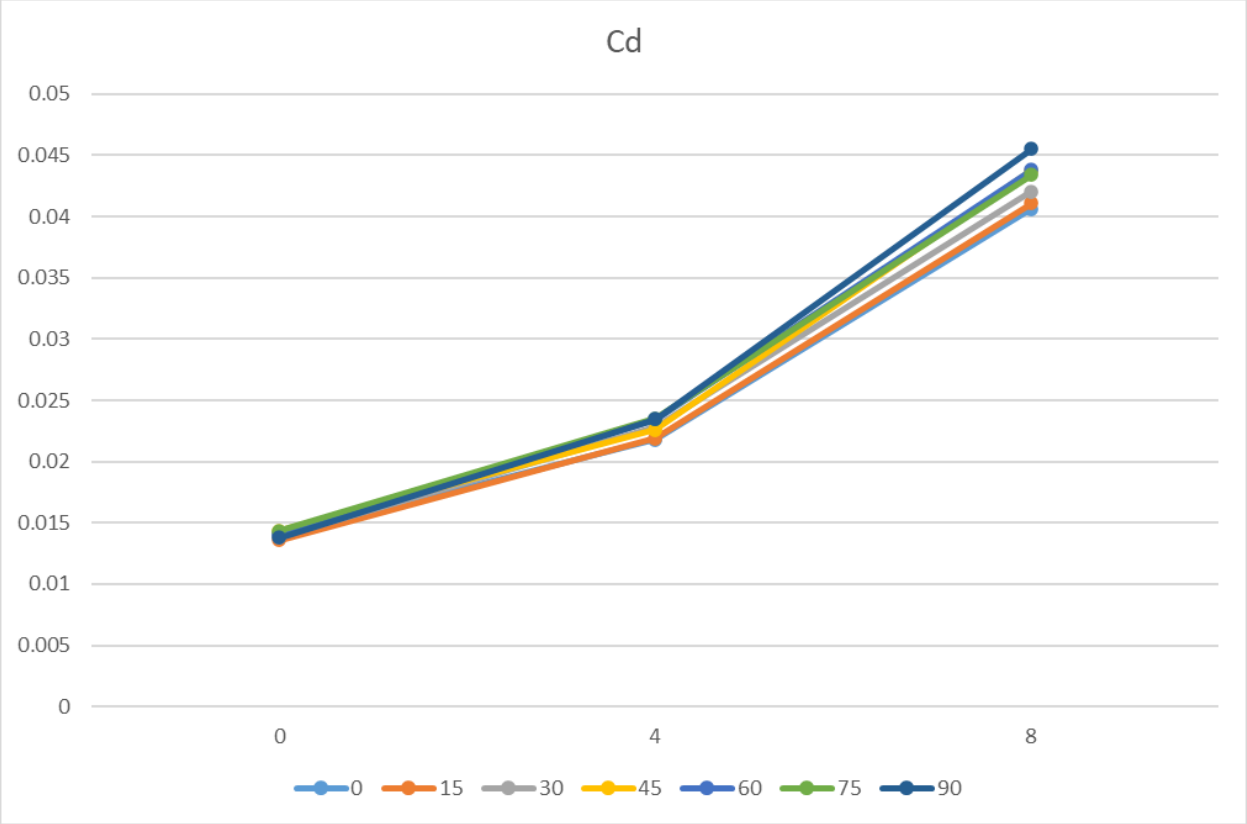

Figure 3.32 - Variation of drag coefficient corresponding to different angles of winglets

According to Figure 3.32, we can find the following changes:

- When the Angle of attack is the same, the drag coefficient of the wing models with different winglet angles changes.
- When the Angle of attack changes, the drag coefficient of the wing model

with winglet deflection also changes correspondingly. When the Angle of attack of the incoming flow is positive, the drag coefficient presents an upward trend.

- As far as the drag coefficient curve of the model wing is concerned, when the rotation Angle of the winglet rotates from 0° to the maximum Angle of 90°, the change curve of the drag coefficient of the model wing is closer and closer to that of the model without winglet deflection.

3.5.2. The variation law of lift-drag ratio (K)

By dividing the lift coefficient of the wing in Table 3.1 by the drag coefficient in Table 3.2, the value of the lift-drag ratio of the model can be obtained. The corresponding relationship between the Angle of attack and the lift-drag ratio is listed in Table 3.3. According to these data coordinates, the change law of lift-drag ratio of the wing model with different winglet angles can be analyzed.

Table 3.3 – Lift-drag ratio of each wing model at different angles of attack

	$\alpha = 0^o$	$\alpha = 4^o$	$\alpha = 8^o$
K at winglet angle 0°	18.50856818	33.90340753	40.73716262
K at winglet angle 15°	18.56484916	33.50998988	29.68655163
K at winglet angle 30°	18.3964052	32.1374967	28.76857608
K at winglet angle 45°	17.70613919	32.15559552	27.46024522
K at winglet angle 60°	17.89365826	30.43634451	27.2124107
K at winglet angle 75°	16.95859485	29.93103597	27.04958647
K at winglet angle 90°	16.93552693	29.5567706	25.19713667

With the data in Table 3.3 as the horizontal and vertical coordinate points, the corresponding lift-drag ratio curve of the wing model under different winglet angles changing with the Angle of attack can be obtained. These are shown in Figure 3.33.

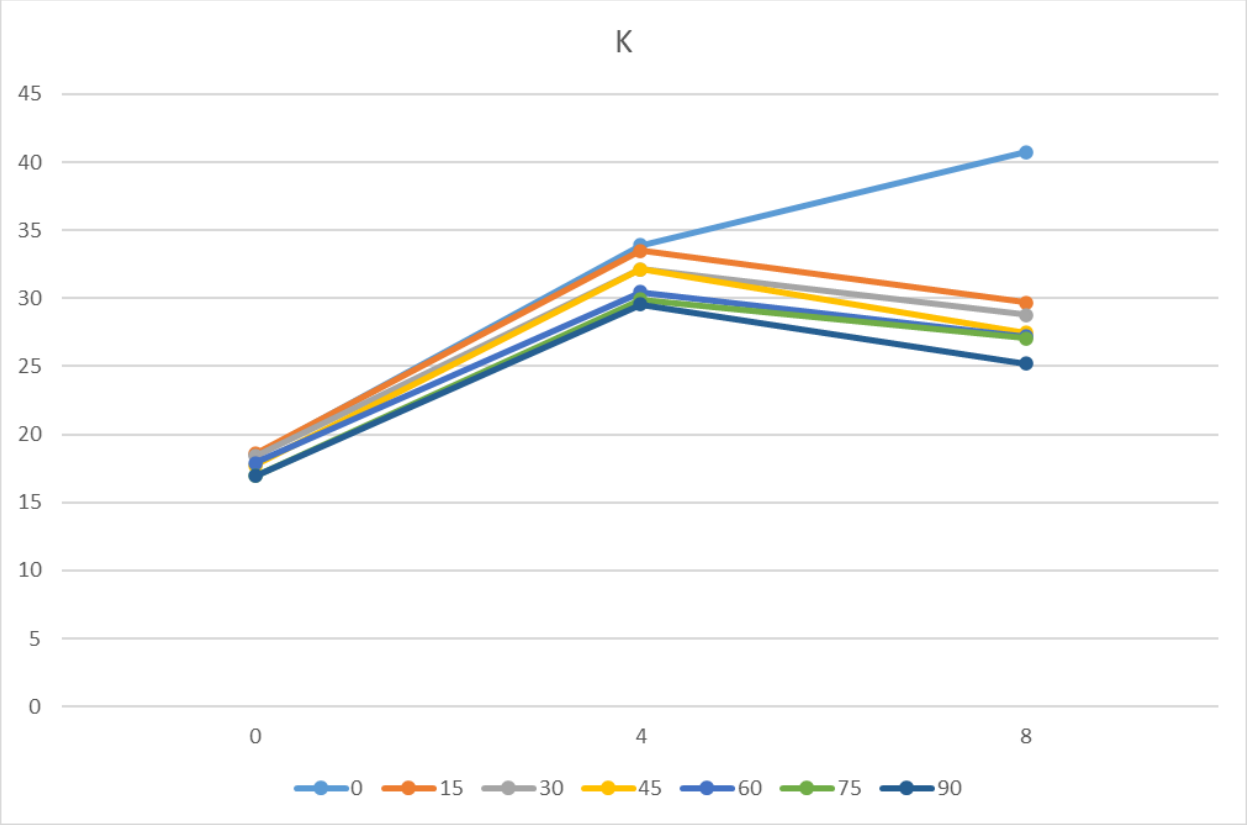

Figure 3.32 - Variation of lift-drag ratio corresponding to different angles of winglets

According to Figure 3.33, we can find the following changes:

- When the Angle of attack of the incoming flow is positive, the lift-drag ratio curves of the wing models corresponding to different winglet angles have little change, but it can still be seen that the lift-drag ratio of the wing models is the maximum when the winglet Angle is 0°.
- When the Angle of attack of the incoming flow is positive, the relation between lift-drag ratio and winglet Angle is obvious. The lift-drag ratio of the winglet model without winglet deflection is larger than that of any case

with winglet deflection. For the winglet model with winglet deflection, the lift-drag ratio is the largest when the Angle of attack is 4°.

3.6. Conclusions

The main resistance of aircraft in flight is differential pressure resistance, viscous resistance and induced resistance. Differential and viscous drag are quickly converted to heat, so only the induced drag can be changed. By reducing induced drag, the wingtip improves the aircraft's ability to climb, takeoff weight and fuel consumption.

The lift generated by the wing is partly used to eliminate induced drag and partly used to provide lift. The lower the induced drag, the higher the lift provided. Therefore, how to reduce induced drag requires a certain understanding of the eddy current distribution of aircraft, as shown in Figure 3.33.

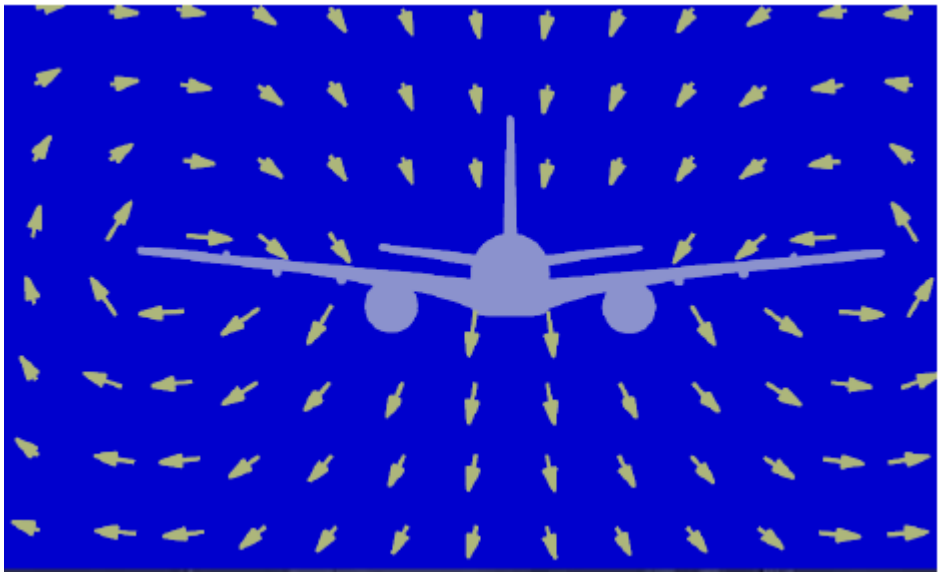

Figure 3.33 - Aircraft vortex diagram

As can be seen from the figure above, the eddy current is generally distributed in the wing tip part of the wing, and the distribution of such eddy current is the main cause of induced drag. If the direction of the eddy current distribution in the wing tip can be

changed, the induced drag can be reduced and lift can be increased. Figure 3.34 The left wing is the lift diagram of the general wing, and the right wing is the lift diagram after the installation of the "wingtip winglet".

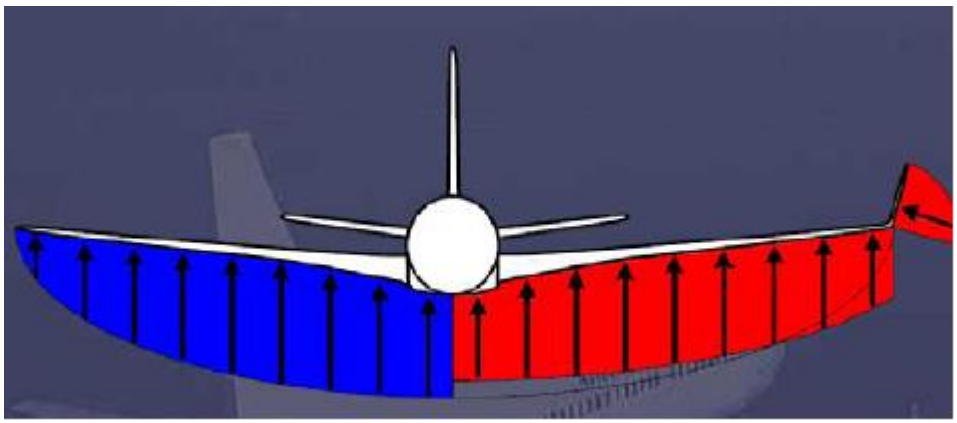

Figure 3.34 - Lift comparison of wing models with or without winglets

From the above analysis, it can be seen that the results obtained in this study are in line with the actual flight conditions of the aircraft. However, due to limited time, this study only analyzes the selected wing model for the transonic flight state, the Mach number of 0.8, and the data points obtained from the study are not comprehensive, so the variation trend of each aerodynamic coefficient can only be roughly represented. The influence of winglet rotation on the aerodynamic characteristics of the whole wing model is briefly analyzed from these changing trends. However, if we want to design a more complete set of variable mechanism to achieve the adaptive winglets, these are far from enough, so this is the deficiency of the design.

Combining theory with practice, we can get the following conclusions:

1. An exquisite rotation mechanism is designed in the study to realize the rotation of the wingtip winglets.
2. The installation of wingtip winglets can hinder the air flow around the upper and lower surfaces of the wings, thus reducing the lift induced drag

caused by the wingtip vortices and reducing the damage of the lift caused by the wingtip vortices. If the data obtained is comprehensive enough, the most reasonable winglet rotation position can be selected according to different Angle of attack.

3. A reasonable choice of wingtip location can increase lift-drag ratio, improve lift, enhance climbing ability, reduce fuel consumption, and improve aircraft flight performance.

REFERENCES

[1] https://en.wikipedia.org/wiki/Aerodynamics

[2] https://en.wikipedia.org/wiki/Airbus_A330

[3] https://en.wikipedia.org/wiki/Airbus_A350

[4] https://en.wikipedia.org/wiki/Boeing_787_Dreamliner

[5] https://en.wikipedia.org/wiki/Boeing_777

[6] Jason Bowman，Brian Sanders，Bryan Cannon，et al．Development of Next Generation Morphing Aircraft Structures，48th AIAA/ASME/ASCE/AHS/ASC Structures[C]．Structural Dynamics and Materials Conference，Honolulu，Hawaii，23-26 April 2007，AIAA 2007-1730．

[7] D H Lee，Terrence A Weisshaar．Aeroelastic Studies on A Folding Wing Configuration，46th AIAA/ASME/ASCE/AHS/ASC Structures[C]．Structural Dynamics and Materials Conference，Austin，Texas，18-21 April 2005，AIAA 2005-1996．

[8] https://www.sciencedirect.com/topics/materials-science/smart-structure

[9] https://en.wikipedia.org/wiki/Wing_tip

[10] Joshi S P, Tidwell Z, Crossley W A, et al. Comparison of morphing wing stategies based upon aircraft performance impacts[C]. 45th AIAA/ASME/ASCE/AHS/ASCS Structures, Strucrural Dynamics &Materials Conference. USA: AIAA, 2004, AIAA 2004-1722:1-7.

[11] LI M, CHEN W M, GUAN D, Improvement of Aircraft Rolling Power by Use of Piezoelectric Actuators[J]. CHINESE JOURNAL OF AERONAUTICS.

2004,17(2).

[12] 桑为民, 陈年旭. 变体飞机的研究进展及其关键技术[J]. 飞行力学. 2009, 27(6).

[13] Wlezien R W, Homer G, McGowan A R, Padula S, Scott M A, Silcox R, Simpson J O. The Aircraft Morphing Program[C]. Proceedings of the 37th AIAA/ASME/ASCE/AHS/ASC Structures, Structural Dynamics and Materials Conference. Long Beach, California, April 1998.

[14] Kudva J N. Overview of the DARPA Smart Wing Project[J]. Journal of Intelligent Material Systems and Structures. 2004,15(4): 261-267.

[15] Nathan P, Marat M, Eli L. Design, Construction, and Tests of an Aeroelastic Wind Tunnel Model of a Variable Camber Continuous Trailing Edge Flap (VCCTEF) Concept Wing[J]. AIAA Paper. NO, AIAA 2014-2442.

[16] Nathan P, Marat M, Eli L. The Design, Construction, and Tests of a Concept Aeroelastic Wind Tunnel Model of a High-Lift Variable Camber Continuous Trailing Edge Flap (HLVCCTEF) Wing Config[J]. NO, AIAA 2015-1406.

APPENDIX A

8 Three View Diagra

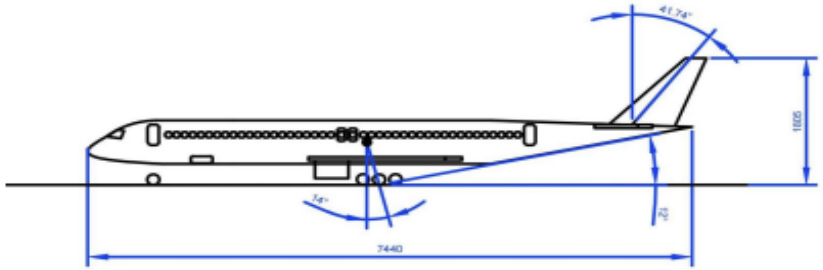

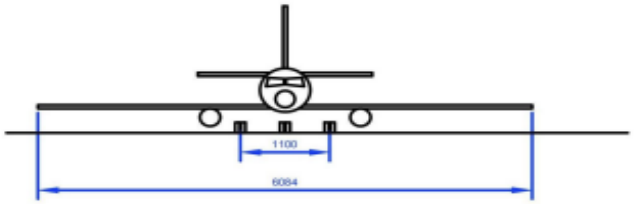

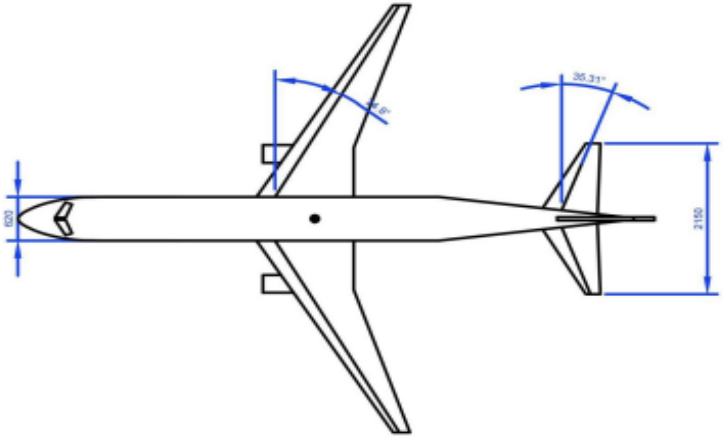

Heading Qualities	1	$H_{cursing}$		km	10
	2	$V_{landing}$		km/h	275
	3	$L_{take-off}$		m	1900
	4	L		km	10000
Mass Data	5	$m_{take-off}$		kg	209700
	6	n_{crew}		persons	15
	7	n_{pass}		persons	450
Power Plant Data	8	P_0		kN	410
	9	t_0			0.39
	10	Number and type of engines			2,Turbofan
Geometry	11	S_{wing}		m^2	426.884
	12	S_{ht}		m^2	101.034
	13	S_{vt}		m^2	53.111
	14	η_{wing}			5.846
	15	χ_{wing}			31.64
	16	λ_{wing}			8.67
	17	$d_{fuselage}$		m	6.2
	18	$\lambda_{fuselage}$			12

					K103-150fd			
	Sheet	Doc NO.	Sign	Date				
Drawn			Zhang Haoyu	27.01.2022		Letter	Mass	Scale
Chng.					Passenger Airplane			
Developed								
Checked by								
T.check								
						Department 103,KhAI		


ZC
XC
YC